AD_____

CONTRACT NO.: DAMD17- 92-C-2071

TITLE: Mechanism of Cutaneous Vesication

PRINCIPAL INVESTIGATOR: Nancy A. Monteiro-Riviere, Ph.D.
CO-AUTHORS: Jason Z. Zhang, B.M.
Alfred O. Inman, M.S.
Jim D. Brooks, M.S.
Jim E. Riviere, D.V.M., Ph.D.

CONTRACTING ORGANIZATION: North Carolina State University
College of Veterinary Medicine
Cutaneous Pharmacology and Toxicology Center
Raleigh, North Carolina 27606

REPORT DATE: February 17, 1994

TYPE OF REPORT: Midterm Report

PREPARED FOR: U.S. Army Medical Research, Development, Acquisition and Logistics Command (Provisional),
Fort Detrick, Frederick, Maryland 21702-5012

DISTRIBUTION STATEMENT: Approved for public release; distribution unlimited

REPORT DOCUMENTATION PAGE

Form Approved
OMB No. 0704-0188

1. AGENCY USE ONLY (Leave blank)	2. REPORT DATE	3. REPORT TYPE AND DATES COVERED
	17 February 1994	Midterm Report (7/17/92 - 2/17/94)

4. TITLE AND SUBTITLE

Mechanism of Cutaneous Vesication

5. FUNDING NUMBERS

C-DAMD17-92-C-2071

6. AUTHOR(S)

Nancy A. Monteiro-Riviere, Ph.D., Jason Z. Zhang, B.M., Alfred O. Inman, M.S., Jim D. Brooks, M.S., Jim E. Riviere, D.V.M., Ph.D.

7. PERFORMING ORGANIZATION NAME(S) AND ADDRESS(ES)

North Carolina State University
College of Veterinary Medicine
Cutaneous Pharmacology and Toxicology Center
Raleigh, North Carolina 27606

8. PERFORMING ORGANIZATION REPORT NUMBER

9. SPONSORING / MONITORING AGENCY NAME(S) AND ADDRESS(ES)

U.S. Army Medical Research Development Acquisition and Logistics Command (Provisional)
Fort Detrick
Frederick, Maryland 21702-5012

10. SPONSORING / MONITORING AGENCY REPORT NUMBER

11. SUPPLEMENTARY NOTES

12a. DISTRIBUTION / AVAILABILITY STATEMENT

Approved for public release; distribution unlimited

12b. DISTRIBUTION CODE

13. ABSTRACT (Maximum 200 words)

This project investigated the mechanism of bis (2-chloroethyl) sulfide [sulfur mustard, HD]-induced cutaneous vesication using the isolated perfused porcine skin flap (IPPSF) and in vitro cell cultures. Treatment of IPPSFs with 5.0 mg/ml of HD results in a characteristic increase in vascular resistance, decrease in glucose utilization, and the formation of gross and microblisters. The first study demonstrated that the vascular changes associated with HD vesication are accompanied by increases in the efflux of prostaglandins E_2 and F_2. Assessment of extracellular and intravascular space using radiolabeled inulin and albumin infusions, respectively, demonstrated that HD primarily produced an increase in intravascular space. Thus these studies unequivocally demonstrate a vascular component to HD vesication directly mediated by cutaneous elements, since the IPPSF is an isolated system not associated with a systemic immune response. A second study probed the molecular basis of HD interaction with laminin, a basement membrane component previously implicated by our group to be primarily involved in HD-induced epidermal-dermal separation. HD directly alkylated laminin and reduced its cell adhesive activity through a noncytotoxic mechanism. This is a significant finding,

14. SUBJECT TERMS	15. NUMBER OF PAGES
Pig; Skin; Porcine; Integument; Percutaneous Absorption; Pharmacology; Vesicants; Sulfur Mustard; Laminin; Prostaglandins; Toxicokinetics; Chemical Warfare; Morphology	114
	16. PRICE CODE

17. SECURITY CLASSIFICATION OF REPORT	18. SECURITY CLASSIFICATION OF THIS PAGE	19. SECURITY CLASSIFICATION OF ABSTRACT	20. LIMITATION OF ABSTRACT
Unclassified	Unclassified	Unclassified	Unlimited

NSN 7540-01-280-5500

Standard Form 298 (Rev 2-89)
Prescribed by ANSI Std. Z39-18
298-102

GENERAL INSTRUCTIONS FOR COMPLETING SF 298

The Report Documentation Page (RDP) is used in announcing and cataloging reports. It is important that this information be consistent with the rest of the report, particularly the cover and title page. Instructions for filling in each block of the form follow. It is important to *stay within the lines* to meet *optical scanning requirements*.

Block 1. Agency Use Only (Leave blank).

Block 2. Report Date. Full publication date including day, month, and year, if available (e.g. 1 Jan 88). Must cite at least the year.

Block 3. Type of Report and Dates Covered. State whether report is interim, final, etc. If applicable, enter inclusive report dates (e.g. 10 Jun 87 - 30 Jun 88).

Block 4. Title and Subtitle. A title is taken from the part of the report that provides the most meaningful and complete information. When a report is prepared in more than one volume, repeat the primary title, add volume number, and include subtitle for the specific volume. On classified documents enter the title classification in parentheses.

Block 5. Funding Numbers. To include contract and grant numbers; may include program element number(s), project number(s), task number(s), and work unit number(s). Use the following labels:

C	- Contract	PR	- Project
G	- Grant	TA	- Task
PE	- Program Element	WU	- Work Unit Accession No.

Block 6. Author(s). Name(s) of person(s) responsible for writing the report, performing the research, or credited with the content of the report. If editor or compiler, this should follow the name(s).

Block 7. Performing Organization Name(s) and Address(es). Self-explanatory.

Block 8. Performing Organization Report Number. Enter the unique alphanumeric report number(s) assigned by the organization performing the report.

Block 9. Sponsoring/Monitoring Agency Name(s) and Address(es). Self-explanatory.

Block 10. Sponsoring/Monitoring Agency Report Number. *(If known)*

Block 11. Supplementary Notes. Enter information not included elsewhere such as: Prepared in cooperation with...; Trans. of...; To be published in.... When a report is revised, include a statement whether the new report supersedes or supplements the older report.

Block 12a. Distribution/Availability Statement. Denotes public availability or limitations. Cite any availability to the public. Enter additional limitations or special markings in all capitals (e.g. NOFORN, REL, ITAR).

DOD	- See DoDD 5230.24, "Distribution Statements on Technical Documents."
DOE	- See authorities.
NASA	- See Handbook NHB 2200.2.
NTIS	- Leave blank.

Block 12b. Distribution Code.

DOD	- Leave blank.
DOE	- Enter DOE distribution categories from the Standard Distribution for Unclassified Scientific and Technical Reports.
NASA	- Leave blank.
NTIS	- Leave blank.

Block 13. Abstract. Include a brief *(Maximum 200 words)* factual summary of the most significant information contained in the report.

Block 14. Subject Terms. Keywords or phrases identifying major subjects in the report.

Block 15. Number of Pages. Enter the total number of pages.

Block 16. Price Code. Enter appropriate price code *(NTIS only)*.

Blocks 17. - 19. Security Classifications. Self-explanatory. Enter U.S. Security Classification in accordance with U.S. Security Regulations (i.e., UNCLASSIFIED). If form contains classified information, stamp classification on the top and bottom of the page.

Block 20. Limitation of Abstract. This block must be completed to assign a limitation to the abstract. Enter either UL (unlimited) or SAR (same as report). An entry in this block is necessary if the abstract is to be limited. If blank, the abstract is assumed to be unlimited.

13. **ABSTRACT (continued)**

since it not only offer insight into HD-induced epidermal-dermal separation, but also suggests hypotheses as to the reasons for delayed epidermal regeneration and healing in HD wounds. To further probe the molecular basis of HD-induced basement membrane damage, the effect of HD treatment on six epidermal-dermal epitopes (laminin, type IV collagen, bullous pemphigoid (BPA), pidermolysis bullosa acquisita (EBA), fibronectin, and GB3) was characterized using indirect immunohistochemistry and immunoelectron microscopy. These studies confirmed the laminin alkylation data by localizing the HD-induced blister cleavage plane within the laminin and fibronectin, above the type IV collagen, EBA, and GB3, but below the BPA sites. Finally, in an effort to get a better understanding of the relationship between HD absorption and toxicologic effect, a toxicokinetic model of ^{14}C-HD percutaneous absorption and intracutaneous disposition was formulated. We believe that the studies reported herein have made significant progress in probing the mechanism of cutaneous vesication, characterizing the use of the IPPSF to study this phenomenon, and identifying the molecular targets of HD in the basement membrane which lead to epidermal-dermal separation.

FOREWORD

Opinions, interpretations, conclusions, and recommendations are those of the author and are not necessarily endorsed by the U.S. Army.

NAMR Where copyrighted material is quoted, permission has been obtained to use such material.

N/A Where material from documents designated for limited distribution is quoted, permission has been obtained to use the material.

NAMR Citations of commercial organizations and trade names in this report do not constitute an official Department of Army endorsement or approval of the products or services of these organizations.

NAMR In conducting research using animals, the investigator(s) adhered to the "Guide for the Care and Use of Laboratory Animals," prepared by the Committee on Care and Use of Laboratory Animals of the Institute of Laboratory Resources, National Research Council (NIH Publication No. 86-23, Revised 1985).

N/A For the protection of human subjects, the investigator(s) adhered to policies of applicable Federal Law 45 CFR 46.

N/A In conducting research utilizing recombinant DNA technology, the investigator(s) adhered to current guidelines promulgated by the National Institutes of Health.

N/A In the conduct of research utilizing recombinant DNA, the investigator(s) adhered to the NIH Guidelines for Research Involving Recombinant DNA Molecules.

N/A In the conduct of research involving hazardous organisms, the investigator(s) adhered to the CDC-NIH Guide for Biosafety in Microbiological and Biomedical Laboratories.

Nancy A Montes-Rivera 2/14/94

PI - Signature DATE

ACKNOWLEDGMENT

The technical assistance of Rick Rogers, Lillian Kidd, Katrina Winter, Becky Vaughn, and Dawn Chasse is deeply appreciated in the surgical procedure, caring, dosing and histological preparation of the skin flaps. The assessment of HD alkylation of laminin represents partial fulfillment of the requirements for the Doctor of Philosophy (Ph.D.) degree in toxicology for Jason Zili Zhang under the direction of Dr. Nancy Monteiro-Riviere. Thanks are also given to Drs. Patrick Williams and Barry Peters for assistance. Only with the dedication and conscientiousness of all these individuals was this project possible.

TABLE OF CONTENTS

TABLE OF CONTENTS (continued)

TABLE OF CONTENTS (continued)

List of Tables

List of Figures

TABLE OF CONTENTS (continued)

TABLE OF CONTENTS (continued)

INTRODUCTION

The purpose of this contract is to study the mechanism of action of the cutaneous vesicant sulfur mustard, bis (2-chloroethyl) sulfide (HD), in the isolated perfused porcine skin flap (IPPSF), an in vitro model previously shown to be a useful system to investigate the actions of topically applied vesicants on skin. The morphological, biochemical, and physiological changes induced by HD in the IPPSF have been fully described previously in the final report of the USAMRDC contract (DAMD17- 87-C-7139), during which the model was developed (Monteiro-Riviere et al., 1991). Based on this previous research, a number of interesting phenomena were noted and a hypothesis developed that is the subject of the present contract. It must be stressed that this is a midterm report and therefore must be viewed as a report of **"studies in progress"**. Final conclusions have yet to be made.

These previous studies generated two relatively independent lines of research related to the pathogenesis of HD blisters in the skin: the inflammatory reaction and the molecular mechanism of HD damage to the basement membrane zone. These were independently investigated in the present proposal in Sections I & IV and II & III, respectively.

A characteristic physiological change seen with HD treatment in the IPPSF is an increase in total flap vascular resistance (VR) shortly after exposure. In fact, compared to all historical IPPSF data collected to date (≈ 2,000 IPPSFs), this increase in VR is a hallmark of chemical vesication. Similar manifestations of vascular changes (e.g. erythema, edema, etc.) have also been reported by other investigators (Vogt et al., 1984). What is the mechanism of this change which precedes morphological evidence of vesication? Section I of this report provides data which strongly suggest that it is mediated by release of prostaglandins. Section IV further documents an HD-induced increase in intravascular volume as assessed by albumin space which suggests an increase in capillary permeability. Since these changes occur in the

IPPSF, an in vitro model which lacks a functional immune system, the mediators responsible must be produced by cutaneous elements via a mechanism triggered by HD.

Earlier studies demonstrated that HD-induced vesication occurred at the level of the lamina lucida of the epidermal-dermal junction (EDJ; basement membrane). What specific molecular components of this structure are involved, and is HD capable of directly interacting with these components? The results documented in Sections II and III of the present report strongly suggest that laminin may be directly alkylated by HD. Furthermore, after a blister is formed, laminin remaining on the dermis is altered and may be directly responsible for the delayed wound healing that is characteristic of HD-induced vesication. This altered laminin, which normally serves as a scaffold for epidermal regeneration, is now deficient in this function. Additional studies reported herein have further defined the molecular epitope mapping of the EDJ zone antigens after HD treatment which localizes the blister cleavage plane to the region occupied by laminin and fibronectin.

The final component of this report deals with our attempts to develop an integrated toxicokinetic-toxicodynamic (TK-TD) model of HD vesication in the IPPSF. Such a model would be useful in tying together the multiple toxicologic end points observed after HD treatment and correlating them to the disposition of HD and its metabolites within the skin. For example, what is the concentration of HD seen in the basement membrane of HD-treated flaps? Also, these studies shed light on the source of the variability seen after HD treatment since a great deal of variability in HD penetration and absorption was documented. Ultimately, a formal TK-TD model encompassing time-related changes in vascular volumes and permeability will be constructed. In this report, the IPPSF venous efflux and intra-cutaneous disposition profiles of ^{14}C - HD are reported. A preliminary TK model based on individual flaps is presented in addition to the previously mentioned changes in vascular volume seen with HD.

I. CUTANEOUS TOXICITY OF SULFUR MUSTARD IN ISOLATED PERFUSED PORCINE SKIN

Introduction

Sulfur mustard, bis (2-chloroethyl) sulfide (HD), an old warfare chemical, is well-documented for its severe cutaneous damage as well as systemic toxicity (Papirmeister et al., 1991). At the molecular level, HD represents a classical alkylating agent, which forms a DNA adduct and can cause mutagenesis and carcinogenesis (Boberts, 1978). Recently, derivatives of mustard have been used as potential antineoplastic drugs (Calabresi and Chabner, 1992). Therefore, the study of HD may provide interesting toxicological and pharmacological perspectives to this family of compounds.

Skin is a principal site of exposure to HD and demonstrates a characteristic lesion of HD exposure, namely vesication. Traditional in vitro models used to study skin toxicity usually do not contain an intact anatomic structure, and therefore fail to mimic the complicated physiological responses. The isolated perfused porcine skin flap (IPPSF), developed in our laboratory as a novel in vitro model for percutaneous absorption and cutaneous toxicity has been shown to be a rational tool to evaluate dermally toxic compounds, especially vesicants. This model responded with biochemical, vascular, and morphological changes that were identical to human cutaneous exposure to HD, including the formation of macroscopic blisters (Monteiro-Riviere and King, 1989; Monteiro-Riviere et al., 1990; 1991). Recent studies have shown a complex immune network in the skin, suggesting that determination of inflammatory mediators may offer a unique insight into the evaluation of dermal toxicity (Rheins, 1992). The IPPSF maintains the normal anatomical structure, including a functional microcirculation and therefore it provides a new approach to study the immunological activity in the skin.

The objective of this study was to characterize HD effects in the IPPSF by topical exposure to 5.0 mg/ml and 10.0 mg/ml of HD, and to determine the changes in viability,

vascular resistance, and morphology. In addition, the production of inflammatory mediators prostaglandin E_2 (PGE_2) and prostaglandin $F_{2\alpha}$ ($PGF_{2\alpha}$), were characterized in HD-treated IPPSFs.

Materials and Methods

IPPSF preparation and dosing

Weanling, female Yorkshire pigs (18-24 kg) were given atropine sulfate (0.04 mg/kg) and then anesthetized with ketamine hydrochloride (10.0 mg/kg) and xylazine hydrochloride (4.0 mg/kg) intramuscularly. Anesthesia was maintained during surgery using halothane delivered via tracheal intubation. The first stage of IPPSF preparation involved the creation of two skin flaps, with one on either side of the midline in the inguinal region of the pig. Two days later, the arterial supply to each flap was cannulated and the flaps were removed for perfusion (Figure 1). Each flap was gently flushed with heparinized saline to remove blood from the IPPSF vasculature and placed in a perfusion chamber (Figure 2) within a specially designed chemical fume hood (Riviere et al., 1986; Monteiro-Riviere et al., 1987; Monteiro-Riviere, 1990; Bowman et al., 1991).

Each flap was perfused in a nonrecirculating manner with a media containing bovine serum albumin (BSA) and glucose in a Kreb's-Ringer bicarbonate buffer solution. Environmental parameters in the chamber were held constant during all of the IPPSF experiments. Target ranges for these parameters are as follows: temperature, 36-38 $^{\circ}$C; relative humidity, 50-65%; and media flow rate, 1.5 ml/min. Media were gassed during perfusion with 95% O_2/5% CO_2 using a silastic tube oxygenator. Each flap was perfused for 1 hour prior to dosing to ensure perfusion viability and stability.

Immediately prior to dosing, perfusion was temporarily suspended and each IPPSF was fitted with a flexible plastic template (Stomahesive, ConvaTec-Squibb, Princeton, NJ) which was adhered with Skin Bond (Pfizer Hospital Products, Inc., Largo, FL). A 7.5 cm^2

nonoccluded dosing surface was defined by the template. A total of 300 µl of the appropriate dosing solution was applied inside the template with a positive displacement pipette (Gilson Microman, Gilson Medical Electronics, France). The dosing solution was allowed to air dry before perfusion was resumed. Nineteen IPPSFs were treated with 5.0 mg/ml or 10.0 mg/ml of HD (n= 6/treatment) in ethanol (n=7) and perfused for 8 hours. Stock HD in ethanol was obtained from the U.S. Army Medical Research and Development Command. Concentrations greater than 10.0 mg/ml could not be used in this study because greater concentrations would exceed the surety limits established for university laboratories. Vehicle controls were dosed with 300 µl of absolute ethanol (AAPER Alcohol & Chemical Co., Shelbyville, KY) and perfused for 8 hours.

Biochemical and vascular parameters

Samples of the arterial and venous media were collected hourly throughout the perfusion period and analyzed for glucose. Cumulative glucose utilization (CGU) has been used in previous IPPSF studies to determine the status of flap viability and chemical effects on IPPSF metabolism (King and Monteiro-Riviere, 1990; Riviere and Monteiro-Riviere, 1991). Hourly glucose utilization was the primary biochemical marker of flap viability during perfusion. A plateau in CGU was used as a retrospective indicator of a loss in flap viability.

Arterial pressure and media flow rate were monitored throughout the perfusion period. The physiological parameter vascular resistance (VR) is defined as the ratio of arterial pressure to media flow rate. This parameter has been used as an indirect measure of vascular activity in previous IPPSF studies and shown to characteristically increase after HD exposure (Monteiro-Riviere et al., 1990; 1991).

Tissue preparation and morphological parameters

After 8 hours of perfusion, skin from the dosed region of each IPPSF was excised and tissues prepared for light microscopy (LM). LM samples were fixed in 10% neutral buffered formalin, processed through a graded series of alcohols and embedded in paraffin. Sections

were cut at 6 μm, stained with hematoxylin and eosin (H&E) and then examined under an Olympus PM-10AD photographic microscope (Olympus Optical Co., LTD., Tokyo, Japan).

Prostaglandin parameters

PGE_2 and $PGF_{2\alpha}$ were measured with an enzyme-linked immunosorbent assay (ELISA) (Pradelles et al., 1990). This assay is based on the competition of variable amounts of PGE_2 or $PGF_{2\alpha}$ in the samples with a fixed amount of acetylcholinesterase (AChE)-labeled PGE_2 or $PGF_{2\alpha}$ for a limited number of binding sites on anti-PGE_2 or $PGF_{2\alpha}$ antibody. With more unlabeled PGE_2 or $PGF_{2\alpha}$, less labeled PGE_2 or $PGF_{2\alpha}$ is bo to the specific antibody. The resulting pellet containing labeled PGE_2 or $PGF_{2\alpha}$ was incu d with the AChE substrate. A distinct yellow color produced by the AChE metabolite was measured at 412 nm. The intensity of absorbance was correlated to the concentration of labeled-PGE_2 or $PGF_{2\alpha}$, and was inversely proportional to the amount of sampling prostaglandins by means of a standard curve.

In each of the 250-μl hourly venous effluent samples, 8 ml of 0.1 M KH_2PO_4 solution was added. PGE_2 and $PGF_{2\alpha}$ were extracted from the diluted IPPSF medium sample using a Sep-Pak Plus^R extraction cartridge (Waters, Milford, MA), then washed with ethyl acetate (EA) (8 ml EA for each column). After the EA was evaporated, the remaining PGE_2 and $PGF_{2\alpha}$ was dissolved in an enzyme immunosorbent assay (EIA) buffer (1 ml) and then placed in a 96-well polystyrene microtiter assay plate (Caymen Chemical, Ann Arbor, MI). PGE_2 and $PGF_{2\alpha}$ EIA kits were developed according to the manufacturer's instructions and the samples were assayed on a Fisher Biotech ELISA Reader (Fisher Scientific, Pittsburgh, PA).

Statistical methods

Statistical comparisons were made for all parameters on the basis of responses of individual IPPSF over the time course of each hour after HD treatment using the General Linear Models procedure (SAS Institute, Inc., Cary, NC) at the 0.05 significance level. Where

significant differences were noted between treatment responses, multiple comparison tests were conducted using Student's *t* test.

Results

Viability parameters

CGU was evaluated to determine baseline IPPSF viability and whether HD altered cutaneous glucose metabolism and IPPSF viability. All HD-treated groups (5.0 mg/ml and 10.0 mg/ml) showed a significant decrease ($p < 0.05$) in CGU compared to the ethanol-treated control group (Figure 3) by 6 hours after HD dosing.

Vascular resistance parameters

VR was evaluated for all IPPSFs in as an indirect assessment of vascular activity. Figure 4 shows the VR profiles for all study groups. At 4 hours, all HD-treated groups demonstrated a higher VR response than did the controls and the 5.0 mg/ml concentration of HD had a higher VR than did the 10.0 mg/ml of HD. Although differences between 10.0 mg/ml HD and ethanol or 5.0 mg/ml HD treatment were not statistically significant ($p > 0.05$), VR of the 5.0 mg/ml HD was significantly greater than the ethanol controls (Figure 4).

Morphological parameters

Morphological findings, including macroscopic and microscopic changes, were examined and are summarized in Table I. Macroscopically, approximately 30% of the HD-treated IPPSFs demonstrated the formation of gross visible blisters. One out of six IPPSFs treated with 5.0 mg/ml of HD developed macroscopic blisters, while three out of six developed gross blisters with the 10.0 mg/ml of HD. In general, blisters on the dosing surface started as small vesicles at 6 hours after dosing and then coalesced into larger bullae by the end of perfusion. These bullae were filled with a clear fluid that often resulted in a marked elevation of the skin surface. However, LM observation of the H&E stained sections showed that microvesicles occurred in 100% of the HD-treated IPPSFs. All of these

microvesicles were localized at the EDJ (Figures 5 and 6). In addition, lymphocyte infiltration, pyknotic basal cells, and intracellular and intercellular epidermal edema were noted at both the 5.0 mg/ml and 10.0 mg/ml of HD. Neither macroscopic nor microscopic lesions were found in the ethanol control flaps (Figure 7).

Prostaglandin parameters

The venous concentrations of PGE_2 and $PGF_{2\alpha}$ for all HD treatments and for the ethanol controls are shown in Figures 8 and 9. In the ethanol-treated group, the PGE_2 level did not increase during the perfusion time, except at 6 hours where it continued to increase until 8 hours. However, the 5.0 mg/ml of HD demonstrated a significant increase ($p< 0.05$) of PGE_2 release at 6 hours after dosing and continued to increase until 8 hours. Interestingly, PGE_2 was unaffected in the flaps treated with the 10.0 mg/ml (Figure 8). Similarly, we did not find any significant changes of $PGF_{2\alpha}$ levels in the ethanol or 10.0 mg/ml of HD-treated groups. However, the 5.0 mg/ml of HD caused the highest increase in $PGF_{2\alpha}$ by 6 hours (Figure 9).

Table I. Frequency of Macroscopic and Microscopic Blisters in HD -Treated IPPSFs.

Treatment	Macroscopic	Microscopic
ethanol	0/7	0/7
5.0 mg/ml	1/6	6/6
10.0 mg/ml	3/6	6/6

Discussion

Sulfur mustard is a highly reactive electrophilic molecule, and reacts with DNA, RNA, protein and other biological macromolecules. As a result, HD interferes with a variety of critical biochemical processes (Boursnell, 1951; Levy, 1946; Singer, 1975; Fox and Scott, 1980; Smith et al., 1992). Many studies have demonstrated that HD damages vital cellular organelles and membranes (Ray et al., 1990). In this regard, HD has been shown to cause degeneration of mitochondria which can lead to inhibition of cellular metabolism and energy production. Also, HD has been shown to disrupt the intracellular calcium homeostasis and release of proteinases, leading to cellular injury (Orrenius and Nicotera, 1987; Nicotera et al. 1989; Higuchi et al., 1988).

In HD-induced cutaneous toxicity studies, most of the traditional in vitro models only provide information of HD toxicity affecting the epidermal cells, with no reports of gross blisters occurring in any of the in vitro models. A few reports of blister formation have been made in in vivo studies with HD (Mitcheltree et al., 1989; Wade et al., 1989; Marlow et al., 1990; Petrali et al., 1990). The IPPSF has been shown to be a useful model for studying cutaneous toxicity because it maintains a viable dermal structure identical to that of the human and simultaneously provides information on the biochemical, vascular, and morphological changes; therefore, it is possible to analyze the relationship of these responses over a time course. In addition, our model is the only in vitro model that has successfully produced gross blisters. In this study, all HD-treated flaps developed microvesicles and/or blisters which followed a concentration-dependent response. Further, these morphological alterations were all located at the EDJ, consistent with that of human skin exposed to HD (Ginzler and Davis, 1943; Momeni et al., 1992; Requena et al., 1988). Our previous transmission electron microscopy studies of the mustard analog 2-chloroethyl methyl sulfide (CEMS) (King and Monteiro-Riviere, 1990), HD and lewisite (L) (Monteiro-Riviere et al., 1990) also revealed

these morphological changes, including separation of the EDJ. Hence, it is possible that HD causes vesication by directly altering several proteins within the basement membrane, a hypothesis that is addressed in the next section of this report.

Previous IPPSF studies have evaluated glucose utilization (CGU) as a measure of flap viability and alterations in cutaneous metabolism (Riviere et al., 1986). In this study, the CGU decreased in all IPPSFs treated with HD. This could indicate that HD is a metabolic inhibitor affecting cell viability. Other IPPSF studies have demonstrated a decrease in glucose utilization in flaps treated with L (Monteiro-Riviere, 1990), a potent organic arsenical, and with CEMS (King and Monteiro-Riviere, 1990). A decrease in CGU was correlated to the degeneration of the mitochondria, site of the citric acid cycle, based on the time-course studies (King and Monteiro-Riviere, 1990; King et al., 1992). Detriment of the glucose metabolism pathways was proposed as a mechanism of HD-induced cytotoxicity by other groups (Dixon and Needham, 1946; Holzer, 1964). Therefore, these effects may contribute to the change of CGU caused by HD.

On exposure to HD, rapid fluid transudation from capillaries and resulting edema are prominent features in both human and animal studies (see final section of this report for vascular volume studies). Some studies have demonstrated that HD can release certain vasoactive substances (e.g., prostaglandins) and cause an increase in proteinases after HD exposure (Rudin, 1953; Rikimaru et al., 1991). These factors could affect the vascular permeability and vascular tone. VR was used in this study to measure the potential activity of the cutaneous vasculature in response to HD exposure. All IPPSFs had an increase in VR with the 5.0 mg/ml HD, resulting in a higher vascular response than the 10.0 mg/ml. It is conceivable that 10.0 mg/ml of HD may cause more severe capillary injury, and therefore inhibit the vascular response. In addition, some inflammatory mediators (e.g., PGE_2 and $PGF_{2\alpha}$) were found to alter the vascular permeability and activity. As we will discuss later, the levels of both PGE_2 and $PGF_{2\alpha}$ increased only in the 5.0 mg/ml rather than in the 10.0

mg/ml of HD. The consistency of change between these vasoactive mediators and VR after HD exposure indicates that PGE_2 and $PGF_{2\alpha}$ may be involved in the HD-induced VR change seen during this study.

Products of arachidonic acid (AA) metabolism by cyclooxygenase and lipoxygenase enzymes are known to be potent inflammatory mediators present in many skin diseases. The skin is an organ which displays a highly active metabolism of AA (Ziboh, 1992). High levels of PGE_2, $PGF_{2\alpha}$, and LTB_4 have been shown to elicit a cutaneous inflammatory reaction. Injection of these prostaglandins resulted in erythema and edema by either altering the vascular responses or by chemotaxis (Willis and Cornelson, 1973). Although the specific cell type responsible for the release of prostaglandins in the skin is uncertain, the epidermal cells and endothelial cells are likely candidates. This conclusion is based on the evidence that these cells possess an enzyme system that is needed to convert prostaglandins (Dahlen, 1987; Grabbe et al., 1985) and that lymphocytes are not present in the IPPSF perfusion media. Treatment with indomethacin, a cyclooxygenase inhibitor, prevented an increase in PGE_2 and reduced the inflammatory reaction caused by ultraviolet light (Snyder, 1975). In this study, we attempted to assess changes in AA metabolism in HD-treated IPPSFs by examining the production of PGE_2 and $PGF_{2\alpha}$ and the role of the prostaglandins in vesication. In the control group, PGE_2 levels only begin to increase at 7 hours. The 5.0 mg/ml of HD increased in both PGE_2 and $PGF_{2\alpha}$ as early as 6 hours. However, we detected no increase in PGE_2 or $PGF_{2\alpha}$ levels in the flaps treated with 10.0 mg/ml of HD when compared to the controls. Another study conducted in human skin cultures has found similar results (Rikimaru et al., 1991). Thus, this may suggest that the no effect of 10.0 mg/ml of HD on the production of PGE_2 and $PGF_{2\alpha}$ is due to the concentration of HD rather than to imperfections in our model. Studies in our laboratory have shown no changes in LTB_4, major lipoxygenase metabolite in the skin, after HD treatment (unpublished studies). It appears unlikely that 10.0 mg/ml of HD switches the AA metabolism from cyclooxygenase to

lipoxygenase pathway. Thus, it is reasonable to postulate that 10.0 mg/ml concentration of HD either inhibits both AA metabolism enzymes, produces other factor(s), or causes cell death, which prevents PGE_2 and $PGF_{2\alpha}$ release. Further studies need to be conducted.

II. ASSESSMENT OF DIRECT HD INTERACTION WITH BASEMENT MEMBRANE COMPONENTS

Introduction

Bis-2-chloroethyl sulfide (sulfur mustard, HD) is a bifunctional agent that is highly reactive with many biological macromolecules, especially those containing nucleophilic groups such as the thiol group, and it is known for its severe cutaneous damage, as well as systemic toxicity. The HD-induced dermal lesion is characterized by vesication and slow wound healing (Papirmeister et al., 1991). Our laboratory has shown that epidermal-dermal separation occurs at the lamina lucida of the cutaneous basement membrane in HD-induced dermal injury (Monteiro-Riviere et al., 1991; Monteiro-Riviere and Inman, 1992). In spite of extensive research, there have been no published studies presenting a clear and underlying mechanism for HD-induced toxicity to the basement membrane.

During the past decade, considerable information has accumulated regarding tne cutaneous basement membrane (Timpl, 1989). Ultrastructurally, the basement membrane consists of hemidesmosomes, the lamina lucida, lamina densa, and the subbasal lamina. Anchoring filaments, anchoring fibrils, and microfibril bundles further stabilizes the EDJ. From a biochemical standpoint, the basement membrane zone and attendant anchoring structures are composed of collagen, proteoglycans, and noncollagenous glycoproteins. It has been well-documented that not only does the basement membrane provide a mechanical support of epidermal-dermal interaction but it can also influence cell behavior and wound healing (Paulsson, 1992; Burgeson, 1993). Further, defects of the basement membrane components, evident in many of the inherited and autoimmune blister diseases (Fine, 1991), may play a role in weakening the basement membrane in the process of vesication. However, little research has been performed on the chemical interaction with the vesicant HD.

The purpose of this study was to examine the potential role of laminin, a key thiol-rich protein in the basement membrane, as a molecular target for alkylation by HD in the formation of HD-induced epidermal-dermal separation and in resultant slow wound healing. This was accomplished by examining the effect of HD treatment on the cell adhesive activity of laminin.

Materials and Methods

Biosynthetic labeling of human UM-UC-9 bladder carcinoma cells

Proliferating human UM-UC-9 bladder carcinoma cells were cultivated in Dulbecco's modified Eagle's medium containing D-glucose (4500 mg/liter) and supplemented with 10% FBS (Gibco BRL, Gaithersburg, MD). They were maintained in an atmosphere of 95% air, 5% CO_2, at 37°C, with fresh growth medium added every 2-3 days.

Cultures near confluence were biosynthetically labeled with L-^{35}S-cysteine (1113 Ci/mmol) (ICN Biochemical, Costa Mesa, CA). The cells were preincubated in serum-free, cysteine-free, methionine-free Dulbecco's modified Eagle's medium for 30 minutes prior to labeling. Then, the UM-UC-9 cells were labeled with 100 μCi/ml of ^{35}S-cysteine in the cysteine-free medium (5 ml/flask). After a 4-hour labeling incubation, the labeling medium was removed and replaced with complete growth medium for chase incubation intervals up to 20 hours. The medium was collected and the cells harvested by lysis with 5 ml/flask of cold (4°C) phosphate buffered saline (PBS) containing 1% Triton X-100, 0.5% sodium deoxycholate, and 0.1% sodium dodecyl sulfate (PBS-TDS). Flasks were scraped to remove adherent cellular remnants and the extracellular matrix. The harvested medium was clarified of any cellular debris by centrifugation at 350 X g for 5 minutes and then adjusted to the same concentration of PBS-TDS as the cell lysate by adding 1/4 volume of a fivefold concentrated solution. The cell lysate and chase media were frozen at -70°C overnight. The cell lysate was

thawed, clarified by centrifugation at 100,000 X g for 60 minutes, and then submitted to immunoprecipitation with antibody against laminin.

Immunoprecipitation of UM-UC-9 laminin

Both the medium and cell lysate were first incubated with 160 μl/ml sample of gelatin S4B suspension overnight at 4°C. This served as a clearing round to remove fibronectin and diminish nonspecific immunoprecipitation in subsequent rounds. Once cleared of fibronectin, the medium and cell lysate were immunoprecipitated with rabbit antiserum against murine Englebreth-Holm-Swarm (EHS) sarcoma laminin obtained commercially (Gibco BRL, Gaithersburg, MD) tumor laminin. One microliter of anti-laminin antibody per milliliter of the medium was used to immunoprecipitate laminin. Recovery of the resulting immune complexes was accomplished by adsorption to protein A-Sepharose (Sigma, St. Louis, MO; 20 μl packed beads/μl antiserum used for immunoprecipitation). The resulting protein A-Sepharose pellets were washed three times with PBS-TDS for sodium dodecyl sulfate-polyacrylamide gel electrophoresis (SDS-PAGE).

Incubation of laminin with HD

UM-UC-9 laminin immunoprecipitate adsorbed to protein A-Sepharose (40 μl/ml of packed beads) was suspended in 200 μl of 50 mM Tris buffer (pH 7.4) and was incubated at room temperature for 2 hours with 10.0 μl of ethanol (ETOH), 1.0 mg/ml, or 10.0 mg/ml HD in ETOH, respectively. In addition, 0.5 mg of murine EHS tumor laminin was treated with 25 μl of 10.0 mg/ml ^{14}C-HD or ETOH under the same conditions described above.

Gel filtration was carried out to separate HD-alkylated EHS laminin using a Sephadex G-10 column (31 cm X 1 cm). The reaction solution was eluted with isocratic mobile phase consisting of 0.15 M sodium chloride, and 0.01 M Tris-chloride (pH 7.4). Five-minute (1 ml) fractions of the eluent were collected. ^{3}H-EHS laminin (NEN) standard was eluted at 30-35 minutes, as was a nonradioactive EHS laminin detected by UV absorbance at 274 nm.

Unconjugated ^{14}C-HD standard was eluted at 55-60 minutes. Thus, the G-10 column effectively separated unreacted HD from the HD-laminin adduct.

Nonreduced and reduced SDS-PAGE

These treated laminins were fractionated by both nonreduced and reduced SDS-PAGE using vertical slab gels (3-10% polyacrylamide gradient with a 3% stacking gel) in the Laemmli buffer system. Prior to fractionation, the samples were boiled for 5 minutes in an equal volume of two-fold concentrated Laemmli sample buffer either with or without 2-mercaptoethanol (2%) to reduce disulfide bonds. Gels were fixed, dried, and exposed to X-ray film to visualize radioactive bands.

Coating of culture dishes and cell adhesion assay

Falcon 1029 bacteriological culture dishes were coated with 5.0 ml of PBS, 10.0 μg/ml of EHS laminin, and 1.0, 3.0, and 10.0 μg/ml of HD-alkylated laminin in PBS for 2 hours at 4°C.

A suspension of UM-UC-9 cells was prepared by trypsinization of a flask of confluent cells with 0.05% trypsin and 0.02% EDTA in PBS. The trypsin was quenched by adding 5.0 ml of serum, and the cells were suspended in Dulbecco's modified Eagle's medium. The cells were plated onto the laminin-coated dishes at a density of 7 X 10^5/ml. After a 20-hour incubation at 37°C, nonadherent cells were removed with two 10.0-ml PBS washes. Adherent cells were detached with trypsin and counted in a hemacytometer.

Results

Chemical modification of laminin by HD

In order to determine if HD alkylates laminin, ^{35}S-cysteine-labeled UM-UC-9 laminin immunoprecipitates were treated either with HD in ethanol (1.0 mg/ml, or 10.0 mg/ml) or with ethanol alone as a control. Analysis of these treated laminins by nonreduced SDS-PAGE or reduced SDS-PAGE is shown in Figures 10 and 11. Both control and the HD-treated UM-UC-9 laminin migrated similarly on nonreduced SDS gels as one 900-kDa band corresponding to undissociated A.B1.B2. laminin trimer. On reduced SDS gels, laminin not treated with HD showed the typical profile of dissociated A and B chains at 400 kDa and 200 kDa. In contrast, HD-treated UM-UC-9 laminin exhibited two new higher molecular weight bands on reduced SDS gels at 900 kDa and 600 kDa. These two new bands correspond to undissociated laminin trimer and a partially dissociated laminin form. The intensity of these bands was greater with the higher concentration of HD in the reaction mixture.

In a similar manner, EHS laminin was incubated with ^{14}C-HD (10.0 mg/ml). Figure 12 reveals the profile of HD-treated EHS laminin on reduced SDS-PAGE. The HD treatment of laminin from this source also caused the appearance of a new predominant band of cross-linked laminin at 900 kDa on the reduced SDS gel. In addition, two radioactive bands of lower intensity corresponding to native EHS laminin subunits at 400 kDa and 200 kDa were also visible on the reduced gel. These results suggest that HD covalently binds laminin subunits in part by cross-linking and that cross-linking of HD is concentration-dependent.

Cell adhesion to HD-alkylated laminin

EHS laminin treated by HD was purified from a Sephadex column and used to coat the cell culture dishes to examine the effect of HD on its ability to promote cell adhesion. SDS-PAGE was conducted to prove that the eluted laminin was alkylated by HD. As shown in Figures 13 and 14, 10.0 μg/ml of untreated laminin increased the number of UM-UC-9 cells

adherent to the dish, whereas 1.0, 3.0, and 10.0 μg/ml of HD-alkylated laminin significantly inhibited cell adhesion and appeared to cause cell disaggregation in a concentration-dependent manner. When cells were plated and allowed to attach to the tissue culture flask in the usual manner for 24 hours and UM-UC-9 cells were exposed to HD-alkylated laminin, neither cytotoxicity nor cell detachment were observed. Also, the cells showed the adhesive response to 10.0 μg/ml of laminin in the presence of 3.0 μg/ml HD-alkylated laminin, which indicated that the effect of HD-alkylated laminin on cell adhesion was not a cytotoxic effect.

Discussion

The experiments described a one-step approach in testing the hypothesis that HD decreases epidermal-dermal adhesion by alkylating laminin, a key adhesive thiol-rich glycoprotein located at the site of epidermal-dermal separation on HD-induced blisters. HD is a highly toxic bifunctional alkylating agent with well-described vesicant properties in the skin. However, the mechanism of HD cutaneous toxicity has not been clearly represented. Although HD has long been known to react with a variety of other biomolecules, alkylation of DNA by HD was traditionally described to be responsible for its cytotoxicity. Recently, studies suggest that the genotoxicity of HD may not play a crucial role in the acute cutaneous HD injury (Papirmeister, 1993). Tissue injury requires a higher dose than does genotoxicity, takes less time to develop, and is not dependent on DNA cross-links. Our previous studies have shown that all HD-induced vesications were exclusively localized at the lamina lucida of the cutaneous basement membrane. Further, blisters and dark basal cells develop as early as 5 hours after HD exposure in our IPPSF model (Monteiro-Riviere et al., 1991; Monteiro-Riviere and Inman, 1992). This raises the possibility of a direct chemical modification of proteins in the basement membrane by HD, leading to diminished stability of the EDJ in the process of its dermal toxicity and vesication.

The basement membrane zone is a complex structure composed of a variety of molecular components bridging the epidermis and dermis, and represents a major site of pathological changes associated with blister diseases. A number of the basement membrane components have been identified. Defects in basement membrane zone components have been associated with autoimmune blister disease, thus suggesting their role in the process of vesication. Among those components, laminin, a major glycoprotein in the basement membrane, has been studied extensively (Schittny et al., 1988; Steele et al., 1990). Cysteine-rich laminin is a multidomain protein made of three disulfide-linked polypeptide chains designated as an A chain with a molecular weight of 400 kDa and two B chains of 210 kDa (B1) and 200 kDa (B2). Our previous study has shown that 30% of the thiol group in laminin is available for alkylation (King et al., 1994). As mentioned above, immunohistochemical mapping of HD-induced vesication has been accomplished in our laboratory and shows that the epidermal-dermal separation is exclusively localized to the lamina lucida, just above the level of the prominent staining for laminin (Monteiro-Riviere and Inman, 1992; Monteiro-Riviere et al., 1993). Thus, it is plausible that thiol-rich laminin is a target for HD action and leads to blister formation.

This study evaluated HD alkylation of laminin by incubation of radiolabeled laminin from UM-UC-9 cell with HD. Native laminin trimer is dissociated under reduced conditions because of the breakage of intersubunit disulfide bonds. However, after HD treatment, two new bands at 900 kDa and 600 kDa were identified on the reduced gel. The 900-kDa band migrates on the gel like undissociated laminin (A.B1.B2.) trimer. The 600-kDa band migrates on the gel like a partially dissociated A.B laminin form as we have previously observed in partially reduced laminin preparations (King et al., 1994). In addition, murine laminin from the EHS tumor was treated with ^{14}C-HD in a similar manner. Radioactive bands labeled with ^{14}C-HD were visible at the positions of laminin trimer (900 kDa) and the dissociated A and B chains (400 and 200 kDa). These results suggest that HD covalently binds and cross-links

laminin chains. This is consistent with the idea that laminin is one of the basement membrane components at the EDJ that is reactive with HD.

Laminin has a well-defined role in maintaining epidermal-dermal interaction. In addition, recent studies show that laminin is implicated in the regulation of cell differentiation and migration (Kleinman et al., 1985; Sakashiti et al., 1980; Goodman et al., 1989). Further, laminin is one of the earliest detectable proteins appearing at the wound site (Fine et al., 1987), suggesting a functional role of laminin in tissue repair. So far, several functional domains of laminin, such as cell binding sites and epidermal growth factor-like regions have been determined and sequenced. Not surprisingly, some of these domains are composed of cysteine-repeats (Sasaki et al., 1987; Sasaki and Yamada, 1987; Sasaki et al., 1988; Hartl et al., 1988). Thus, it is likely that HD may destroy the biological functions of laminin by alkylating these domains.

The adhesion and spreading of cells to the basement membrane seem to be a multistep process that requires the recognition of those components by specific receptors. The interaction between cells and laminin is not completely understood. However, several integrins have been suggested as laminin receptors (Mercurio, 1990; Bouzon et al., 1990). These receptors may neither recognize nor respond to the laminin modified by HD or other chemicals. Further, HD-alkylated laminin may also function as a receptor blocker preventing cell-cell and/or cell-matrix interaction. Our cell adhesive assay shows that HD-alkylated laminin inhibits cell adhesion without any signs of cytotoxicity, whereas laminin enhances cell adhesion. Further, normal laminin restores cell adhesive activity in the presence of HD-alkylated laminin, which opens the possibility of HD-alkylated laminin as an antagonist for competition of laminin binding and alteration of cell adhesion. This binding has significant clinical implications in the pathogenesis of the slowly healing HD lesions.

In conclusion, we find that alkylation of laminin and possibly other basement membrane components may play a role in HD-induced vesication, and this results in the

delayed wound-healing characteristic of HD vesication. Our study provides a new hypothesis regarding the mechanism of cutaneous toxicity caused by HD and other chemical vesicants. Because of the biological diversity of different cell types, similar studies need to be accomplished on cultured human keratinocytes. In addition, further investigations will be performed to localize the HD-alkylated domains within the laminin molecule, and to identify other basement membrane molecules as potential targets for HD alkylation.

III. THE HISTOCHEMICAL AND ULTRACTRUCTURAL DISTRIBUTION OF LAMININ, TYPE IV COLLAGEN, BULLOUS PEMPHIGOID, EPIDERMOLYSIS BULLOSA ACQUISITA , FIBRONECTIN, AND MONOCLONAL GB3 ANTIBODIES IN THE HD-TREATED ISOLATED PERFUSED PORCINE SKIN FLAP.

Introduction

Porcine skin is similar morphologically (Montagna Yun, 1964; Meyer et al., 1978; Monteiro-Riviere and Stromberg, 1985; Monteiro-Riviere, 1986) and histochemically (Meyer et al., 1986; Woolina et al., 1991; Rigal et al., 1991) to human skin and has been touted as a model for the study of percutaneous absorption and toxicity (Bartek et al., 1972; Reifenrath et al., 1984). The isolated perfused porcine skin flap (IPPSF), an alternative in vitro model, is similar to human skin morphologically (Monteiro-Riviere et al., 1987), and correlates well to in vitro (Carver et al., 1989; Williams et al., 1990) and human absorption studies (Riviere and Monteiro-Riviere, 1991). The in vivo and in vitro models employed to study vesicant exposure either lack the structural and functional similarities to human skin or fail to produce gross blisters. Micheltree et al. (1989) showed that HD and lewisite (L) cutaneous exposure to pigs resulted in microvesicle formation. Studies utilizing other in vivo models, such as rabbit, guinea pig, hairless guinea pig, and human skin graft/nude mouse model (Marlow et al., 1990; Vogt et al., 1984; Petrali et al., 1990; Wade et al., 1989; Papirmeister et al., 1984a,b) have reported similar results. The IPPSF does produce gross blisters in response to 2-chloroethyl methyl sulfide (King and Monteiro-Riviere, 1990) and to HD (Monteiro-Riviere et al., 1991) and L (King et al., 1991).

The effects of cutaneous exposure of HD and L on EDJ antigens has been briefly explored (Monteiro-Riviere et al., 1991; King et al., 1991; Monteiro-Riviere and Inman, 1993). Therefore, the primary objective of this study is to (1) determine the presence of laminin, type IV collagen, bullous pemphigoid antibody (BPA), epidermolysis bullosa acquisita antibody (EBA), fibronectin, and GB3 antibodies in the IPPSF, (2) determine the

integrity of HD on these epitopes in the IPPSF, and (3) determine the EDJ cleavage plane within the blister of the HD-treated IPPSFs.

Materials and Methods

Creation and perfusion of the IPPSF was previously described in detail in Section I. All flaps were dosed with 300 µl of ethanol or HD within a 7.5 cm^2 Stomahesive (ConvaTec-Squibb, Princeton, NJ) dosing template using a Microman positive displacement pipette (Gilson Medical Electronics S.A., France). Flaps were perfused for 8 hours with 5.0 mg/ml of HD, 10.0 mg/ml of HD (n= 6/treatment) or ethanol (n=7). See Section I for more details.

Following flap perfusion, frozen tissue samples were taken from the dosed area for immunohistochemistry (IH), immunofluorescence (IF), and immunoelectron microscopy (IEM). Samples were oriented in an aluminum foil boat, quenched in isopentane well immersed in liquid nitrogen and embedded in OCT Compound (Tissue-Tek, Miles Inc., Elkhart, IN). For this study, indirect IH, indirect IF, indirect IEM were performed on the IPPSFs using laminin (polyclonal rabbit anti-mouse EHS tumor), type IV collagen (polyclonal rabbit anti-mouse EHS tumor), human BPA (IgG titer >1:2560), human EBA (IgG titer of 1:320), fibronectin (polyclonal rabbit anti-human), and monoclonal GB3 antibody. Additional human monoclonal antibodies L3d and 19-DEJ-1 did not cross-react to the porcine basement membrane epitopes and therefore no attempt was made to further characterize them. Indirect IH was carried out using routine biotin/streptavidin methodology. Cryosections (8 µm) were cut on a cryostat (Histostat, AO Reichert Scientific Instruments, Buffalo, NY), mounted on poly-l-lysine-coated slides, and air-dried. The sections were incubated in 3% hydrogen peroxide and rinsed in 0.1M PBS (pH 7.6). The tissue was then incubated in normal goat serum, followed by the primary antibody (laminin, type IV collagen, BPA, EBA, fibronectin

and GB3) or the control (normal rabbit or normal human serum). Biotinylated IgG conjugate (anti-rabbit or anti-human) (Boehringer-Mannheim Biochemica) was applied followed by an incubation in the streptavidin-peroxidase conjugate label (Boehringer-Mannheim Biochemica). Sections were then fixed in formol saline and the reaction product developed in the substrate diaminobenzidine (DAB) (Polysciences Inc., Warrington, PA). The tissue was dehydrated through a graded ethanol series, cleared, mounted in Permount^{R}, and screened with an Olympus PM 10-ADS bright field light microscope (Olympus Optical, Ltd., Tokyo, Japan).

For indirect IF, cryosections (8 μm) were incubated in the primary antibody (GB3) or the control serum followed by the secondary antibody (fluorescein isothiocyanate) [FITC] labeled goat anti-rabbit IgG). Sections were mounted in a glycerol mounting medium and viewed on a Zeiss IM 35 inverted light microscope equipped with epifluorescence (Carl Zeiss, Inc., West Germany).

Indirect IEM was performed using a modification of the method described by Yaoita et al. (1976). Cryosections (20 μm) were mounted on chrome alum slides, air-dried and incubated in normal goat serum. The sections were incubated with the primary antibody or the control. The secondary antibody (goat anti-rabbit IgG (Sigma Chemical Co., St. Louis, MO) or biotinylated goat anti-human IgG) was applied to the sections and followed by an incubation of the tertiary antibody (rabbit peroxidase antiperoxidase complex (Sigma Chemical Co.) or streptavidin-peroxidase conjugate label). The sections were fixed in half-strength Karnovsky's fixative (Monteiro-Riviere et al., 1987) at 4°C and the reaction product developed in DAB. The tissue was postfixed in 1% osmium tetroxide, dehydrated through graded ethanols, cleared in propylene oxide, and infiltrated in Poly/Bed 812 (Polysciences, Inc., Warrington, PA). Each section was topped with resin and polymerized overnight at 60°C. Tissue sections (600-900Å) were cut on a Reichert Ultracut E ultramicrotome (Leica, Nussloch, Germany) and mounted on 200-mesh copper grids. Unstained sections were

evaluated and photographed on a Philips EM 410 transmission electron microscope (Philips Electronics, Mahwah, N.J.).

Results

Indirect IH and IF

Light microscopic observations of antibody binding are summarized below.

Laminin:

The laminin antibody identically stained both the ethanol- and the nonblistered HD-treated IPPSFs with a continuous band at the EDJ and along the capillary basement membrane (Figure 15). In the blistered areas of HD-treated flaps, laminin stained the dermal side (blister floor), with fragmented staining at the basal pole of the stratum basale cells (blister roof) (Figure 16). Staining of the dermis was more intense in the blistered areas than in the adjacent nonblistered areas.

Type IV Collagen:

Type IV collagen stained the EDJ and capillary basement membranes of all the ethanol and HD-treated IPPSFs in a pattern similar to that of laminin (Figure 17). In all the HD-treated blistered IPPSFs, staining was limited exclusively to the dermis and appeared more intense than the adjacent nonblistered areas (Figure 18).

Bullous Pemphigoid:

BPA, localized within the hemidesmosomes, exhibited a continuous staining of the EDJ in all the ethanol- and HD-treated IPPSFs (Figure 19). The antibody staining of the blistered areas was limited to the basal pole of the stratum basale cells (Figure 20).

Epidermolysis Bullosa Acquisita:

EBA stained a continuous linear band along the EDJ in all the ethanol- and HD-treated IPPSFs (Figure 21). In the blistered areas of the HD-treated flaps, the antibody was bound to the dermis (Figure 22).

Fibronectin:

Fibronectin, which binds to the lamina lucida region of the EDJ, stained a continuous faint linear band in all of the ethanol- and HD-treated flaps (Figure 23). In blistered areas of the HD-treated IPPSFs, the staining was localized primarily to the dermis, with fragmented staining of the basal pole of the stratum basale cells (Figure 24).

GB3:

The GB3 monoclonal antibody bound to the EDJ to stain a prominent continuous band in all of the ethanol- and HD-treated IPPSFs (Figure 25). In blistered areas, the staining was localized to the dermal surface (Figure 26).

Normal serum controls (rabbit or human) paired with the antibodies in all the ethanol- and HD-treated IPPSFs revealed no specific staining within the EDJ or capillary basement membrane.

Indirect IEM

Ultrastructural observations of antibody binding are described below and summarized in Table II.

Laminin:

Antibody binding in all of the ethanol- and HD-treated IPPSFs exhibited a well-defined staining pattern within the lamina lucida of the EDJ (Figure 27) and around the dermal vasculature. In flaps with HD-induced blisters, staining occurred predominantly on the dermal interface (blister floor), with fragmented staining on the basal pole of the stratum basale cells (blister roof) (Figure 28).

Type IV Collagen:

Type IV collagen bound to the lamina densa in all of the ethanol- and HD-treated IPPSF's in a discrete, linearly continuous band (Figure 29). Antibody localization in the blistered areas was limited to the dermal side of the split (Figure 30).

Bullous Pemphigoid:

BPA was bound to the hemidesmosomes in most of the ethanol- and HD-treated flaps in a diffuse broken pattern along the EDJ. In the blistered areas of HD-treated flaps, focal staining of the hemidesmosomes was diffuse and localized to the basal pole of the stratum basale cells.

Epidermolysis Bullosa Acquisita:

EBA bound to the EDJ of all the ethanol- and HD-treated IPPSFs, but the cross-reactivity was very low. Therefore, the antibody staining has not been fully characterized.

Fibronectin:

The cross-reactivity of this antibody was low, but preliminary staining did show a very discrete band along the EDJ.

GB3:

This antibody has not been completely characterized by indirect immunoelectron microscopy due to low cross-reactivity to the EDJ of the IPPSF.

Control sera (normal rabbit or normal human) for all of the antibodies produced no staining in the ethanol- and HD-treated IPPSFs.

Table II. Indirect Immunoelectron Microscopic Mapping of Basement Membrane Epitopes in HD-Induced Blisters in the IPPSF.

Antigen	Localization	Blister Floor	Blister Roof	Capillary
Laminin	lamina lucida	continuous (+++)	fragmented	+++[1]
Type IV Collagen	lamina densa	continuous (+++)	–	+++[1]
BPA	hemidesmosomes	–	discontinuous (++)	–
EBA	lamina densa	continuous (+)	–	–
Fibronectin	lamina lucida	continuous (+)	fragmented	–
GB3	lamina densa	continuous[2] (+)	–	–
L3d	*	*	*	*
19-DEJ-1	*	*	*	*

1 Stained capillary basement membrane.
2 Characterized by immunohistochemistry due to poor reactivity.
(+++) = intense staining; (++) = moderate staining; (+) = light staining
* No antibody cross-reactivity with the IPPSF

Discussion

The EDJ of porcine skin has been described to be ultrastructurally similar to that of humans (Monteiro-Riviere and Stromberg, 1985; Monteiro-Riviere, 1986). Ultrastructural evaluation reveals that the EDJ consists of the basal cell membrane of basal cells (which includes the hemidesmosomes), the lamina lucida, the lamina densa (basal lamina), and the subbasal lamina. The antibodies chosen for this study bind to different epitopes, and therefore to different sites within the EDJ. Our HD-treated IPPSF had severe cutaneous injury in which epidermal-dermal separation occurred at the lamina lucida area. Only by performing indirect immunoelectron microscopy could we discern the specific localization of the blister cleavage plane. Foidart et al. (1980) originally reported that laminin was located within the lamina lucida of human skin. Other studies suggest laminin was found primarily (Fleischmajer et al., 1985) or exclusively (Laurie et al., 1982) within the lamina densa. It is now believed that the laminin molecule spans at least a portion of both layers (Briggaman, 1990; Horiguchi et al., 1991). Type IV collagen, the major structural protein of the EDJ (Briggaman, 1983), is localized within the lamina densa. The BP epitope is spatially associated with the hemidesmosomes of the cell membrane, although a portion of the molecule is possibly found within the lamina lucida (Fine, 1991). Woodley et al. (1984) defined the EBA epitope from autoantibodies in the sera of EBA patients and localized the antigen to the lamina densa of the human basement membrane. Fibronectin, a macromolecule that may not be a true component of the basement membrane (Clark, 1983), also has been demonstrated in the lamina lucida of fetal rodent skin and in the upper papillary dermis and around the vasculature in adult human skin. The monoclonal antibody GB3 was raised against human amnion and reacts with the basement membrane, binding specifically to the lamina lucida (probably associated with hemidesmosomes) and the lamina densa (Verrando et al., 1987).

The EDJ of normal pig skin has been found to be antigenically similar to that of normal human skin. Stanley et al. (1981) reported that laminin, type IV collagen, and BPA bound to the EDJ of normal skin of weanling Yorkshire pigs. Also, porcine skin has been found to exhibit a high degree of cross-reactivity to murine laminin and to human type IV collagen and BPA (Rigal et al., 1991).

In this study, immunohistochemical staining has proven that antibodies to laminin, type IV collagen, BP, EBA, fibronectin and GB3 cross-react with EDJ epitopes in the IPPSF. Immunoelectron microscopy has shown the staining patterns to be similar, though usually more diffuse in the IPPSF. Since the DAB substrate is insoluble in water and presumably binds to the cellular proteins, the EDJ antigens may actually diffuse slightly during perfusion of the IPPSF.

HD, its analog CEMS, and L caused the formation of macroscopic (gross) blisters and microscopic vesicles which caused basement membrane separation similar to that described in human skin exposed to HD (Monteiro-Riviere et al., 1991; Monteiro-Riviere, 1992; King et al., 1992; Monteiro-Riviere and Inman, 1992). Immunohistochemistry of blistered and nonblistered skin from the dose site of the IPPSF has revealed moderate to strong staining of these antibodies. Epitope mapping of the blistered skin has demarcated the cleavage plane within the laminin and fibronectin, above the type IV collagen, EBA and GB3 and below the bullous pemphigoid (BP) antigenic sites.

Immunoelectron microscopy precisely defined the plane of epidermal-dermal cleavage. The laminin and fibronectin antibodies bound primarily to the dermis with fragmented areas of attachment to the basal pole of the stratum basale cells. Woodley et al. (1983) found laminin bound in this same pattern using immunofluorescence in split human skin. This indicates that the cleavage plane in the HD-treated IPPSFs is localized in the upper portion of the lamina lucida. Type IV collagen, EBA and GB3 bind to the lamina densa and exclusively

stain the dermal (blister floor) surface. Since BPA bound to hemidesmosomes, staining remained with the epidermis.

In conclusion, antibodies to laminin, type IV collagen, BPA, EBA, fibronectin, and GB3 all appear to similarly bind the EDJ of ethanol-treated and HD-treated IPPSFs . The EDJ cleavage plane of the blistered HD-treated IPPSFs was identical to that found in both experimental (suction, sodium chloride, heat shock, EDTA, various proteases) and diseased (junctional epidermolysis bullosa, autoimmune bullous diseases) states.

IV. FORMULATION OF A TOXICOKINETIC MODEL OF HD ABSORPTION IN THE ISOLATED PERFUSED PORCINE SKIN FLAP

Introduction

The purpose of this section of the report is to characterize the dermatopharmacokinetic profile of topically applied HD in the IPPSF. There are four major components to this task which would culminate in a toxicokinetic-toxicodynamic (TK-TD) model of HD action in the IPPSF. These are (1) formulation of the dermatopharmacokinetic model based on an analysis of individual skin flap data, (2) definition of the proper physiologic end points of HD effect in the IPPSF, (3) definition of the biotransformation profile of HD, and (4) coupling of all of these data into a comprehensive TK-TD model. This report will present the individual IPPSF dermatopharmacokinetic model analyses proposed in (1) and some aspects of (2) related to inulin/albumin physiological space studies. The previously presented physiological studies of prostaglandin efflux in this report should also be consulted since this data will ultimately be integrated into the model. Component (3) is presently being conducted using gas chromatography and mass spectrometry to characterize the nature of the HD-related radiolabel presented in this report. Component (4) cannot be attempted until all three earlier components are completed. All individual IPPSF modeling experiments will then be combined into a single model during this phase.

Materials and Methods

General: All IPPSF experiments were conducted as previously described in this report. There were essentially two parts to this study, the radiolabeled HD penetration and the inulin/albumin infusion studies.

Phase 1: Mustard Penetration Study

Nine IPPSFs were used in the study. Following a 1-hour predosing period, the first six skin flaps were perfused for 8 hours, the last three for 4 hours. All nine flaps received a 300 µl dose of 10.0 mg/ml ^{14}C-labeled HD (.56 mCi/mol) in ethanol which was obtained from the U.S. Army Medical Research and Development Command. Total dose for each flap was 10 µCi in the 1.25 cm X 6 cm (7.5 cm^2) Stomahesive template. The templates were secured to the skin flaps using Skin-Bond (Pfizer Hospital, Inc., Largo FL).

Sampling for all nine skin flap experiments was the same. Venous efflux samples were taken at 5, 10, 20, 30, 45, 60, 75, 90, 105, and 120 minutes, and then every 30 minutes for either 4 or 8 hours to determine the absorption profiles. At termination, several steps were taken to determine location and mass balance of the labeled compound. The Stomahesive template used to demarcate the dosing area was removed and soaked in a known volume of ethanol for subsequent radioanalysis. The dose area was swabbed twice with a soap solution and gauze and then tape-stripped 12 times with cellophane tape. The underside of the skin flap was rinsed to remove label that had collected over the 4- or 8-hour perfusion period. The skin flap cradle was rinsed twice and all the rinses were retained. The dose site was dissected from the skin flap with a razor blade and a 1 cm X 1 cm core sample was removed from the center of the dose area and snap-frozen for the penetration study. The remainder of the dose site was retained. The skin under the Stomahesive template was dissected with a razor blade and separated from the subcutaneous fat after snap-freezing in liquid nitrogen. All the tissue samples (except the excised frozen core sample) and subcutaneous samples were dissolved

individually in Soluene-350 (Packard Instrument Co., Downers Grove, IL). The leaks that resulted from the dissection of the skin flap, the fingertips of the gloves, and the instruments used during dissection were cleaned and the swabs retained for analysis.

Each 1.0 cm X 1.0 cm cryostat core sample was placed epidermal side down in an aluminum foil boat embedded in Tissue-Tek OCT (Miles, Inc., Diagnostics Division, Elkhart, IN), snap-frozen in an isopentane well immersed in liquid nitrogen, and stored at -80°C until sectioned. Sectioning was performed on a Reichert-Jung Cryocut Model 1800 (Reichert Ophthalmic Instruments, Werner-Lambert Technologies, Inc., Buffalo, NY). Two 40-μm sections were combined for each sample taken from the core. Steps were taken during sampling to minimize evaporation of the radiolabeled compound.

All the above samples were assayed for radiolabel via a Packard Model 306 Tissue Oxidizer and the samples were counted on a Packard Model 1900 TR Tri-Carb Liquid Scintillation Analyzer (Packard Instrument Co., Downers Grove, IL). The individual assay values were used in the subsequent modeling analysis.

Rate constants were estimated with the CONSAM computer program (Foster and Boston, 1983; Berman, et al., 1983) using an iterative least-squares criterion. A multi-compartmental pharmacokinetic model (Figure 31) was utilized to analyze these data. This model is based on similar studies previously reported by our group (Williams et al., 1990; Williams and Riviere, 1994). Please note that the 4- and 8-hour flaps were handled separately in this analysis.

The results of the assays from the IPPSF experiments were utilized as constraints for parameter estimation in several of the compartments in the multicompartment passive topical kinetic model used to describe compound penetration and distribution. Compartment 8 (evaporative loss) is represented by the unrecovered compound. Compartment 4 (surface) is represented by the swabs used to remove the surface compound. Compartment 9 (stratum corneum) is represented by the tape strips plus 75% of the first 80-μm cryostat core sample.

Compartment 2 (viable epidermis) is represented by 25% of the first 80-μm cryostat core sample. Compartment 3 (dermis) is represented by the label found in the cryostat core samples from 80 μm through 1100 μm. Compartment 5 (subcutaneous fat) is represented by the label found in the fat plus the remainder of the cryostat core samples. Compartment 12 is the sum of compartments 1 + 2 + 3 + 9. This corresponds to the whole flap measure, excluding fat--that is, the tape strips plus all the skin measures (including the cryostat core samples) and the leaks. Compartment 7 (effluent) is represented by the absorption, which is the amount of label measured in the venous effluent.

Phase 2: Vascular and Extracellular Volume Study

A total of nine skin flaps were used for the vascular and extracellular volume study. All skin flaps were dosed intra-arterially through the perfused media with ^{125}I-labeled bovine serum albumin (BSA) and ^{14}C-labeled inulin--approximately 45 mg/ml BSA and 3.5 μg/ml inulin in IPPSF media. Four of the skin flaps received no topical dose (1674, 1675, 1660, 1661) while five received 300 μl of 5.0 mg/ml (1796, 1797, 1804) or 10.0 mg/ml (1812,1813) of HD in ethanol. Additionally, the data from four historical control inulin/albumin flaps (400-403) were used since they illustrate the consistency of the control preparations. All topical doses were administered within a 1.25 cm X 6.0 cm (7.5 cm^2) Stomahesive template. In these rather complex studies, a great deal of variability was observed in the response of individual IPPSFs. Initially, another eight skin flaps were also studied to work out this technique. Since the purpose of this study was to characterize the vascular volume changes which occur during HD toxicosis, flaps analysed were selected on the basis of the presence of the characteristic increase in VR after exposure. As seen in the original HD studies from the previous contract (DAMD17-87-C-7139), this was the most predictive marker of HD toxicosis. Also, this is the best correlate that ties into the prostaglandin efflux studies previously reported and the actual HD kinetic studies described above.

Arterial samples (the media before it entered the skin flap) and venous efflux samples were taken at 5, 10, 15, 20, 25, 30, 40, 50, 60, 75, 90, and 120 minutes, and then every 30 minutes for 6 hours to determine the absorption profiles. At termination, steps were taken to determine location and mass balance of the infused labeled compounds. The Stomahesive template used to demarcate the dosing area was removed. The underside of the skin flap was rinsed to remove the label that had collected over the 6-hour perfusion period. The skin flap cradle was rinsed twice and all the rinses were retained. Then the skin was separated from the subcutaneous fat after snap-freezing in liquid nitrogen. The skin and fat tissue samples were dissolved individually in Soluene-350 (Packard Instrument Co., Downers Grove, IL). The leaks that resulted from the dissection of the skin flap, the fingertips of the gloves, and instruments used during dissection were cleaned and the swaps retained for analysis.

All the above samples were assayed for ^{14}C-radiolabel via a Packard Model 306 Tissue Oxidizer and the samples were counted on a Packard Model 1900 TR Tri-Carb Liquid Scintillation Analyzer (Packard Instrument Co., Downers Grove, IL). All the above samples were assayed for ^{125}I-radiolabel via an LKB Model 1272 CliniGamma (Pharmacia LKB Biotechnology, Inc., Gaithersburg, MD). The individual assay values were used in the subsequent analysis. Vascular volumes were calculated as previously reported and described on the next page.

Concentrations were calculated using equation 1.

$$C(t) = \frac{D(t)}{(2.22 \times 10^6 \text{ DPM}/\mu\text{Ci})\alpha} \qquad (1)$$

where $C(t)$ = radiolabel concentration (μg/mL) at time t.
$D(t)$ = measured DPM/mL.
α = specific activity of radiolabeled material.

Flux was calculated using equation 2.

$$J(t) = C(t)Q(t) \qquad (2)$$

where $Q(t)$ = perfusate flow (mL/min) at time t.

The volumes of distribution for both inulin and BSA spaces were estimated using equation 3.

$$V(T) = M(T)/C_V(T) \qquad (3)$$

where T = length of infusion (experiment length).
$M(T)$ = estimated mass of radiolabel in skin flap at t=T.
$C_V(T)$ = mean concentration of radiolabel emerging at t=T.

The estimation of M(T) was calculated using equation 4.

$$M(T) = \int_0^T J_A(t)dt - \int_0^T J_V(t)dt \qquad (4)$$

where $J_A(t)$ = calculated (eq. 2) arterial flux at time t.
$J_V(t)$ = calculated venous flux at time t.

$C_V(T)$ was calculated as the mean of the final three venous concentration measures, assumed to be under equilibrium conditions. The integrals were approximated using the trapezoidal rule. The above method is presented in detail elsewhere (Williams and Riviere, 1989).

Results

Phase 1: Mustard Penetration Study

Table III lists the results in percentage of the initial dose for the six 8-hour and the three 4-hour skin flap experiments. Listed are the doses, swabs and tape strips, the cradle rinses and leaks, skin and fat measures, absorption and penetration totals, cryostat totals, totals remaining on the dosing template, total recoveries, and the time of peak flux. In the table, additional assays include cradle rinses, leaks, and fingertip measures. The whole flap measure is the total of all the skin samples, the cryostat core sample, the subcutaneous fat, and the leaks resulting from the skin flap dissection. Absorption is the amount of label detected in the venous efflux. Penetration is absorption plus the whole flap measure.

Figures 32-40 illustrate (1) the observed and calculated venous flux, (2) the cryostat core sample penetration profiles, and (3) the vascular resistance in these nine skin flap experiments. All received the same dose: 3000 μg of ^{14}C-HD in ethanol. As seen by examining these plots, all flaps demonstrated the typical increase in VR noted with HD exposure and thus are relevant for ultimately correlating with the physiological data presented elsewhere in this report.

The rate constants (mean $\pm$ standard deviation) for the six 8-hour and three 4-hour skin flaps are listed in Table IV. Figures 41 and 42 show the observed and calculated mean profiles in the 4- and 8-hour experiments. Figures 43 and 44 show the predicted compartmental mass profiles for each series of flaps. The main effect seen with these data is that the larger penetrated tissue masses seen in the 4-hour studies are decreased as penetration and absorption continue. This is seen with the much higher concentrations in the core biopsies at the earlier time point.

Phase 2: Vascular and Extracellular Volume Study

Figures 45 and 46 illustrate the mean: (1) vascular resistance, (2) inulin differential flux (flux resulting from the difference between the arterial media measure minus the venous media measure), and (3) BSA differential flux from thirteen skin flap experiments. Table V lists the calculated volumes of distribution for the markers according to treatment. The volume of distribution normalized for flap weight (e.g., volume fraction) is the most pertinent parameter to analyze. As seen from these data, the HD-treated flaps demonstrate different BSA and inulin profiles than control flaps, suggesting that HD alters the vascular permeability and extracellular fluid space of the IPPSF. Based on an assessment of the volume fractions, the primary effect of HD is on the BSA space.

Table III: ^{14}C-HD Penetration Results in Percentage of Dose.

8-HOUR DOSING PERIOD

SF #	Dose	Dose Area	Swab	Tape	Cr. Rinse	Leaks	Deseed Skin	Template Skin	Skin	Fat
	(ug)	(cm2)	(% Dose)	(% Dose)	(% Dose)	(% Dose)	(% Dose)	(% Dose)	(% Dose)	(% Dose)
1828	3000	7.5	0.076	0.114	0.067	0.020	0.091	0.287	0.804	0.722
1829	3000	7.5	0.031	0.157	0.395	0.066	0.196	0.759	2.504	0.434
1834	3000	7.5	0.050	0.017	0.091	0.036	0.040	0.134	0.804	0.163
1835	3000	7.5	0.012	0.072	0.073	0.074	0.152	1.102	2.110	0.534
1836	3000	7.5	0.024	0.184	0.066	0.024	0.067	0.296	0.222	0.115
1837	3000	7.5	0.076	0.048	0.110	0.066	0.321	0.418	0.491	0.139
Mean	3000	7.5	0.045	0.095	0.127	0.048	0.145	0.499	1.139	0.351
Std. Dev.	0.000	0.000	0.027	0.060	0.118	0.024	0.104	0.363	0.939	0.251

SF #	Penetration	Absorption	Whole Flap	Cryostat Total	Template	Additional Assays	Total Recovered	Total Unrecovrd	Time of Peak Flux	Observed Peak Flux
	(% Dose)	(% Dose)	(% Dose)	(% Dose)	(% Dose)	(% Dose)	(% Dose)	(% Dose)	(hours)	(ug/min)
1828	6.192	4.134	2.058	0.034	1.469	0.066	7.801	92.069	0.25	1.66
1829	9.724	5.575	4.148	0.189	1.533	0.567	11.818	88.182	0.50	0.91
1834	2.763	1.768	1.015	0.037	0.536	0.133	3.482	96.518	0.06	1.61
1835	13.083	9.031	4.062	0.091	1.460	0.169	14.716	85.284	0.33	9.36
1836	4.323	3.552	0.771	0.047	0.663	0.117	5.444	94.556	0.06	3.92
1837	5.838	4.329	1.508	0.072	0.717	0.186	6.793	93.207	0.75	2.51
Mean	6.992	4.732	2.260	0.078	1.065	0.212	8.359	91.641	0.333	3.333
Std. Dev.	3.781	2.445	1.496	0.058	0.440	0.177	4.179	4.179	0.258	3.142

4-HOUR DOSING PERIOD

SF #	Dose	Dose Area	Swab	Tape	Cr. Rinse	Leaks	Deseed Skin	Template Skin	Skin	Fat
	(ug)	(cm2)	(% Dose)	(% Dose)	(% Dose)	(% Dose)	(% Dose)	(% Dose)	(% Dose)	(% Dose)
1888	3000	7.5	0.062	1.041	0.041	0.026	0.186	0.550	0.028	0.034
1889	3000	7.5	0.027	0.249	0.170	0.144	0.509	1.194	0.746	0.100
1891	3000	7.5	0.039	0.832	0.822	0.323	0.626	2.827	3.636	1.620
Mean	3000	7.5	0.039	0.641	0.344	0.164	0.440	1.524	1.436	0.585
Std. Dev.	0.000	0.000	0.013	0.396	0.419	0.150	0.228	1.174	1.863	0.897

SF #	Penetration	Absorption	Whole Flap	Cryostat Total	Template	Additional Assays	Total Recovered	Total Unrecovrd	Time of Peak Flux	Observed Peak Flux
	(% Dose)	(% Dose)	(% Dose)	(% Dose)	(% Dose)	(% Dose)	(% Dose)	(% Dose)	(hours)	(ug/min)
1888	1.648	0.988	0.662	0.139	2.066	0.206	4.068	95.132	0.75	0.13
1889	6.059	2.639	3.421	0.728	7.063	0.977	13.617	86.383	0.75	0.60
1891	21.282	11.619	9.663	0.732	10.720	1.828	33.539	66.461	1.00	2.58
Mean	9.663	4.982	4.682	0.533	6.623	0.937	17.341	82.659	0.833	1.103
Std. Dev.	10.301	5.830	4.486	0.341	4.346	0.712	14.694	14.694	0.144	1.300

Table IV: ^{14}C-HD Penetration Rate Constants.

8-HOUR DOSING PERIOD

IPPSF #	1828	1829	1834	1835	1836	1837	Mean	Std. Dev.
k48	0.15	0.15	0.15	0.15	0.15	0.15	0.150	0.0000
k49	4.00	4.00	4.00	4.00	4.00	4.00	4.000	0.0000
k94	0.90	0.55	0.90	0.82	0.90	0.80	0.812	0.1357
k92	0.45	0.45	0.45	0.75	0.50	0.55	0.525	0.1173
k29	0.84	0.50	0.84	0.88	0.84	0.92	0.803	0.1520
k23	0.08	0.05	0.08	0.20	0.10	0.11	0.103	0.0516
k32	0.64	0.20	0.74	0.84	0.64	0.88	0.657	0.2448
k31	0.055	0.01	0.055	0.09	0.066	0.06	0.056	0.0260
k13	0.45	0.30	0.45	0.45	0.45	0.45	0.425	0.0612
k35	0.0081	0.0010	0.0025	0.0022	0.0021	0.0020	0.00298	0.0026
k53	0.0014	0.0013	0.0014	0.0013	0.0022	0.0019	0.00158	0.0004
k17	0.28	0.25	0.28	0.40	0.45	0.28	0.323	0.0812
Peak Flux (ug/min)	1.66	0.91	1.61	9.39	3.92	2.51	3.333	3.1416
Peak Time (hours)	0.25	0.50	0.08	0.33	0.08	0.75	0.333	0.258

4-HOUR DOSING PERIOD

IPPSF #	1888	1889	1891				Mean	Std. Dev.
k48	0.35	0.37	0.37				0.363	0.0115
k49	0.40	0.45	0.55				0.467	0.0764
k94	0.15	0.10	0.17				0.140	0.0361
k92	0.018	0.05	0.15				0.073	0.0689
k29	0.015	0.05	0.05				0.038	0.0202
k23	0.09	0.12	0.13				0.113	0.0208
k32	0.06	0.06	0.04				0.053	0.0115
k31	0.01	0.01	0.01				0.010	0.0000
k13	0.25	0.10	0.045				0.132	0.1061
k35	0.0008	0.0026	0.0019				0.00177	0.0009
k53	0.0094	0.0047	0.0048				0.00630	0.0027
k17	0.024	0.022	0.035				0.027	0.0070
Peak Flux (ug/min)	0.13	0.60	2.58				1.103	1.3002
Peak Time (hours)	0.75	0.75	1.00				0.833	0.144

Table V: ^{125}I-BSA and ^{14}C-Inulin Vascular and Extracellular Volumes.

NO TOPICAL DOSE CONTROLS

SF #	IPPSF Mass (grams)	Inulin Volume (mls)	Volume Fraction (mls/g)	BSA Volume (mls)	Volume Fraction (mls/g)
400	23.6	4.83	0.20	0.56	0.02
401	27.0	5.32	0.20	1.91	0.07
402	28.3	9.07	0.32	5.61	0.20
403	30.9	5.84	0.19	5.51	0.18
1660	32.0	-	-	-	-
1661	29.1	-	-	-	-
1674	28.8	10.29	0.36	-	-
1675	30.0	8.31	0.28	-	-
Mean	28.71	7.28	0.26	3.40	0.12
Std. Dev.	2.58	2.25	0.07	2.56	0.08

XHD TOPICAL DOSE

SF #	IPPSF Mass (grams)	Inulin Volume (mls)	Volume Fraction (mls/g)	BSA Volume (mls)	Volume Fraction (mls/g)
1796	26.6	17.31	0.65	7.87	0.30
1797	27.5	4.37	0.16	3.53	0.13
1804	27.8	-	-	7.17	0.26
1812	29.2	6.33	0.22	3.13	0.11
1813	28.2	6.97	0.25	-	-
Mean	27.86	8.75	0.32	5.43	0.20
Std. Dev.	0.95	5.82	0.22	2.44	0.09

Discussion

Phase 1: Mustard Penetration Study

A total of nine IPPSF studies of the absorption and distribution of HD were conducted with the analysis split into 4- and 8- hour studies. As seen from these data, there was unfortunately a great deal of variability between the groups with peak fluxes occurring later in the 4 hour exposure flaps. This must be considered experimental variation that coincidentally occurred in the flaps terminated at an earlier time point. Since pharmacokinetic modeling is essentially an exercise in partitioning out relative rates of different processes, this occurrence of a delayed peak in the shorter experiments (21% of experimental period of a 4-hour flap vs. 4% of an 8-hour flap) confounds interpretation across experiments. Despite these differences, one can appreciate the time course of HD absorption by examining the data in Table III or Figures 32-40. Significantly, the bulk of the absorption occurs rapidly within the first hour with a majority of the absorbed dose either penetrated into the skin (e.g., whole flap measure) or in the venous efflux. The rapid HD absorption and evaporative loss due to volatility are similar to those previously reported by other investigators (Hambrook et al., 1992; Klain et al., 1988; Nagy et al., 1946). This type of data is difficult to extract from many longer term in vivo studies (Black et al., 1992; Davison et al., 1961). Also, it demonstrates that at earlier time points a large fraction of the HD present in tissue (e.g., that determined in the core biopsies of the present study) is still mobile. It is probable that a large fraction of this radiolabel is not HD but one of numerous metabolites (Black et al., 1992; Davison et al., 1961; Hambrook et al., 1992; Sandelowsky et al., 1992). This will be studied in the third component of the present contract.

The great difference in individual susceptibility to HD vesication has been widely acknowledged since the beginning of research in this area (Marshall et al., 1919). The first source of this variability must relate to the actual dose of topically exposed HD which reaches

its target site within the skin. The quantity of applied HD that penetrates into the viable layers of skin is determined by its rate of surface loss in relation to its rate and extent of percutaneous absorption. As can be seen from these disposition studies (Table III, amount penetrated), this is highly variable. Thus, the actual delivery of HD to its site of action is the first process, which probably accounts for a significant amount of the variability in response to HD often reported.

A major limitation of this study is that only dilute liquid HD was used. This method of dose application precludes presentation of a constant HD vapor concentration to skin and adds the potential confounding effects of a vehicle. Studies have previously demonstrated the correlation of HD vapor absorption to volatility and thus its dependence upon temperature, vapor pressure, and humidity, as well as the large percent of dose lost to evaporation (Klain et al., 1988; Nagy et al., 1946). In contrast, there have been reports of cutaneous hazard from dilute mustard (e.g., dissolved in oil) (Alexander, 1947), for which cutaneous vesication still occurs with a pathogenesis similar to vapor cases. However, the goal of this study is to investigate the relationship of HD penetration to the toxicologic effect under the conditions of an IPPSF study; thus, exposure conditions must be the same.

This frame of reference is important to the interpretation of all IPPSF studies. The variation in vesication previously reported with similar doses of HD is most probably secondary to variations in rate of absorption. What is required for the precise interpretation of HD vesication studies is the actual individual IPPSF disposition profile. This is obviously not possible as the disposition data require destructive tissue sampling.

Phase 2: Vascular and Extracellular Volume Study

A total of 13 IPPSF studies of vascular and extracellular volume changes resulting from topical doses of HD and controls were conducted. The experimental protocol is remarkably stable as seen from the congruence of the previous control data with the more recent flaps conducted in this report. The primary finding from these flaps is the change in BSA volume

over the course of an IPPSF experiment. As discussed in the earlier section of this report, this vascular change may be mediated by HD-induced release of prostaglandins. The present results confirm that significant changes in vascular permeability assessed by BSA space do occur.

Combined Summary

The results of this study clarify a significant amount of work previously done within this and earlier contracts and provides the basic data for construction of a comprehensive TK-TD model. First, most of the compound absorption occurs within the first hour. Second, there is a significant change in BSA volume over the course of the experiment as a result of HD-induced vesication. This is probably mediated by prostaglandin release and is also associated with an increase in VR.

The fact that BSA volume changes with time invalidates the assumptions inherent to constructing the pharmacokinetic (PK) model which assumes constant volumes (Riviere and Williams, 1992). This point is critical and is part of the reason why 4- and 8-hour pharmacokinetic fits result in such different parameter estimates. Since volumes are assumed constant, this actual change in volume is reflected in different parameter estimates for multiple parameters. HD is a potent chemical toxicant which damages tissues upon exposure. This chemical-induced change should thus alter the "pharmacokinetic properties" of the tissue such that a dynamic PK model which incorporates these changes is really required to accurately model HD absorption. The problem is how to independently quantitate the HD-induced damage. The change in BSA volume is such a quantitative end point. Similarly, the earlier reported binding of HD to laminin is a demonstration of covalent binding of HD which in this study is part of the epidermal/dermal HD pool. The present model assumes that every molecule of HD is freely diffusable. A proper PK model should account for this binding.

The studies conducted to date give us the preliminary quantitative data to construct such a comprehensive model. What is presently lacking is more information on the

biochemical makeup of the absorbed HD; a study is being conducted. Future models will incorporate a time-dependent or an HD-dependent change in vascular tissue volume in this model. Similarly, the 4- and 8-hour data will be analyzed simultaneously. The important requirement for such an analysis is a parameter that could be used to "synchronize" the course of HD absorption and effect across different experiments which assessed HD uptake, vascular volume changes, prostaglandin efflux, etc. The correlate for this analysis is probably the characteristic change in VR seen in all HD flaps. This is presently being investigated.

DISCUSSION

The results reported in this midterm report offer significant insight into the pathogenesis of HD-induced vesication in the skin. First, one must take into account that all of these studies were conducted in the IPPSF, an in vitro model whose inflammatory responses occur independent of any systemic influences. Thus HD-induced vesication in this model, which has previously been shown to be similar to in vivo lesions, occurs in a milieu that is only controlled by local cutaneous factors. That is, vesication occurs without the requisite involvement of blood-borne humoral or cellular elements of the immune system. With this knowledge at hand, these experiments attempted to define the potential mediators that are involved in modulating the vascular response (altered VR) seen after HD exposure. It was clearly shown that the alteration in VR is accompanied by the release of prostaglandins $PGF_{2\alpha}$ and PGE_2 at the 5.0 mg/ml of HD. In contrast, yet similar to that reported in human skin cultures by Rikimaru and co-workers (1991), prostaglandins were not released at the higher exposure concentration in spite of the presence of epidermal-dermal separation. As discussed in this section of the report, increased exposure to HD could result in cell death rather than injury, inhibition of arachidonic acid metabolism enzymes, or release of other classes of inflammatory mediators when more severe toxicity is seen. Additionally, direct endothelial cell injury could occur at higher HD concentrations which would ablate the vascular response to any mediator released. Changes in vascular volumes (BSA space) were detected at the 5.0 mg/ml and the 10.0 mg/ml of HD doses, suggesting that vascular involvement occurs at both doses. It must be pointed out that there is a confounding factor in assessing inflammatory mediator profiles in the IPPSF venous effluent. If mediators are locally released and as the vascular volume data suggests, tissue volume of distribution and permeability increases, there will be a local dilution of the mediator within the skin, which would tend to decrease the venous concentrations and confound interpretation of these profiles. Accompanying this vascular exudation is the increase in VR which causes edema and perfusion resistance. This

vascular pooling would also lengthen the residence time of prostaglandins in the skin which, due to their lability, could result in degradation and again a decreased venous efflux in the face of increased tissue production.

Thus, there are several mechanisms which predict that more severe levels of inflammation or toxicity may paradoxically be associated with decreased venous mediator efflux. This phenomenon will be investigated by studies involving prostaglandin infusion into the IPPSF, through selected prostaglandin blockade, and through studies which pharmacologically manipulate vascular function. Additionally, formulation of a quantitative TK-TD model will allow the hypothesis of prostaglandin dilution, degradation, and even consumption to be critically evaluated.

One of the most exciting results generated in the present study involves the molecular mechanism of HD-induced epidermal-dermal separation and vesication. The effect of HD exposure on six basement membrane epitopes in the IPPSF was characterized. As discussed in this section, these studies localized the HD-induced blister cleavage plane to be within the laminin and fibronectin, above the type IV collagen, EBA and GB3, but below the BP antigenic sites. These data focus on the molecular mechanisms of direct HD action to the laminin and fibronectin. These morphological studies thus confirm the in vitro findings that laminin may be a primary target of HD action.

We have demonstrated that exposure of laminin to HD alters laminin structure, probably due to alkylation and cross-linking of laminin chains. Additionally, our studies suggest that HD-alkylated laminin inhibits cell adhesion in the absence of cytotoxicity. These data provide evidence for a direct role of HD-alkylation in the formation of a blister. However, once this blister forms, the HD-alkylated laminin is still present as a remnant at the basement membrane zone. Under normal wound-healing circumstances, normal laminin would promote epidermal cell adhesion to the dermal matrix. It is widely known that HD

blisters require a prolonged time interval for healing. Our data strongly suggest that one reason for this delayed wound healing would be the presence of HD-alkylated laminin in the wound surface which would tend to antagonize epidermal cell adhesion. Thus, the direct alkylation of laminin (and possibly other basement membrane molecules) and not HD-induced genotoxicity, may be the primary blockade to healing of HD blisters. This hypothesis would have major implications on the clinical management of HD blisters as compared to other bullous diseases and will be pursued further in this contract.

The final phase of the present project involves formulating a comprehensive TK-TD model of HD absorption, penetration, and toxicologic effect. The first step in building such a model is to characterize, using classic compartmental modeling techniques, the time course of HD absorption in the IPPSF. These studies, based on tissue and venous efflux analyses, confirm previous worker's findings that HD is rapidly absorbed into skin. Also, they graphically illustrate the great deal of variability seen in HD absorption. This must be the proximate cause for the large variability seen in HD toxicity. However, the primary reason for conducting these initial studies was to formulate a basic kinetic model to beginning the more complex construction of a TK-TD model. These individual analyses presented in this report assume that all pharmacokinetic rate constants do not change over the course of an experiment. Based upon all of the physiological data presented above, we know that this assumption cannot be true. In order to model this, we will use the time course of vascular volume and VR changes to vary the volume of compartments 1,2, 3, and 7 of Figure 31 over the course of an experiment. This change will significantly impact on the value of all estimated rate constants. We are also in the process of determining the metabolic profile of the HD detected in the tissue and perfusate using gas chromotography techniques. When these data are available, the kinetic model may also be modified to handle HD metabolism. This would then result in a more powerful quantitative tool to probe the toxicodynamics of HD interaction with molecular targets such as laminin and cellular targets which result in

inflammation. The ultimate goal would be to define the HD-concentration-response relationship at the level of the basement membrane and epidermis. This would allow a more quantitative evaluation of protective strategies which reduce HD flux across the stratum corneum and help evaluate the requirements for successful antivesicant therapy.

In conclusion, we feel that we have made significant progress in achieving the stated research goals of the present contract. All of these studies have confirmed the utility of the IPPSF to study the mechanism of HD vesication. The studies have validated our previous reported findings and further characterize the response of the IPPSF to HD exposure and the disposition of HD within the model. This is a unique aspect of this particular model system for unlike many in vitro models, both absorption and toxicology studies can be done in the same model. The most exciting aspects of these results are the finding of a direct HD interaction with the laminin molecule and its implications to both the pathogenesis of HD vesication and the healing of the resulting wound.

REFERENCES

Alexander, S.F. (1947). Medical report of the Bari harbor mustard casualties. Military Surgeon 101:1-17.

Bartek, M.J., LaBudde, J.A., and Maibach, H.I. (1972). Skin permeability in vivo: Comparison in rat, rabbit, pig, and man. J. Invest. Dermatol. 58:114-123.

Berman, M, Beltz, W.F., Greif, P.C., Chabay, R., and Boston, R.C. (1983) CONSAM User's Guide. Laboratory of Mathematical Biology, U.S. Department of Health and Human Services, National Cancer Institute, National Institutes of Health, Bethesda, MD 20205.

Black, R.M., Hambrook, J.L., Howells, D.J., and Read, R.W. (1992). Biological fate of sulfur mustard, 1,1'-thiobis(2-chloroethane). Urinary excretion profiles of hydrolysis products and β-lyase metabolites of sulfur mustard after cutaneous application in rats. J. Analytical Toxicol. 16:79-84.

Boberts, J.J. (1978). The repair of DNA modified by cytotoxic, mutagenic, and carcinogenic chemicals. Adv. Radiat. Biol. 9:211-435.

Boursnell, J.C. (1951). Some reactions of mustard gas with protein. Biochem. Soc. Symp. 2:8-15.

Bouzon, M., Dussert, C., Lissitzky, J.C., and Martin, R.M. (1990). Spreading of B16F1 cells on laminin and its proteolytic fragments P1 and E8: Involvement of laminin carbohydrate chains. Exp. Cell Biol. 190:47-56.

Bowman, K.F., Monteiro-Riviere, N.A., and Riviere, J.E. (1991). Development of surgical techniques for preparation of in vitro isolated perfused porcine skin flaps for percutaneous absorption studies. Am. J. Vet. Res. 52:75-82.

Briggaman, R.A. (1983). The epidermal-dermal junction and genetic disorders of this area. In Biochemistry and Physiology of the Skin, (Ed. L.A. Goldsmith). Oxford University Press, New York, NY, pp. 1001-1024.

Briggaman, R.A. (1990). Epidermal-dermal junction: Structure, composition, function and disease relationships. Prog. Dermatol. 24:1-8.

Burgeson, R.E. (1993). Dermal-epidermal adhesion in skin. In Molecular and Cellular Aspects of Basement Membrane. (Eds. D.H. Rohrbach and R. Timpl), Academic Press, Inc., San Diego, CA. pp. 49-66.

Calabresi, P., and Chabner, B.A. (1992). Antineoplastic agents. In The Pharmacological Basis of Therapeutics. (Eds. A.G. Gilman, T.W. Rall, A.S. Nies, and P. Taylor). Elmsford, NY, pp. 1209-1223.

Carver, M.P., Williams, P.L., and Riviere, J.E. (1989). The isolated perfused porcine skin flap. III. Percutaneous absorption pharmacokinetics of organophosphates, steroids, benzoic acid, and caffeine. Toxicol. Appl. Pharmacol. 97:324-337.

Clark, R.A.F. (1983). Fibronectin in the skin. J. Invest. Dermatol. 8:475-479.

Dahlen, S.E. (1987). Prostaglandins and leukotrienes. In Dermatology in General Medicine, Vol.1. (Ed. T.B. Fitzpatrick), McGraw-Hill, New York.

Davison, C., Rozman, R.S., and Smith, P.K. (1961). Metabolism of bis-β-chloroethyl sulfide (sulfur mustard gas). Biochem. Pharmacol. 7: 65-74.

Dixon, M., and Needham, D.M. (1946). Biochemical research on chemical warfare agents: A review. Cancer Res. 22:651-688.

Fine, J-D., Redmar, D.A., and Goodman, A.L. (1987). Sequence of reconstitution of seven basement membrane components following split-thickness wound induction in primate skin. Arch. Dermatol. 123:1174-1178.

Fine, J-D. (1991). Structure and antigenicity of the skin basement membrane zone. J. Cutan. Pathol. 18:401-409.

Fleischmajer, R., Timpl, R., Dziadek, M., and Lebwohl, M. (1985). Basement membrane proteins, interstitial collagens, and fibronectin in neurofilibroma. J. Invest. Dermatol. 85:54-59.

Foidart, J.M., Bere, E.W., Yaar, M., Rennard, S.I., Gullino, M., Martin, G.R., and Katz, S.I. (1980). Distribution and immunoelectron microscopic localization of laminin, a noncollagenous basement membrane glycoprotein. Lab. Invest. 42:336-342.

Foster, D.H., and Boston, R.C. (1983). The use of computers in compartmental analysis: The SAAM and CONSAM programs. In: Compartmental Distribution of Radiotracers. (Ed. J. Robertson), CRC Press, Cleveland, OH, pp.73-142.

Fox, M., and Scott, D. (1980). The genetic toxicology of nitrogen and sulfur mustard. Mutat. Res. 75:131-168.

Ginzler, A.M., and Davis, M.I.J. (1943). The pathology of mustard burns of human skin. U.S. Army Medical Research Laboratory, Edgewood Arsenal, Maryland, Report No.3.

Goodman, S.L., Gundula, R., and von der Mark, K. (1989). The E8 subfragment of laminin promotes locomotion of myoblasts over extracellular matrix. J. Cell Biol. 109:799-809.

Grabbe, J., Rosenbach, T., and Czarnetzki, B.M. (1985). Production of LTB_4-like chemotactic arachidonate metabolites from human keratinocytes. J. Invest. Dermatol. 86: 527-530.

Hambrook, J.L., Harrison, J.M., Howells, D.J. and Schock, C. (1992). Biological fate of sulphur mustard (1,1'-thiobis(2-chloroethane)): Urinary and faecal excretion of ^{35}S by rat after injection or cutaneous application of ^{35}S-labelled sulphur mustard. Xenobiotica 22:65-75.

Hartl, L., Oberbaumer, I., and Deutzmann, R. (1988). The N terminus of laminin A chain is homologous to the B chains. Eur. J. Biochem. 173:629-635.

Higuchi, K., Kajiki, A., Nakamura, M., Harada, S., Pula, P.J., Scott, A.L., and Dannenberg, A.M. (1988). Proteases released in organ culture by acute dermal inflammatory lesions produced in vivo in rabbit skin by sulfur mustard: Hydrolysis of synthetic peptide substrates for trypsin-like and chymotrypsin-like enzymes. Inflammation. 12:311-333.

Holzer, H. (1964). Action of alkylating substances on glycolysis. In Chemotherapy of Cancer. (Ed. P.A. Plattner), Elsevier, Amsterdam.

Horiguchi, Y., Abrahamson, D.R., and Fine, J.D. (1991). Epitope mapping of the laminin molecule in murine skin basement membrane zone: Demonstration of spatial differences in ultrastructural localization. J. Invest. Dermatol. 96:309-313.

King, J.R., and Monteiro-Riviere, N.A. (1990). Cutaneous toxicity of 2-chloroethyl methyl sulfide in isolated perfused porcine skin. Toxicol. Appl. Pharmacol. 104:167-179.

King, J.R., Riviere, J.E., and Monteiro-Riviere, N.A. (1991). Characterization of lewisite vesication in isolated perfused porcine skin. In Proceedings of the Medical Defense Bioscience Review, U.S. Army Medical Research Institute of Chemical Defense, Aberdeen Proving Ground, Maryland, pp. 167-170.

King, J.R., and Monteiro-Riviere, N.A. (1991). Effects of organic solvent vehicles on the viability and morphology of isolated perfused porcine skin. Toxicol. 69:11-26.

King, J.R., Riviere, J.E., and Monteiro-Riviere, N.A. (1992). Characterization of lewisite toxicity in isolated perfused skin. Toxicol. Appl. Pharmacol. 116:189-201.

King, J.R., Peters, B.P., and Monterio-Rivere, N.A. (1994). Laminin in the cutaneous basement membrane as a potential target in lewisite vesication. Toxicol. Appl. Pharmacol. 126:164-173.

Klain, G.J., Bonner, S.J., and Omaye, S.T. (1988). Skin penetration and tissue distribution of ^{14}C butyl 2-chloroethyl sulfide in the rat. J. Toxicol. Cut. & Ocular Toxicol. 7:255-261.

Kleinman, H.K., Cannon, F.B., Laurie, G.W., Hassel, J.R., Aumailley, M., Terranova, V.P., Martin, G.R., and DuBois-Dalca, M. (1985). Biological activities of laminin. J. Cell Biochem. 27:317-325.

Laurie, G.W., LeBlond, C.P., and Martin, G.R. (1982). Localization of type IV collagen, laminin, heparan sulfate proteoglycan, and fibronectin to the basal lamina of basement membranes. J. Cell. Biol. 95:340-344.

Levy, M. (1946). Effects of sulfur and nitrogen mustards on proteins, enzymes, and cells. In Chemical Warfare Agents and Related Chemical Problems - Parts III-VI. Summary technical report of Division 9, National Defense Research Committee of the Office of Scientific Research and Development, Washington, DC. DTIC No.AD-234 249.

Marlow, D.D., Mershon, M.M., Mitcheltree, L.W., Petrali, J.P., and Jaax, G.P. (1990). Sulfur mustard-induced skin injury in hairless guinea pigs. J. Toxicol. Cut. & Ocular Toxicol. 9:179-192.

Marshall, E.K., Lynch V., and Smith H.W. (1919). On dichlorethylsulphide (mustard gas). II. variations in susceptibility of the skin to dichlorethylsulphide. J. Pharmacol. Exp. Therap. 12: 291-301.

Mercurio, A.M. (1990). Laminin: Multiple forms, multiple receptors. Curr. Opin. Cell Biol. 2:845-849.

Meyer, W., Schwarz, R., and Neurand, K. (1978). The skin of domestic mammals as a model for the human skin, with special reference to the domestic pig. Curr. Probl. Dermatol. 7:39-52.

Meyer, W., Gorgen, S., and Schlesinger, C. (1986). Structural and histochemical aspects of epidermis development of fetal porcine skin. Am. J. Anat. 176:207-219.

Mitcheltree, L.W., Mershon, M.M., Wall, H.G., Pulliam, J.D., and Manthei, J.H. (1989). Microblister formation in vesicant-exposed pig skin. J. Toxicol. Cut. & Ocular Toxicol. 8:309-319.

Momeni, A., Enshaeih, S., Meghdadi, M., Amindjavaheri, M. (1992). Skin manifestations of mustard gas. Arch. Dermatol. 128:775-580.

Montagna, W., and Yun, J.S. (1964). The skin of the domestic pig. J. Invest. Dermatol. 43:11-21.

Monteiro-Riviere, N.A., and Stromberg, M.W. (1985). Ultrastructure of the integument of the domestic pig (*Sus scrofa*) from one through fourteen weeks of age. Anat. Histol. Embryol. 14:97-115.

Monteiro-Riviere, N.A. (1986). Ultrastructural evaluation of the porcine integument. In Swine in Biomedical Research. (Ed. M.E. Tumbleson), Plenum, New York, pp. 641-655.

Monteiro-Riviere, N.A., Bowman, K.L., Scheidt, V.J., and Riviere, J.E. (1987). The isolated perfused porcine skin flap (IPPSF). II. Ultrastructural and histological characterization of epidermal viability. In Vitro Toxicol. 1:241-252.

Monteiro-Riviere, N.A., and King, J.R. (1989). The dermatotoxicity of 2-chloroethyl methyl sulfide and solvent vehicles in isolated perfused porcine skin. In Proceedings of the Medical Defense Bioscience Review, U.S. Army Medical Research Institute of Chemical Defense, Aberdeen Proving Ground, Maryland, pp. 53-56.

Monteiro-Riviere, N.A., King, J.R., and Riviere, J.E. (1990). Cutaneous toxicity of mustard and lewisite on the isolated perfused porcine skin flap. DAMD17-87-C-7139; NTIS, ADA229922, pp. 1-144.

Monteiro-Riviere, N.A. (1990). Specialized technique: The isolated perfused porcine skin flap (IPPSF). In Methods for Skin Absorption. (Eds. B.W. Kemppainen and W.G. Reifenrath). CRC Press, Boca Raton, FL, pp. 175-189.

Monteiro-Riviere, N.A., King, J.R., and Riviere, J.E. (1991). Mustard induced vesication in isolated perfused skin: biochemical, physiological, and morphological studies. In Proceedings of the Medical Defense Bioscience Review, U.S. Army Medical Research Institute of Chemical Defense, Aberdeen Proving Ground, Maryland, pp. 159-162.

Monteiro-Riviere, N.A. (1992). Use of the isolated perfused skin model in dermatotoxicology. In Vitro Toxicol. 5:219-233.

Monteiro-Riviere, N.A., and Inman, A.O. (1993). Histochemical localization of three basement membrane epitopes with sulfur mustard induced toxicity in porcine skin. Toxicologist. 13:58.

Monteiro-Riviere, N.A., Inman, A.O., Spoo, S.W., Rogers, R.A., and Riviere, J.E. (1993). Studies on the pathogenesis of bis (2-chloroethyl) sulfide (HD) induced vesication in porcine skin. In Proceedings of the Medical Defense Bioscience Review, U.S. Army Medical Research Institute of Chemical Defense, Aberdeen Proving Ground, Maryland, pp. 31-40.

Nagy, S.M., Golumbic, C., Stein, W.H., Fruton, J.S., and Bergmann, M. (1946). The penetration of vesicant vapors into human skin. J. Gen. Physiol. 29: 441-469.

Nicotera, P., McConkey, D.J., Dypbukt, J.M., Jones, D.P., and Orrenius, S. (1989). Ca^{2+}-activated mechanisms in cell killing. Drug Metabol. Res. 20:193-201.

Orrenius, S., and Nicotera, P. (1987). On the role of calcium in chemical toxicity. Arch. Toxicol. Suppl. 11:11-19.

Papirmeister, B., Gross, C.L., Petrali, J.P., and Hixson, C.J. (1984a). Pathology produced by sulfur mustard in human skin grafts on athymic nude mice. I. Gross and light microscope changes. J. Toxicol. Cut. & Ocular Toxicol. 3:371-391.

Papirmeister, B., Gross, C.L., Petrali, J.P., and Meier, H.L. (1984b). Pathology produced by sulfur mustard in human skin grafts on athymic nude mice. II. Ultrastructural changes. J. Toxicol. Cut. & Ocular Toxicol. 3:393-408.

Papirmeister, B., Feister, A.J., Robinson, S.I., and Ford, R.D. (1991). Medical Defense Against Mustard Gas: Toxic Mechanisms and Pharmacological Implications, CRC Press, Boca Raton, FL.

Papirmeister, B. (1993). Excitement in vesicant research - yesterday, today and tomorrow. Def. Med. Conf. 1:1-14.

Paulsson, M. (1992). Basement membrane proteins: Structure, assembly, and cellular interactions. Crit. Rev. Biochem. Mol. Biol. 27:93-127.

Petrali, J.P., Oglesby, S.B., and Mills, K.R. (1990). Ultrastructural correlates of sulfur mustard toxicity. J. Toxicol. Cut. & Ocular Toxicol. 9:193-214.

Pradelles, P., Grassi, J., and Maclouf, J. (1990). Immunoassays of eicosanoids using acetylcholinesterase. Methods Enzymol. 187:24.

Ray, R., Legere, R.H., and Broomfield, C.A. (1990). Membrane composition and fluidity changes due to alkylating agents. J. Cell Biol. 3:73A.

Reifenrath, W.G., Chellquist, E.M., Shipwash, E.A., and Jederberg, W.W. (1984). Evaluation of animal models for predicting skin penetration in man. Fundam. Appl. Toxicol. 4:S224-S230.

Requena, L., Requena, C., Sanchez, M., Jaqueti, G., Aguilar, A., Sanchez-Yus, E., and Hernandez-Moro, B. (1988). Chemical warfare. Cutaneous lesions from mustard gas. J. Amer. Acad. Dermatol. 19:529-536.

Rheins, L.A. (1992). What s new in cutaneous toxicity? J. Toxicol. Cut. & Ocular Toxicol. 11:225-238.

Rigal, C., Pieraggi, M.T., Vincent, C., Prost, C., Bouissou, H., and Serre, G. (1991). Healing of full-thickness cutaneous wounds in the pig. I. Immunohistochemical study of epidermo-dermal junction regeneration. J. Invest. Dermatol. 96:777-785.

Rikimaru, T., Nakamura, M., Yano, T., Beck, G., Habicht, G.S., Rennie, L.L., Widra, M., Hirshman, C.A., Boulay, M.G., Spannhake, E.W., Lazarus, G.S., Pula, P.J., and Dannenberg, A.M. (1991). Mediators, initiating the inflammatory response, released in organ culture by full-thickness human skin explants exposed to the irritant, sulfur mustard. J. Invest. Dermatol. 96:888-897.

Riviere, J.E., Bowman, K.F., Monteiro-Riviere, N.A., Carver, M.P., and Dix, L.P. (1986). The isolated perfused porcine skin flap (IPPSF). I. A novel in vitro model for percutaneous absorption and cutaneous toxicology studies. Fundam. Appl. Toxicol. 7:444-453.

Riviere, J.E., and Monteiro-Riviere, N.A. (1991). The isolated perfused porcine skin flap as an in vitro model for percutaneous absorption and cutaneous toxicology. Critical Reviews in Toxicol. 21:329-344.

Riviere, J.E. and Williams, P.L. (1992). On the pharmacokinetic implications of changing blood flow in skin. J. Pharm. Sci. 81:601-602.

Rudin, D.O. (1953). A review of the biological action of mustard as a basis for therapy. U.S. Army Chemical Corps Medical Laboratories, Army Chemical Center, Maryland, Special Report No. 21. DTIC No. AD-15 565.

Sakashiti, S., Engvall, E., and Ruoslahti, E. (1980). Basement membrane glycoprotein laminin binds to heparin. FEBS Lett. 116:243.

Sandelowsky, I., Simon, G.A., Bel, P., Barak, R., and Vincze, A. (1992). N^1-(2-hydroxyethylthioethyl)-4-methyl imidazole (4-met-1-imid-thiodiglycol) in plasma and urine: A novel metabolite following dermal exposure to sulphur mustard. Arch. Toxicol. 66: 296-297.

Sasaki, M., and Yamada, Y. (1987). The laminin B2 chain has a multidomain structure homologous to the B1 chain. J. Biol. Chem. 262:17111-17117.

Sasaki, M., Kato, S., Kohno, K., Martin, G.R., and Yamada, Y. (1987). Sequence of the cDNA encoding the laminin B1 chain reveals a multidomain protein containing cysteine-rich repeats. Proc. Natl. Acad. Sci. 84:935-939.

Sasaki, M., Kleinman, H.K., Huber, H., Deutzmann, R., and Yamada, Y. (1988). Laminin, a multidomain protein. The A chain has a unique globular domain and homology with the basement membrane proteoglycan and the laminin B chains. J. Biol. Chem. 263:16536-16544.

Schittny, J.C., Timpl, R., and Engel, J. (1988). High resolution immunoelectron microscopic localization of functional domains of laminin, nidogen, and heparan sulfate proteoglycan in epithelial basement membrane of mouse cornea reveals different topological orientations. J. Cell Biol. 107:1599-1610.

Singer, B. (1975). The chemical effects of nucleic acid alkylation and their relation to mutagenesis and carcinogenesis. Prog. Nucleic Acid Res. Mol. Biol. 15:219-284.

Smith, W.J., Sanders, K.M., Caulfield, J.E., and Gross, C.L. (1992). Sulfur mustard-induced biochemical alterations in proliferating human cells in culture. J. Toxicol. Cut. & Ocular Toxicol. 11:293-304.

Snyder, D.S. (1975). Cutaneous effects of topical indomethacin, an inhibitor of prostaglandin synthesis on UV-damaged skin. J. Invest. Dermatol. 64:322-326.

Stanley, J.R., Alvarez, O.M., Bere, E.W., Eaglstein, W.H., and Katz, S.I. (1981). Detection of basement membrane zone antigens during epidermal wound healing in pigs. J. Invest. Dermatol. 77:240-243.

Steele, J.G., Savolainen, T.A., Dalton, B.A., Smith, L., and Smith, G.J. (1990). Adhesion to laminin and expression of laminin in clonally related transformed and control sublines from an alveolar epithelial cell strain. Cancer Res. 50:3383-3389.

Timpl, R. (1989). Structure and biological activity of basement membrane proteins. Eur. J. Biochem. 180:487-502.

Verrando, P., Hsi, B.L., Yeh, C.J., Pasani, A., Seriegs, N., and Ortonne, J.P. (1987). Monoclonal antibody GB3, a new probe for the study of human basement membranes and hemidesmosomes. Exp. Cell Res. 170:116-128.

Vogt, R.F., Jr., Dannenberg, A.M., Jr., Scofield, B.H., Hynes, N.A., and Papirmeister, B. (1984). Pathogenesis of skin lesions caused by sulfur mustard. Fundam. App. Toxicol. 4: S71-S83.

Wade, J.V., Mershon, M.M., Mitcheltree, L.W., and Woodard, C.L. (1989). The hairless guinea pig model and vesicant vapor exposures for bioassay purposes. In Proceedings of the Medical Defense Bioscience Review, U.S. Army Medical Research Institute of Chemical Defense, Aberdeen Proving Ground, Maryland, pp. 569-575.

Williams, P.L., and Riviere, J.E. (1989). Estimation of physiological volumes in the isolated perfused porcine skin flap. Res. Commun. Chem. Pathol. Pharmacol. 66:145-158.

Williams, P.L., Carver, M.P., and Riviere, J.E. (1990). A physiologically relevant pharmacokinetic model of xenobiotic percutaneous absorption utilizing the isolated perfused porcine skin flap. J. Pharm. Sci. 79:305-311.

Williams, P.L., and Riviere J.E. (1994). A biophysically-based dermatopharmacokinetic compartment model for quantifying percutaneous penetration and absorption of topically-applied agents. Pharm. Res. (Submitted).

Willis, A.L., and Cornelson, M. (1973). Repeated injection PGE_2 in rat paws induces chronic swelling and a marked decrease in pain threshold. Prostaglandin. 3:353-355.

Woodley, D., Sauder, D., Talley, M.J., Silver, M., Grotendorst, G., and Qwarnstrom, E. (1983). Localization of basement membrane components after dermal-epidermal junction separation. J. Invest. Dermatol. 81:149-153.

Woodley, D., Briggaman, R.A., O'Keefe, E.J., Inman, A.O., Queen, L.L., and Gammon, W.R. (1984). Identification of the skin basement membrane autoantigen in epidermolysis bullosa acquisita. New Engl. J. Med. 30: 1007-1013.

Woolina, U., Berger, U., and Mahrle, G. (1991). Immunohistochemistry of porcine skin. Acta Histochem. 90:87-91.

Yaoita, H., Gullino, M., and Katz, S.I. (1976). Herpes gestationis. Ultrastructure and ultrastructural localization of in vivo-bound complement: Modified tissue preparation and processing for horseradish peroxidase staining of skin. J. Invest. Dermatol. 66:383-388.

Ziboh, V.A. (1992). Prostaglandins, leukotrienes, and hydroxy fatty acids in epidermis. Dermatol. 11:114-120.

APPENDIX

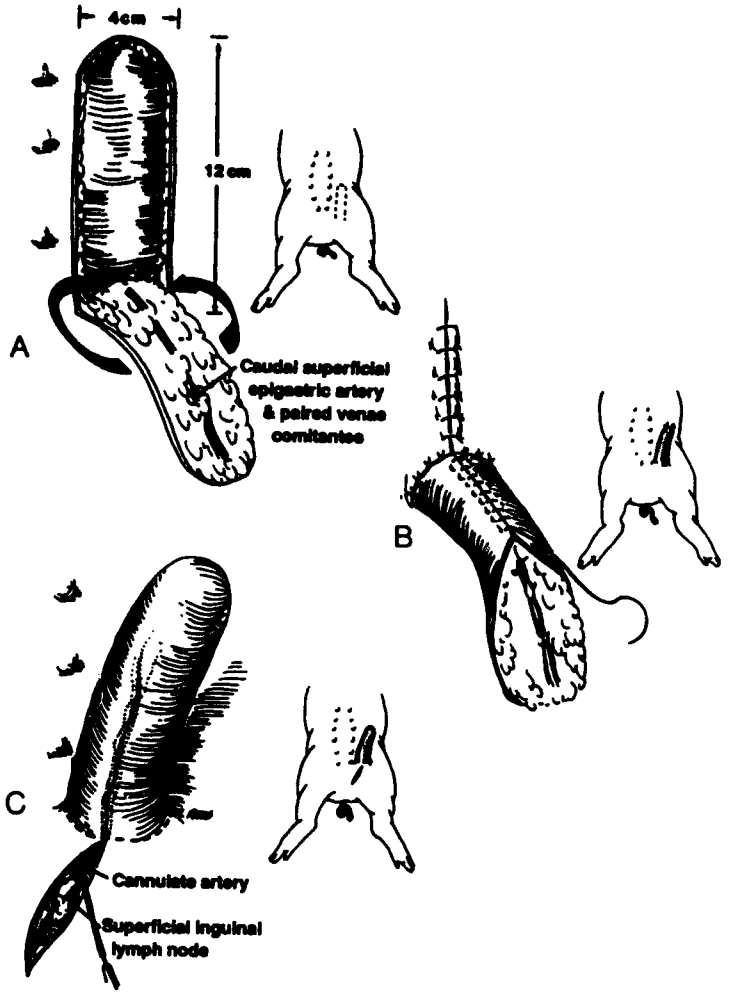

Figure 1. Surgical procedure for creating the IPPSFs.

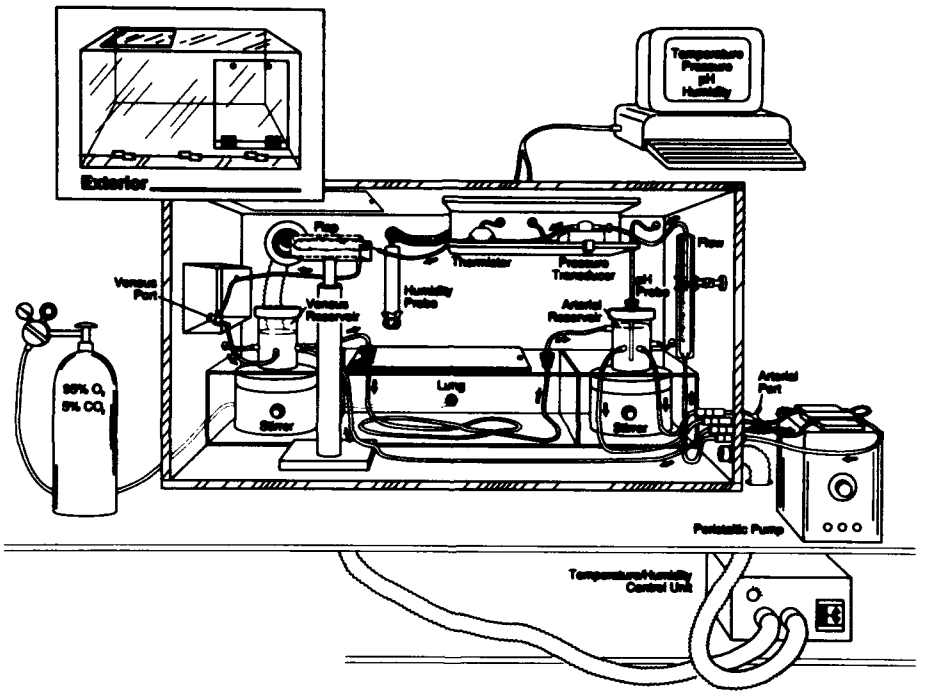

Figure 2. Schematic diagram of the IPPSF perfusion chamber.

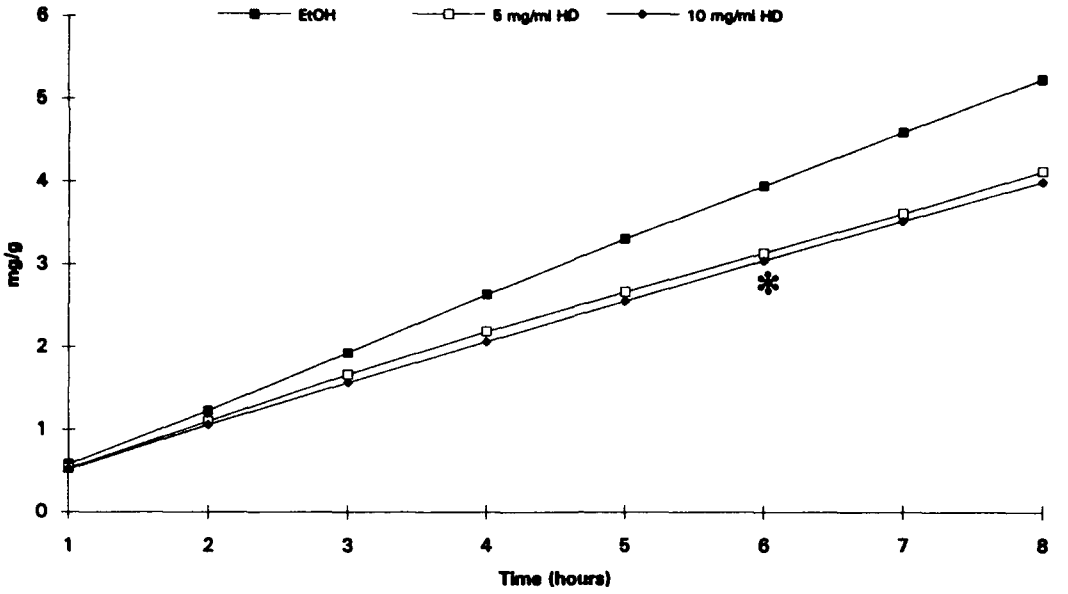

Figure 3. Cumulative glucose utilization in IPPSFs exposed to 5.0 mg/ml and 10.0 mg/ml of HD and ethanol controls. *Significant difference ($p < 0.05$) occurs.

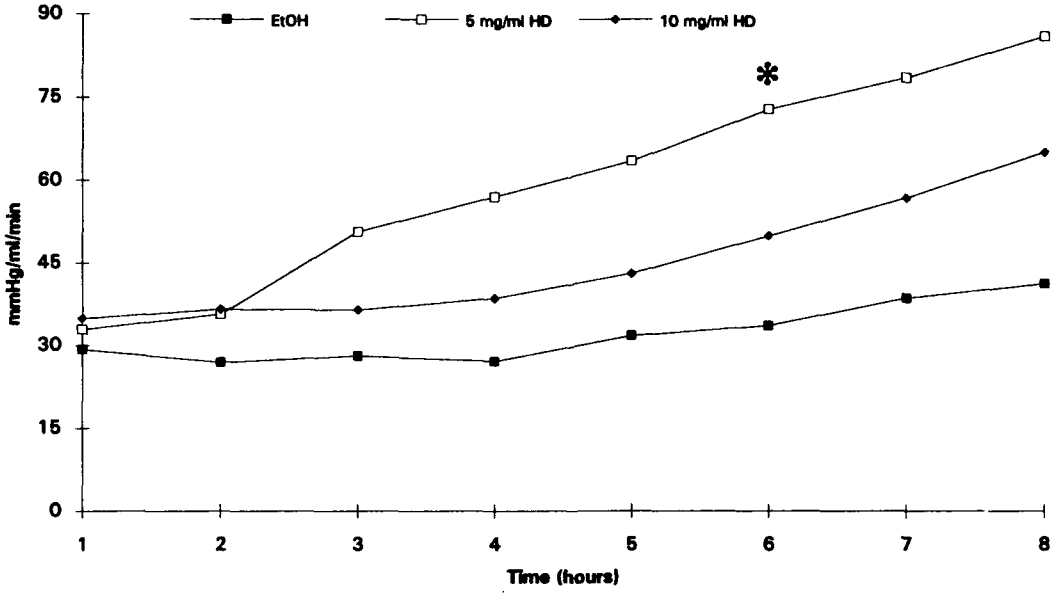

Figure 4. Vascular resistance of IPPSFs exposed to 5.0 mg/ml and 10 mg/ml of HD and ethanol controls.
* Significant difference ($p < 0.05$) occurs.

Figure 5. Light micrograph of an IPPSF exposed to 5.0 mg/ml of HD showing separation of the epidermal-dermal junction. H&E (X 375)

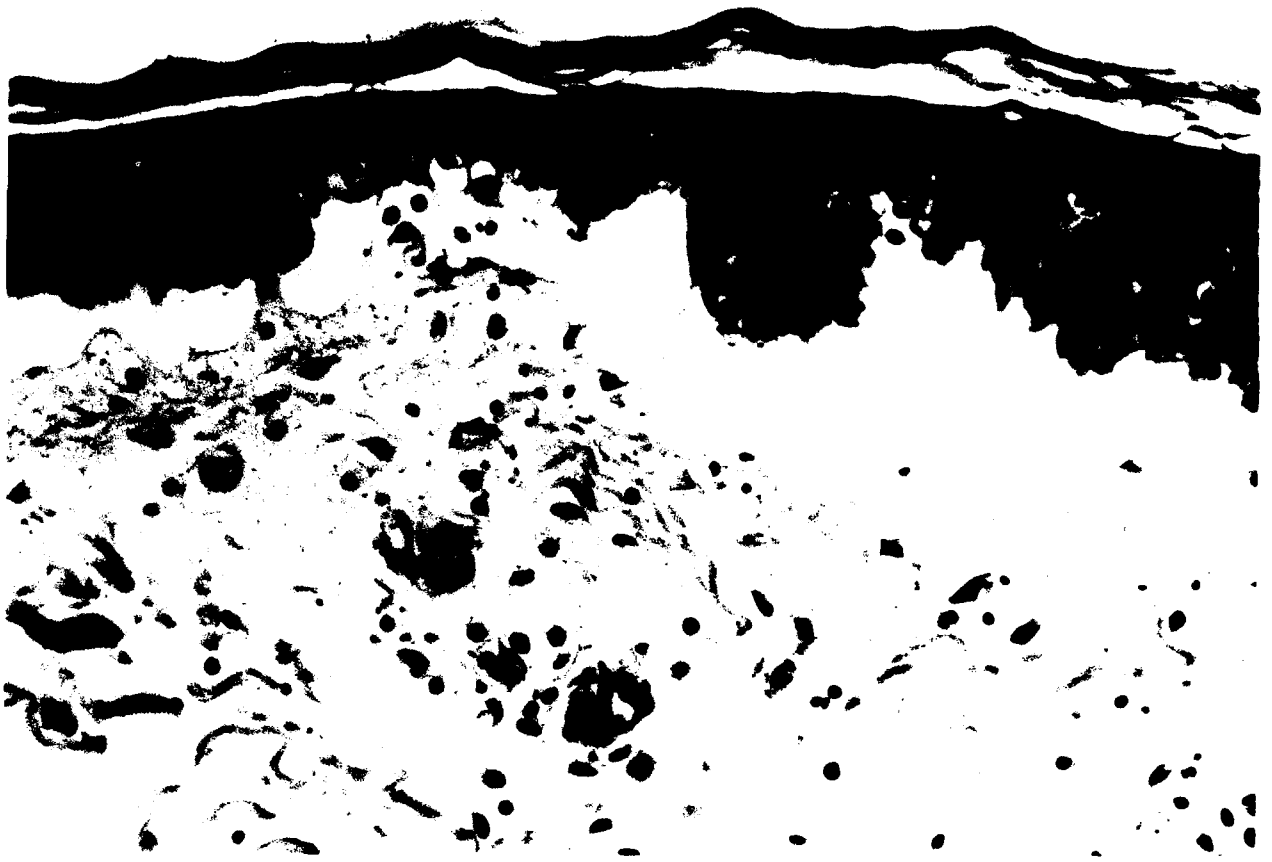

Figure 6. Light micrograph of an IPPSF exposed to 10.0 mg/ml of HD depicting epidermal-dermal separation. H&E (X 420)

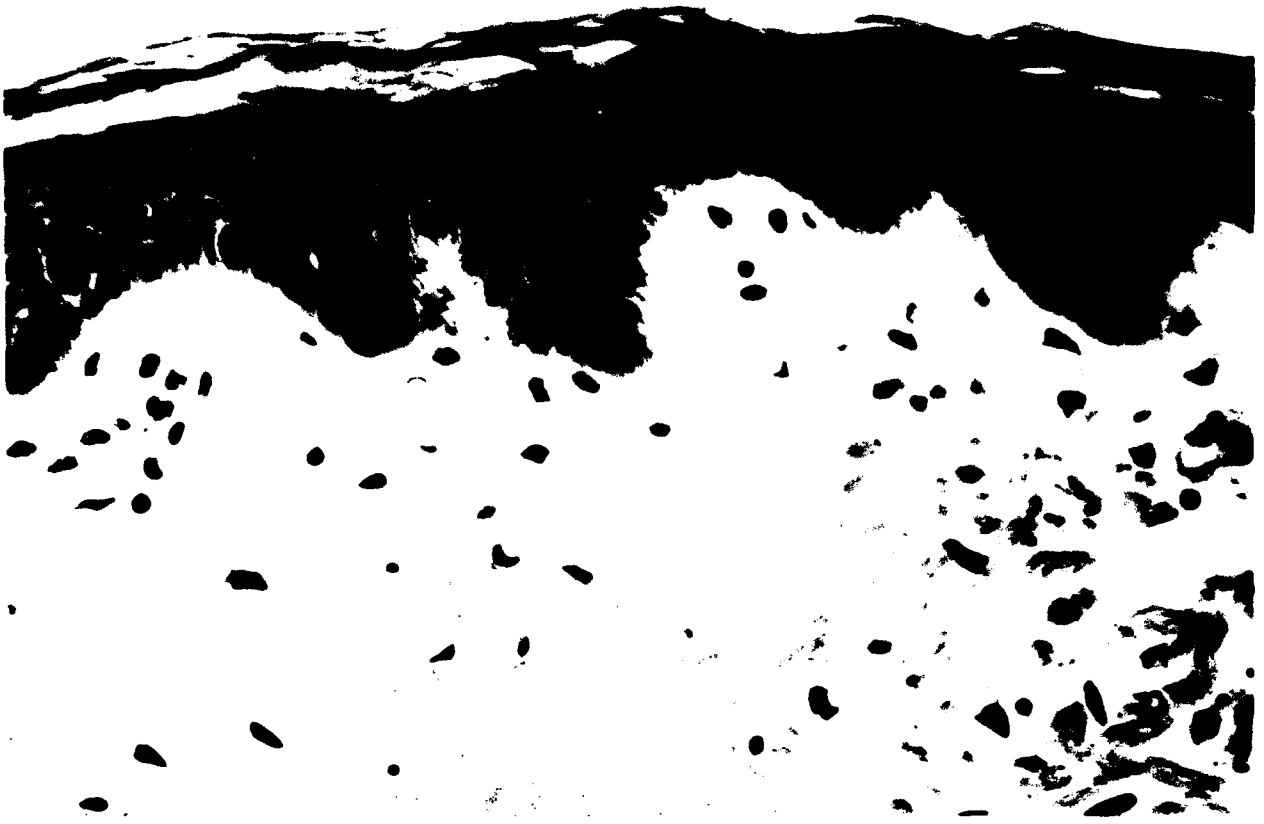

Figure 7. Light micrograph of an IPPSF dosed with ethanol showing normal morphology. H&E (X450)

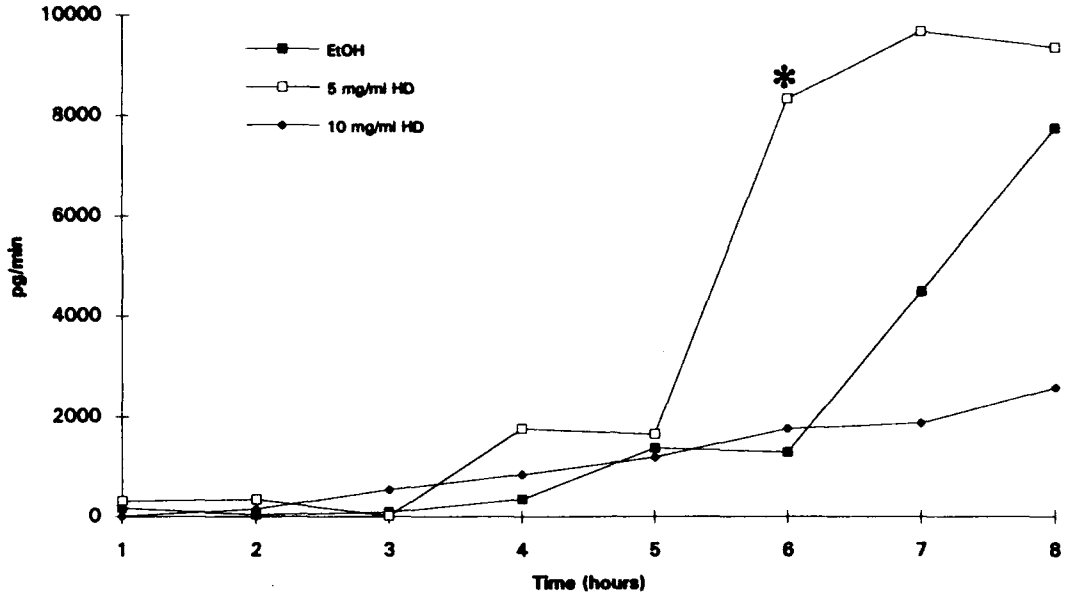

Figure 8. IPPSF venous concentration profiles of PGE_2 for 5.0 mg/ml and 10.0 mg/ml of HD and ethanol controls. *Significant difference ($p < 0.05$) occurs.

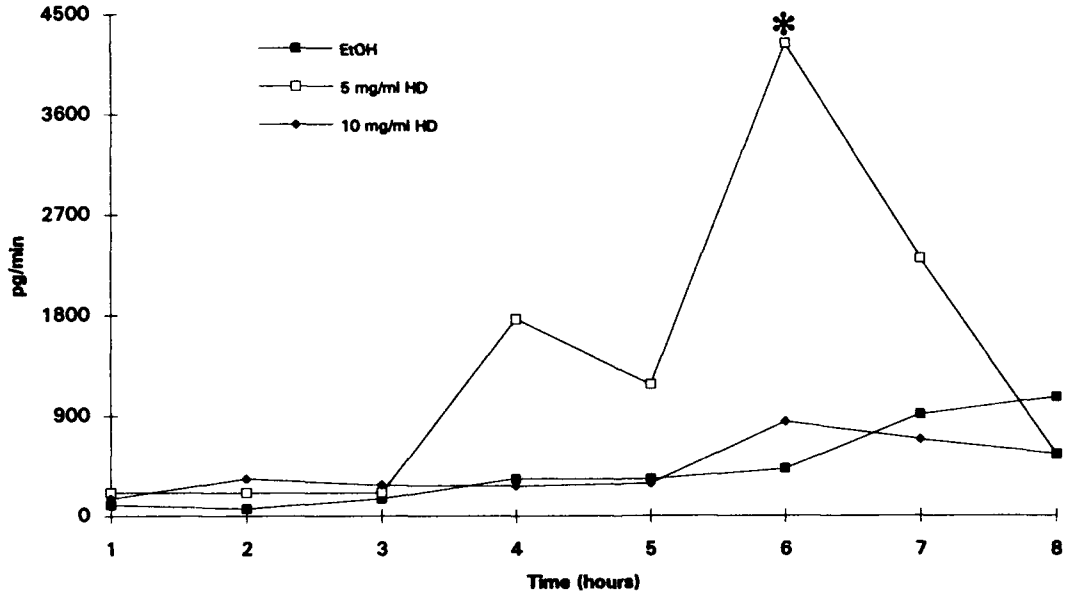

Figure 9. IPPSF venous concentration profile of $PGF_{2\alpha}$ for 5.0 mg/ml and 10.0 mg/ml of HD and ethanol controls. *Significant difference ($p < 0.05$) occurs.

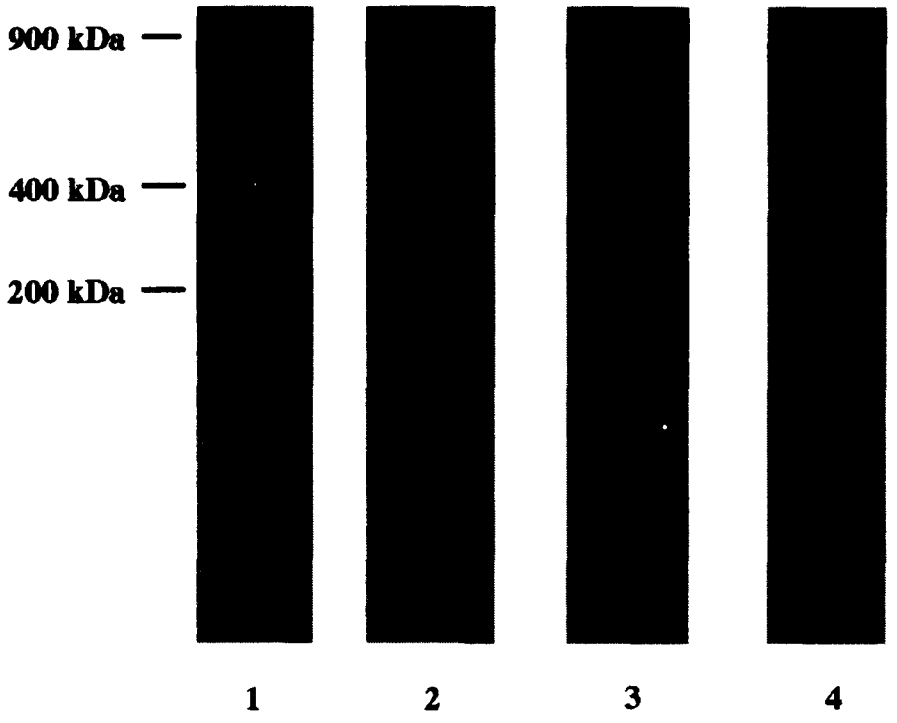

Figure 10. Nonreduced SDS-PAGE analysis of HD-treated UM-UC-9 laminin on a 3-10% acrylamide gradient gel. Lane 1: laminin treated with 10.0 mg/ml HD in ethanol; Lane 2: laminin treated with 1.0 mg/ml HD in ethanol; Lane 3: laminin treated with ethanol control; Lane 4: untreated laminin.

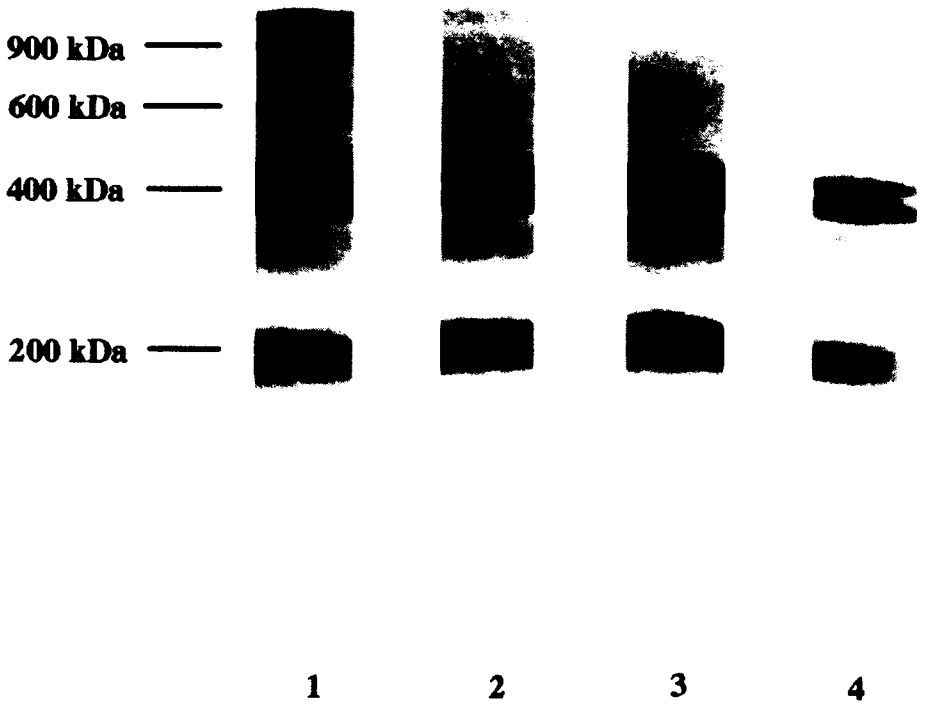

Figure 11. Reduced SDS-PAGE analysis of HD-treated UM-UC-9 laminin on a 3-10% acrylamide gradient gel. Lane 1: laminin treated with 10.0 mg/ml HD in ethanol; Lane 2: laminin treated with 1.0 mg/ml HD in ethanol; Lane 3: laminin treated with ethanol control; Lane 4: untreated laminin.

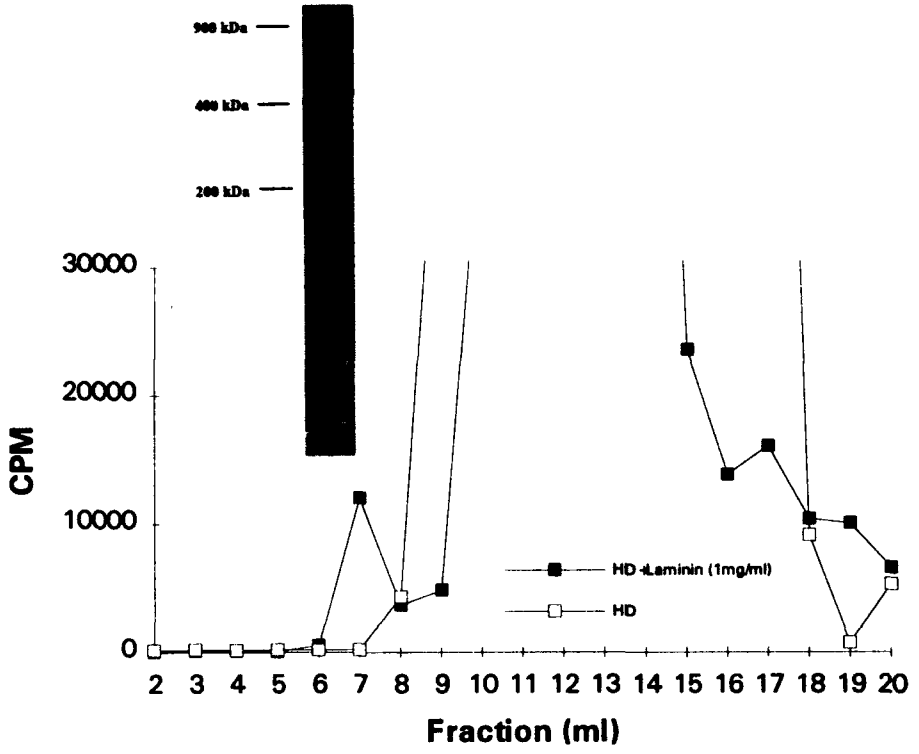

Figure 12. Covalent modification of EHS laminin by ^{14}C-HD. ^{14}C-HD was incubated with either EHS laminin in Tris-Cl buffer (■), or Tris-Cl buffer alone (□). ^{14}C-HD-treated laminin was purified by gel filtration, and analyzed by reduced SDS-PAGE.

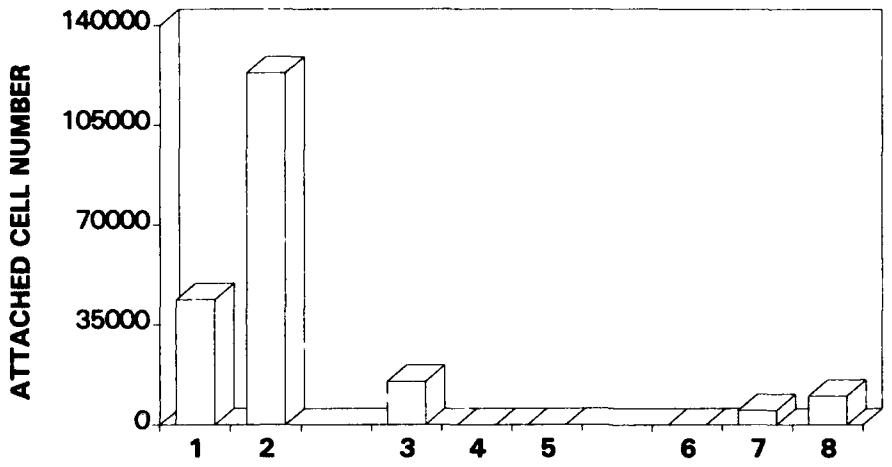

Figure 13. Effect of laminin and HD-alkylated laminin on UM-UC-9 cell adhesion. Cell adhesion to PBS-treated dishes (Column 1); dishes coated with 10.0 μg/ml of laminin (Column 2); 1.0 μg/ml of HD-treated laminin (Column 3); 3.0 μg/ml of HD-treated laminin (Column 4); 10.0 μg/ml of HD-treated laminin (Column 5); 3.0 μg/ml of both laminin and HD-treated laminin (Column 6); 10.0 μg/ml of laminin and 3.0 μg/ml of HD-treated laminin (Column 7); and 20.0 μg/ml of laminin and 3.0 μg/ml of HD-treated laminin (Column 8).

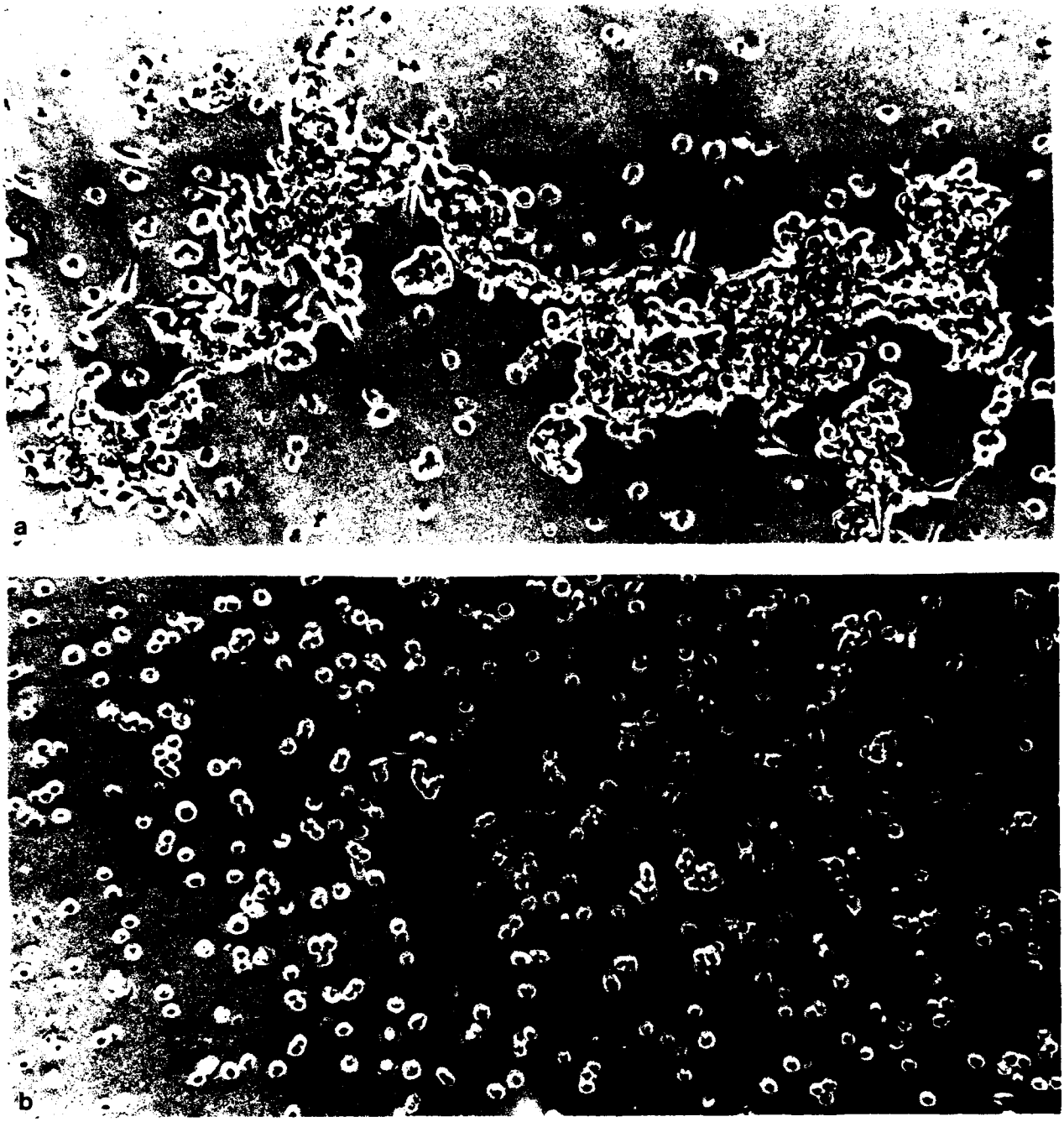

Figure 14. UM-UC-9 cells 20 hours after primary plating on dishes coated with 10.0 μg/ml of laminin (a) and 10.0 μg/ml of HD-treated laminin (b).

Figure 15. IH showing laminin staining in an ethanol-treated IPPSF. Note continuous staining along the EDJ (arrows) and capillary basement membrane (arrowheads). (X400)

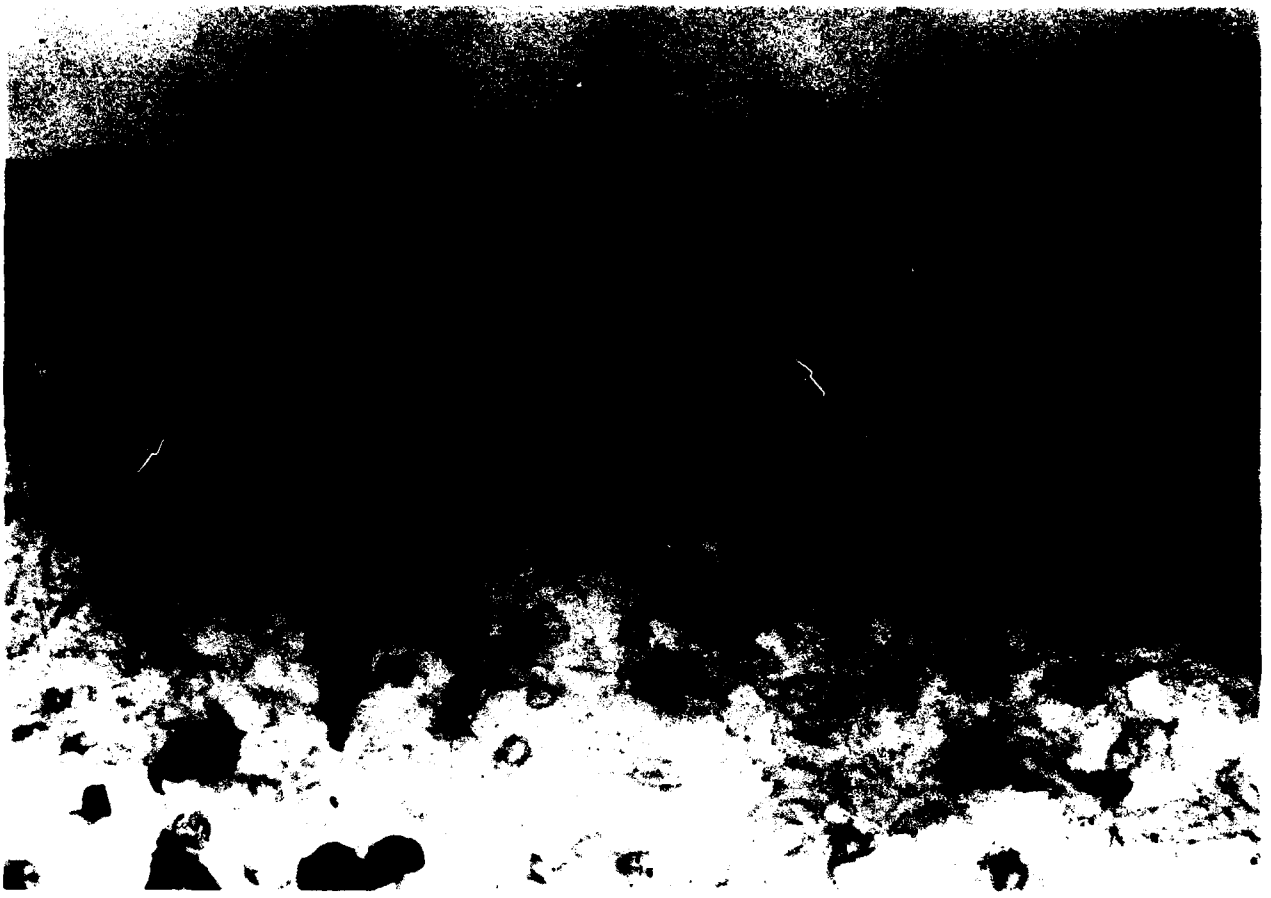

Figure 16. IH showing laminin binding in a 10.0 mg/ml of HD-blistered IPPSF. Laminin stained the dermal side (large arrows) with laminin fragments attached to the stratum basale cells (small arrows). (X400)

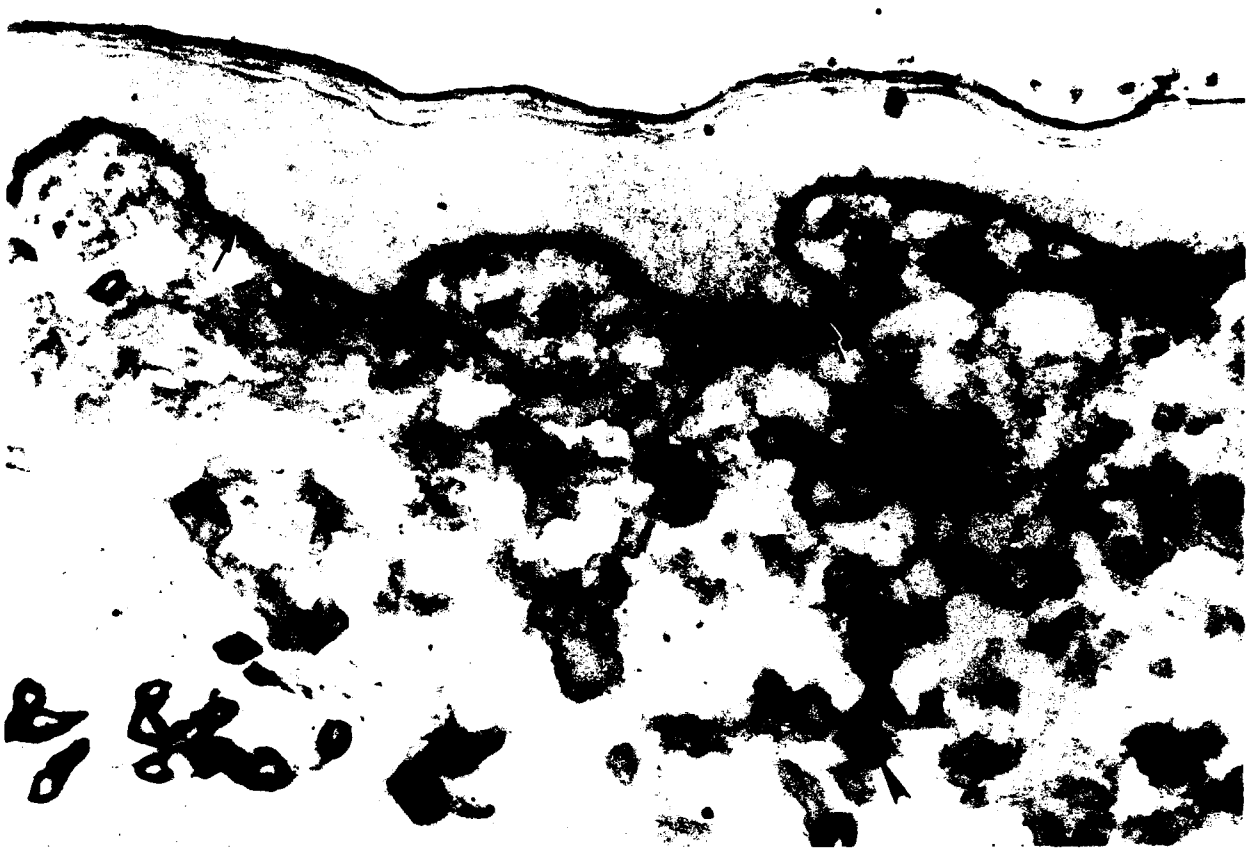

Figure 17. IH showing type IV collagen staining in an ethanol IPPSF. Note continuous staining along the EDJ (arrows) and capillary basement membranes (arrowheads). (X450)

Figure 18. IH showing type IV collagen staining in a 5.0 mg/ml of HD IPPSF. Type IV collagen bound exclusively to the dermis (arrows). (X450)

Figure 19. IH showing BPA staining in an ethanol IPPSF. Note continuous staining along the EDJ (arrows). (X400)

Figure 20. IH showing BPA staining in a 10.0 mg/ml of HD IPPSF. BPA staining was limited to the basal pole of the stratum basale cells (arrows). (X400)

Figure 21. IH showing EBA staining in an ethanol IPPSF. Staining was continuous along the EDJ (arrows). (X400)

Figure 22. IH showing EBA staining in a 10.0 mg/ml of HD IPPSF. Note EBA staining was bound to the dermis (arrows). (X400)

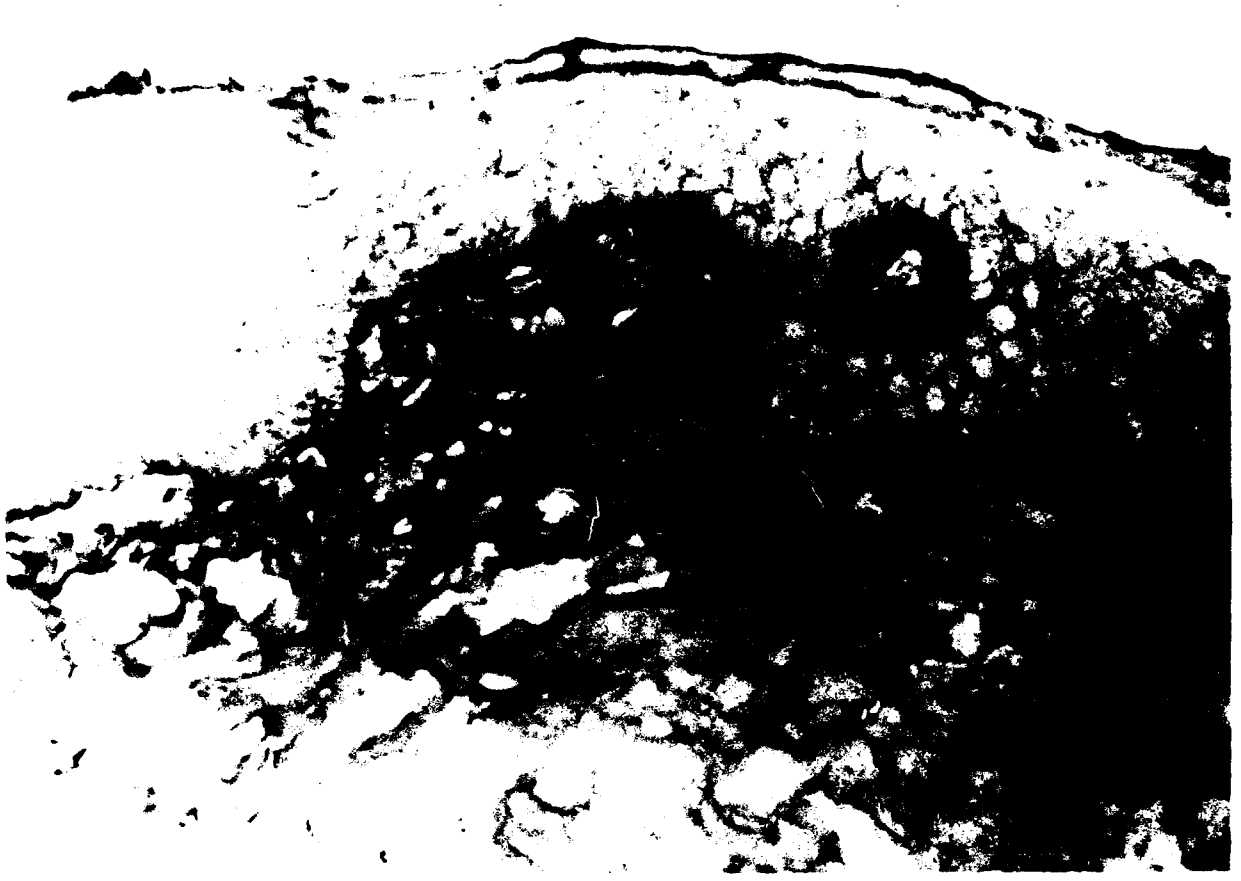

Figure 23. IH showing fibronectin staining in an ethanol IPPSF. Note the weak but continuous stain along the EDJ (arrows). (X450)

Figure 24. IH showing fibronectin staining in a 10.0 mg/ml of HD IPPSF. Fibronectin staining was primarily localized to the dermis (large arrows) but fragmented staining was attached to the basal cells (small arrows). (X400)

Figure 25. IF of GB_3 exhibiting continuous binding along a non blistered area of the EDJ of a 5.0 mg/ml of HD IPPSF (arrows). (X375)

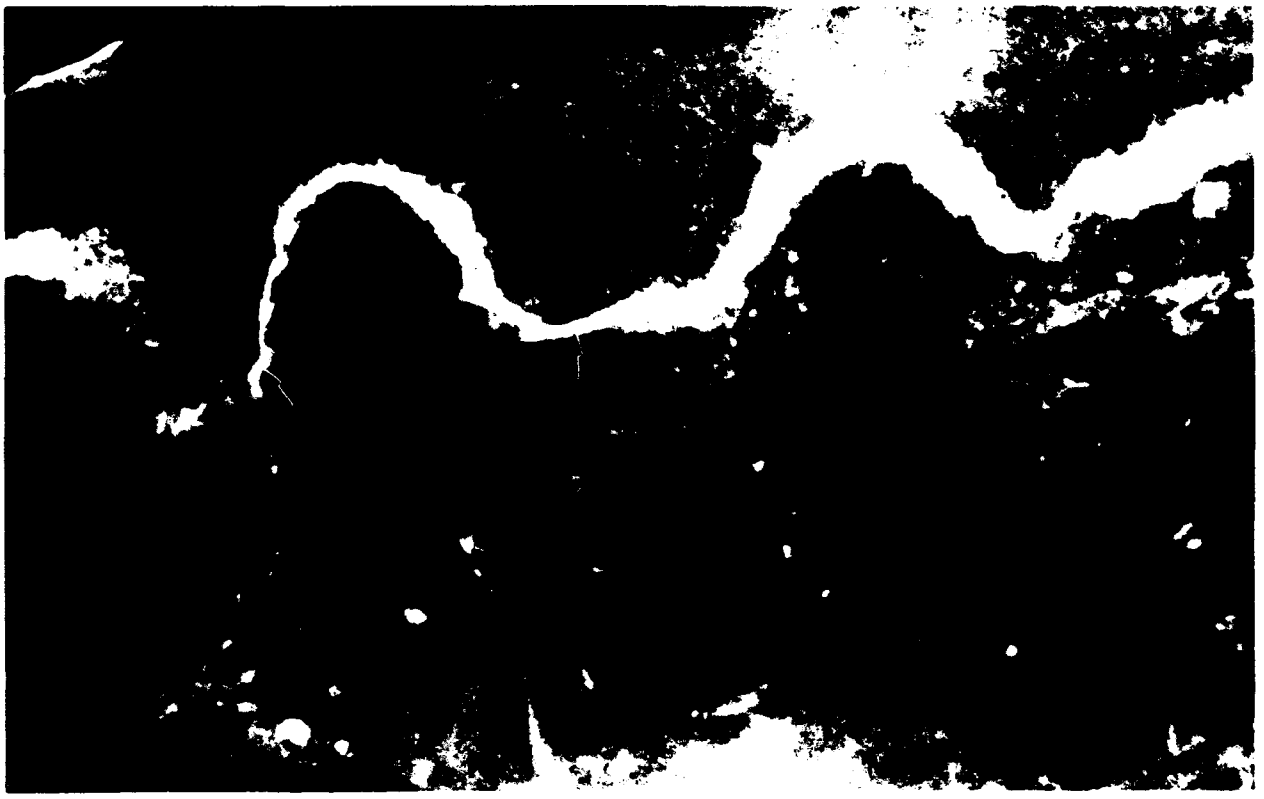

Figure 26. IF of a GB_3 exhibiting continuous staining along the dermis of a 10.0 mg/ml of HD IPPSF (arrows). (X450)

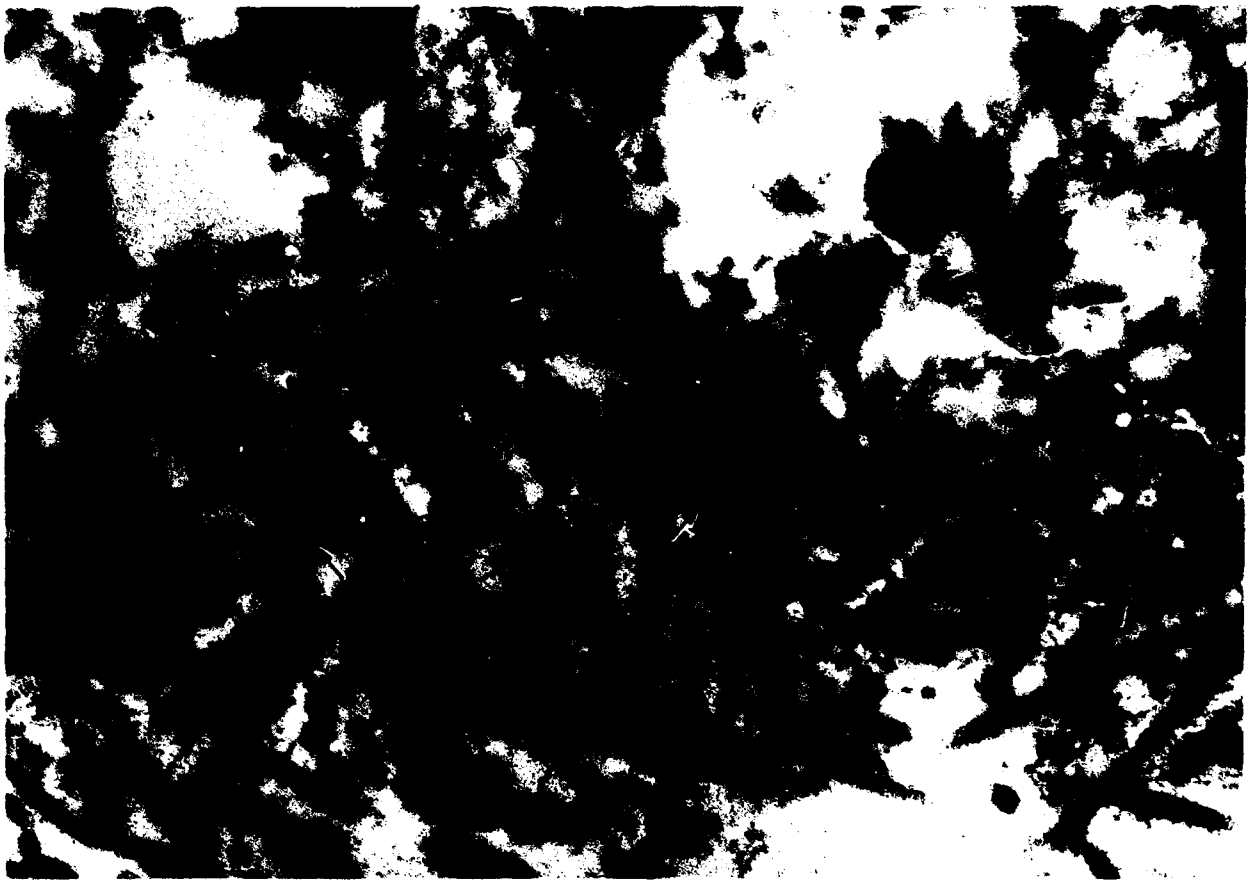

Figure 27. IEM of laminin binding within the lamina lucida (arrows) in an ethanol IPPSF. (X33,900)

Figure 28. IEM of laminin binding to the dermis in a 10.0 mg/ml of HD IPPSF (arrows). Note fragmented staining (arrowheads) along the basal cells of the dermis. (X41,800)

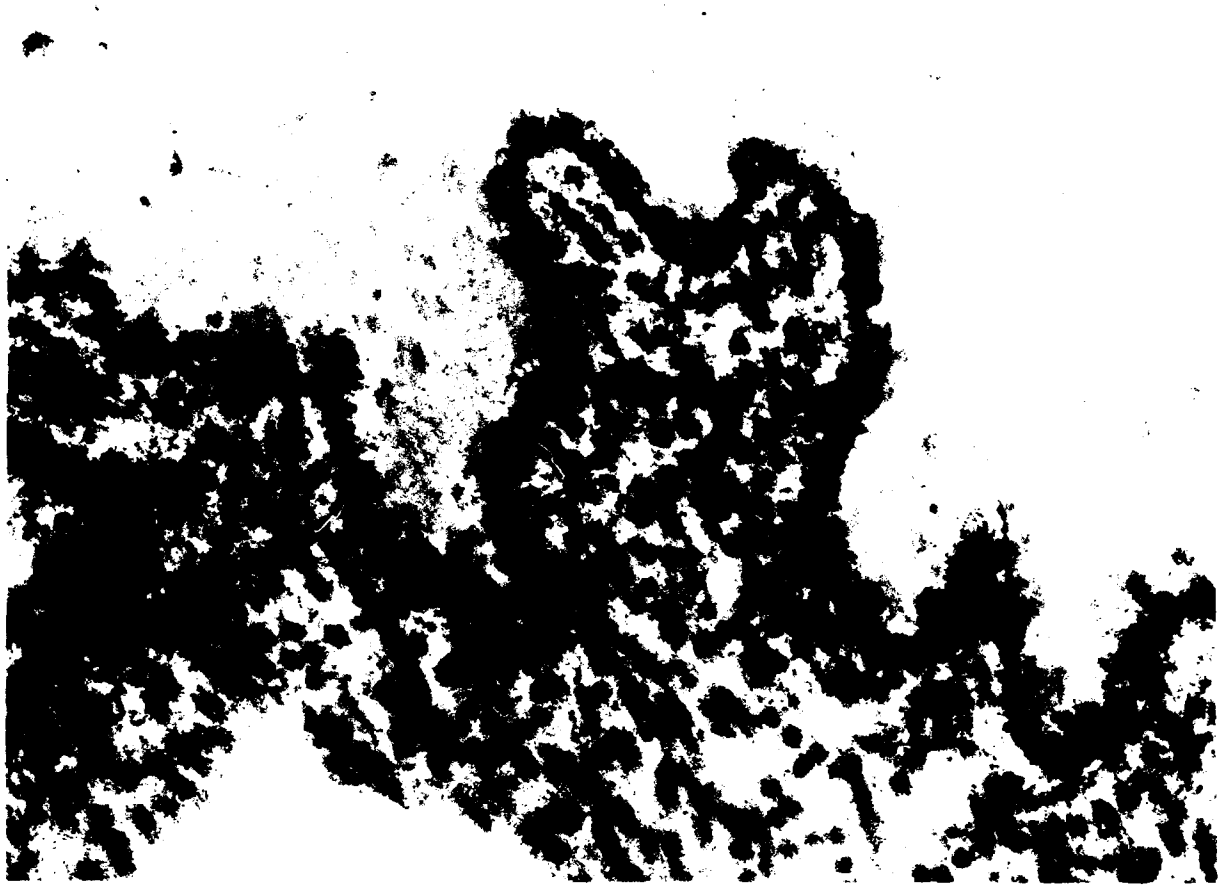

Figure 29. IEM exhibiting type IV collagen binding to the lamina densa (arrows) in an ethanol IPPSF. (X41,800)

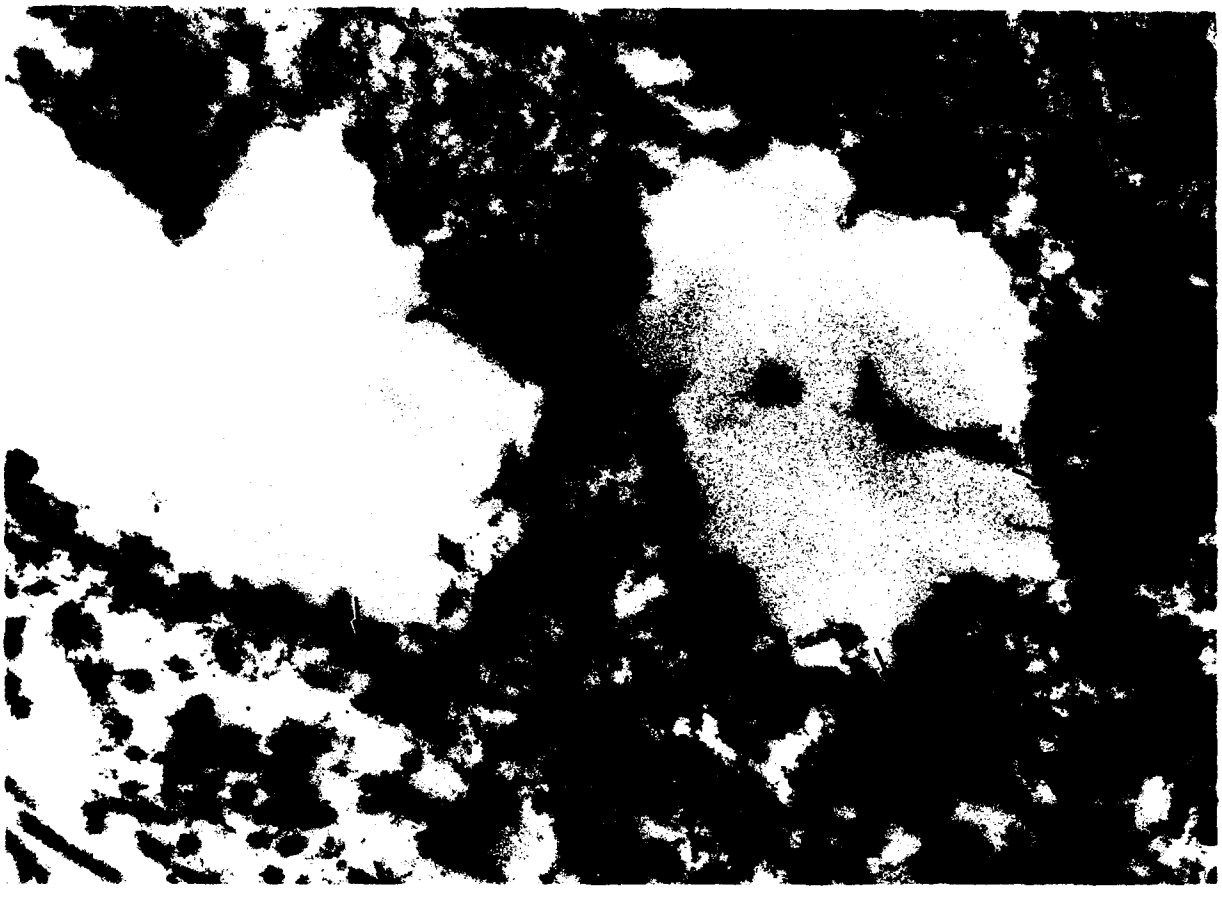

Figure 30. IEM exhibiting type IV collagen binding to the dermis (arrows) of a 10.0 mg/ml of HD IPPSF. (X37,000)

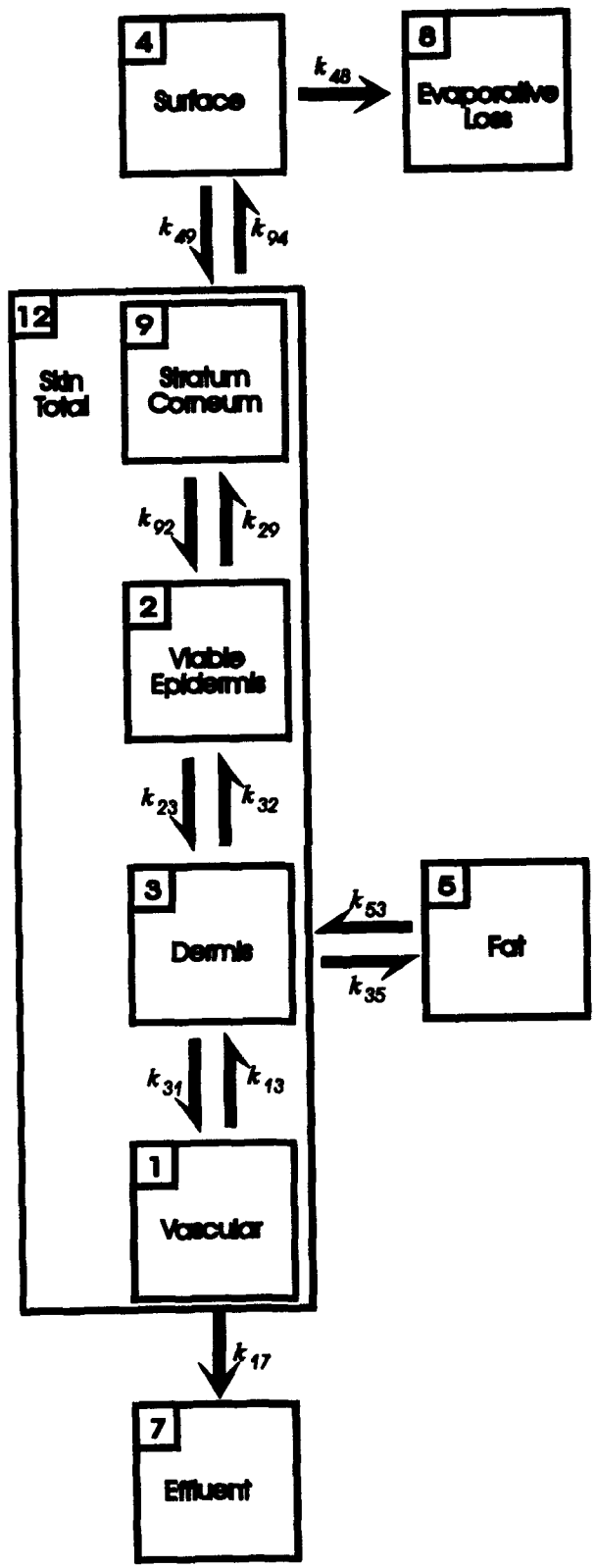

Figure 31: Passive Topical Kinetic Model.

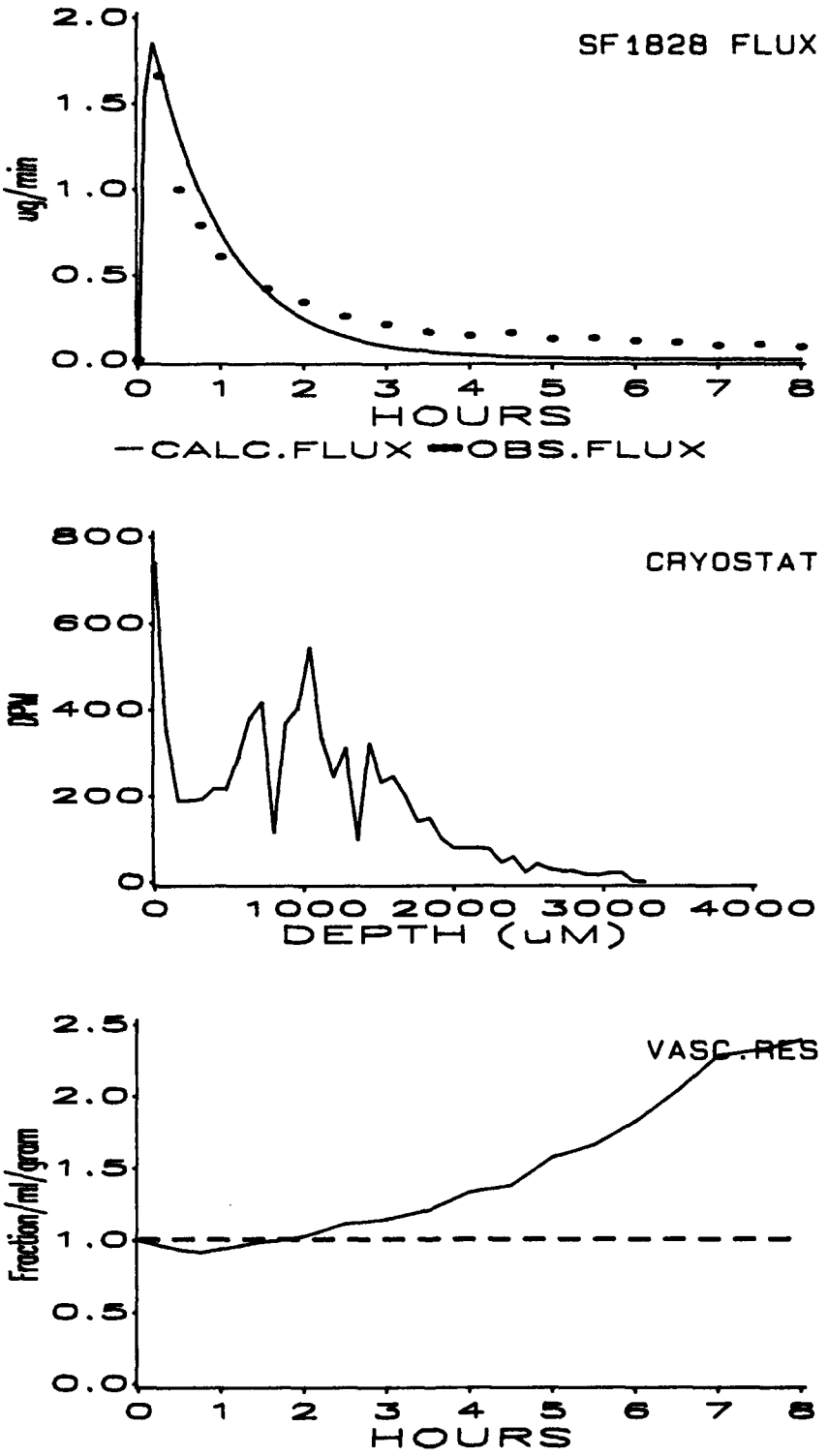

Figure 32: IPPSF 1828: (Dose = 3000 μg ^{14}C-HD in ethanol). Calculated vs observed venous flux; cryostat depth of penetration; and VR fraction of initial value.

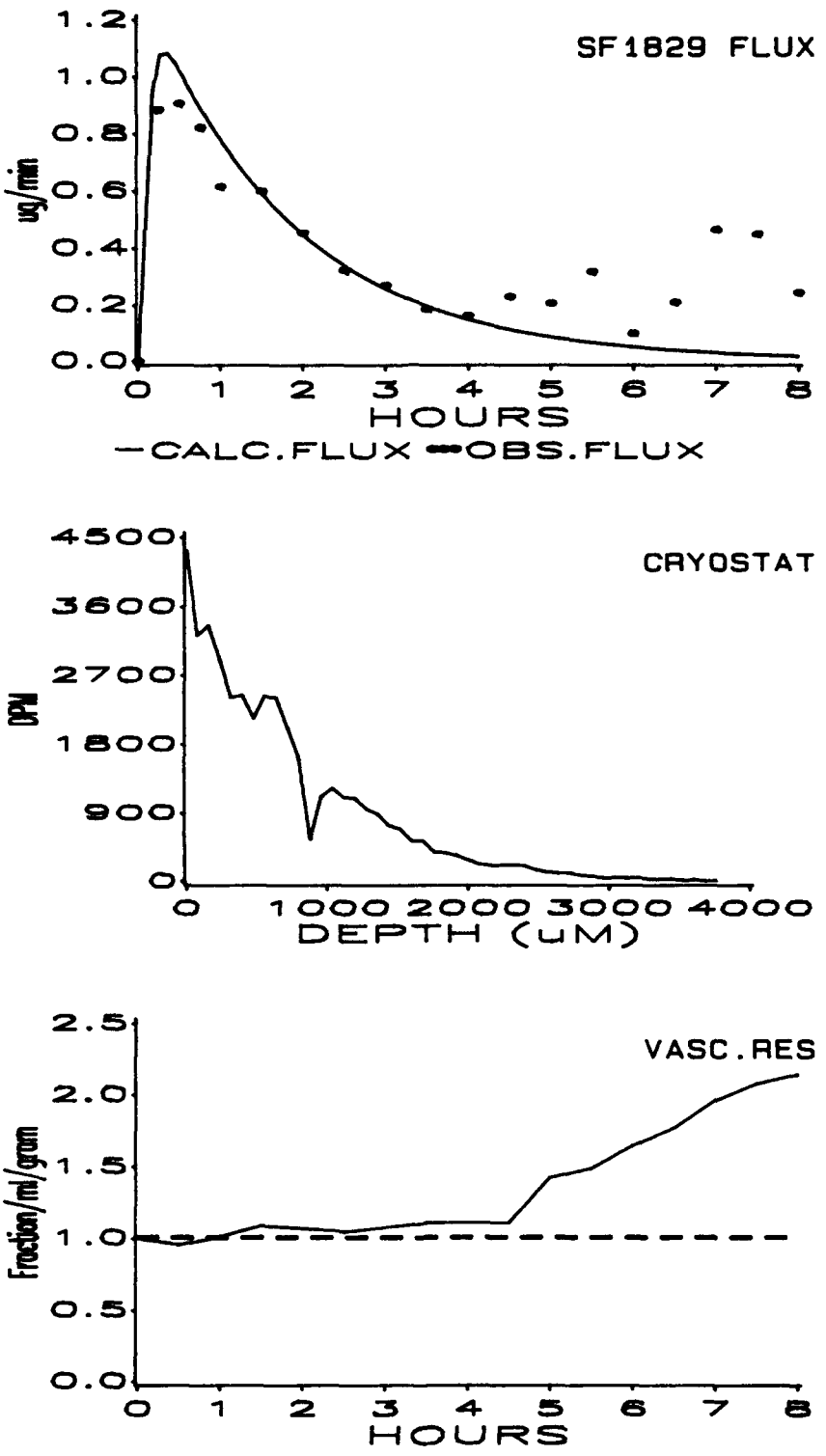

Figure 33: IPPSF 1829: (Dose = 3000 μg ^{14}C-HD in ethanol). Calculated vs observed venous flux; cryostat depth of penetration; and VR fraction of initial value.

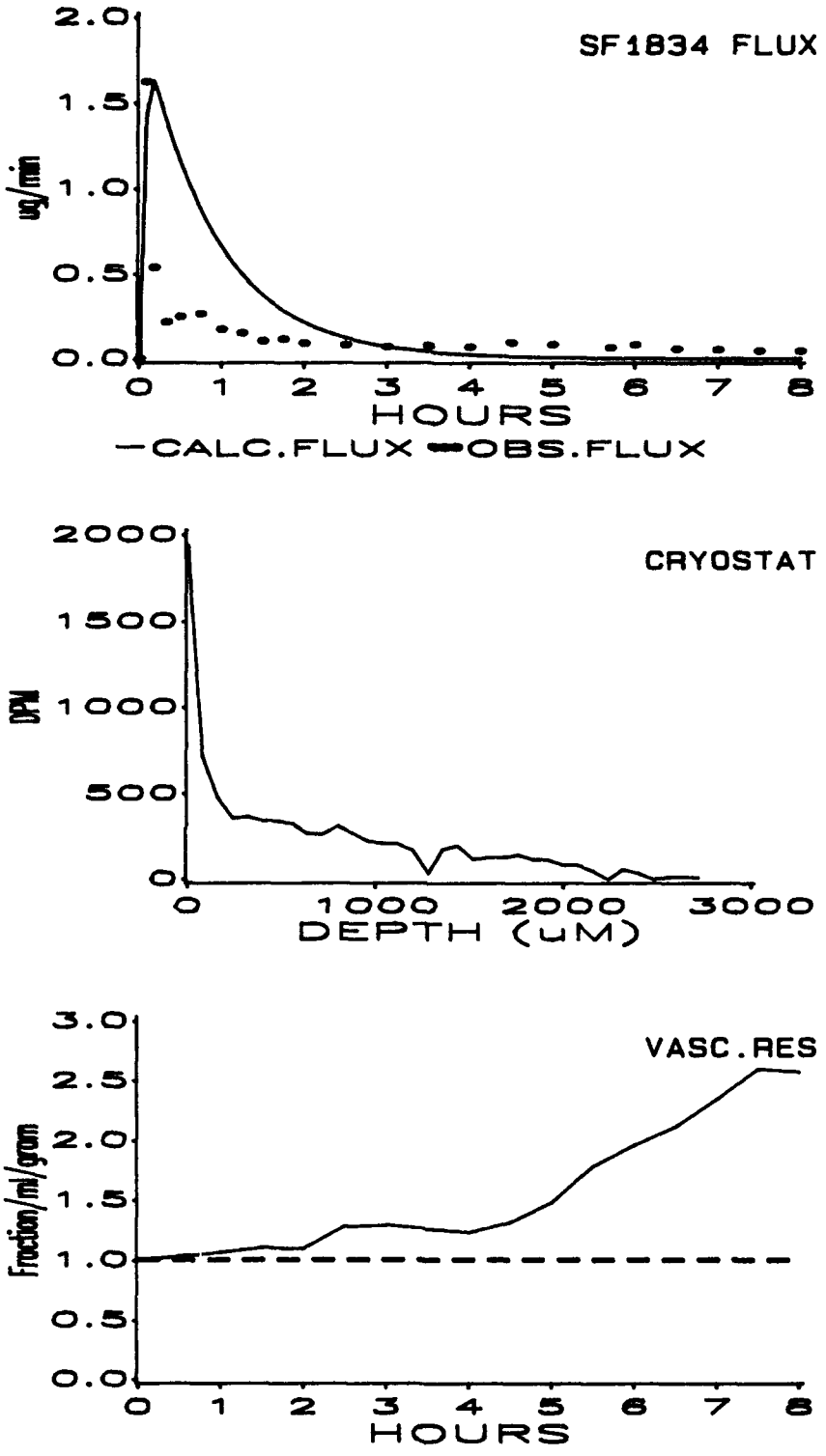

Figure 34: IPPSF 1834: (Dose = 3000 μg ^{14}C-HD in ethanol). Calculated vs observed venous flux; cryostat depth of penetration; and VR fraction of initial value.

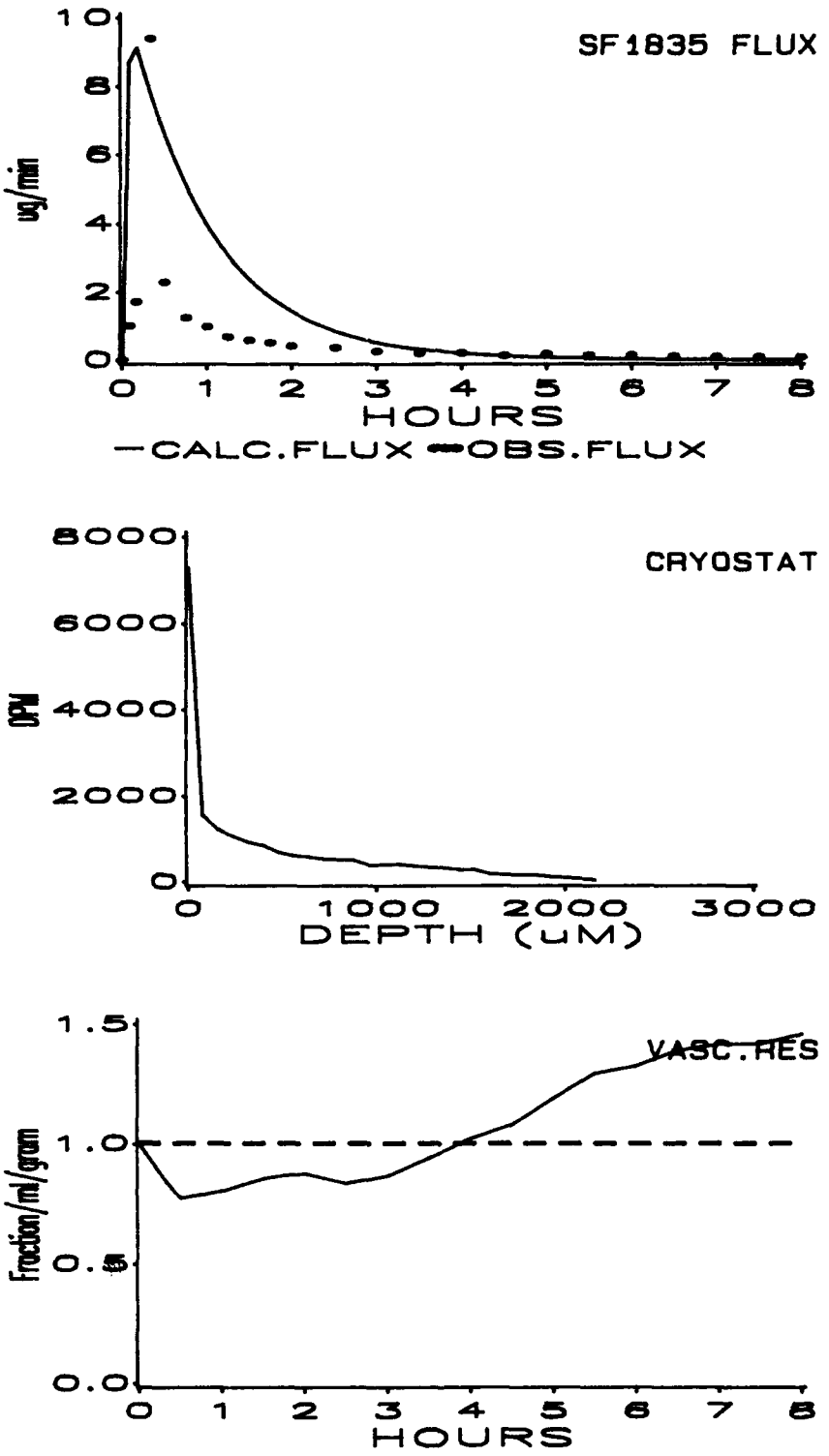

Figure 35: IPPSF 1835: (Dose = 3000 µg ^{14}C-HD in ethanol). Calculated vs observed venous flux; cryostat depth of penetration; and VR fraction of initial value.

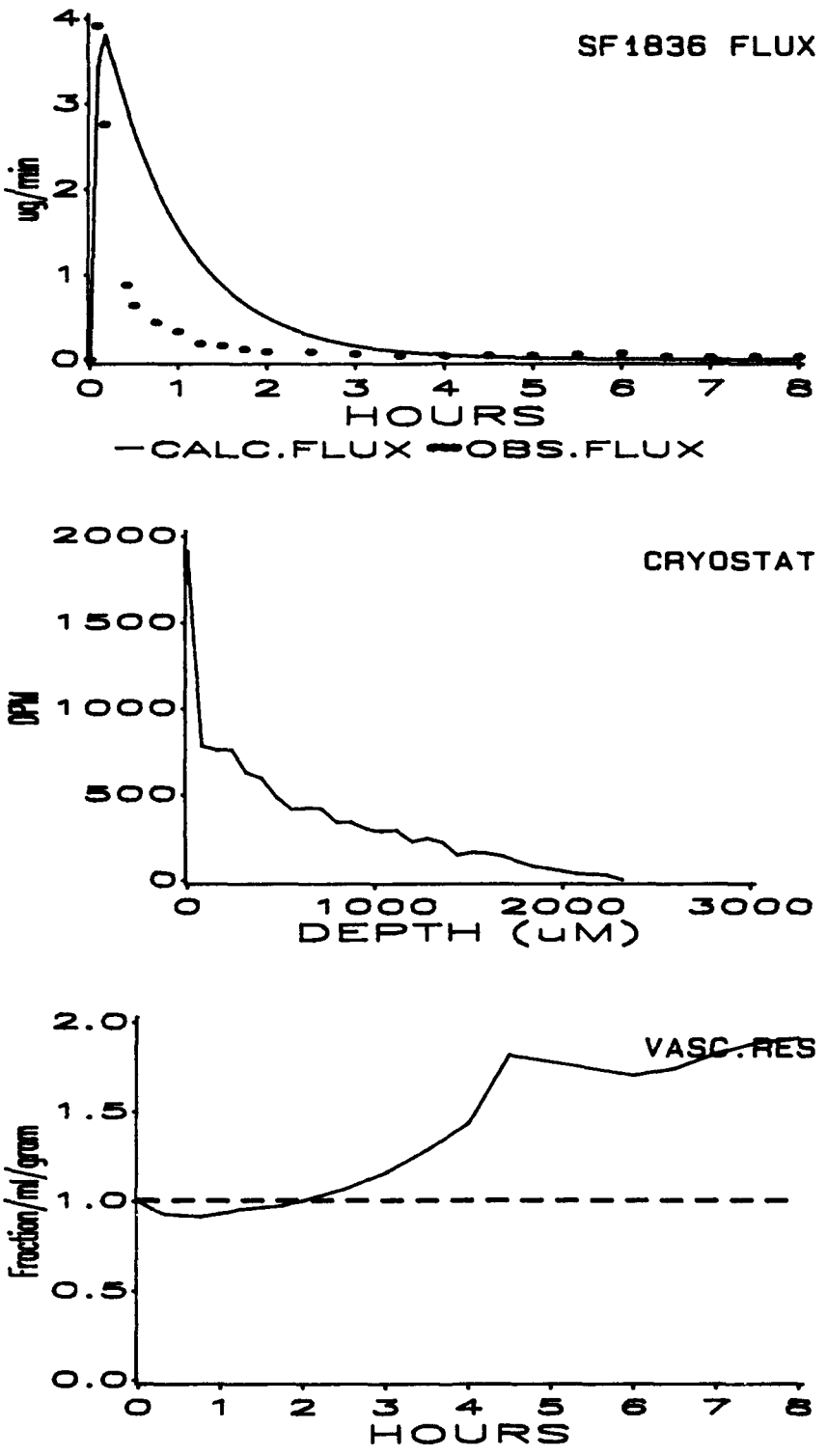

Figure 36: IPPSF 1836: (Dose = 3000 μg ^{14}C-HD in ethanol). Calculated vs observed venous flux; cryostat depth of penetration; and VR fraction of initial value.

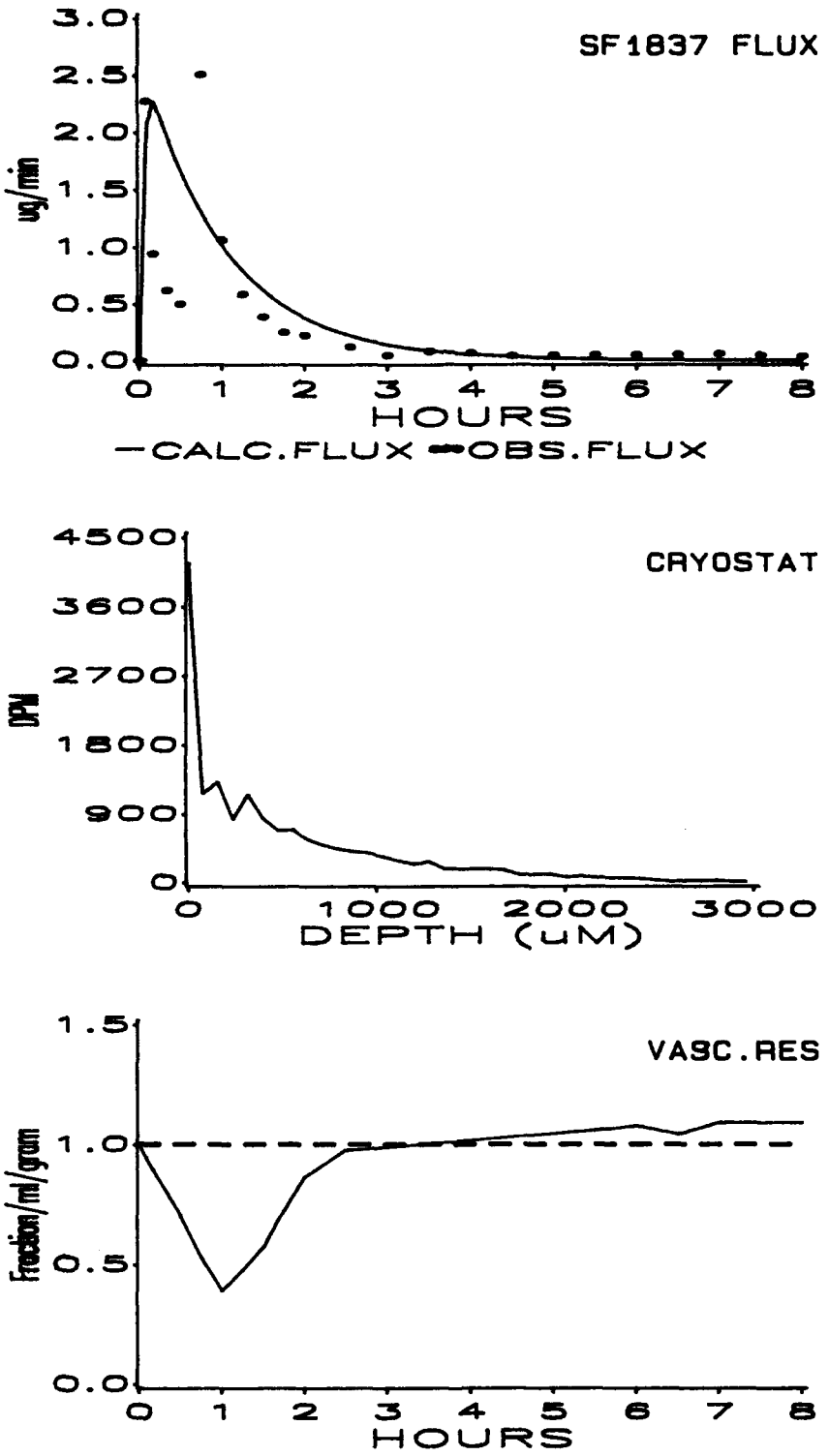

Figure 37: IPPSF 1837: (Dose = 3000 μg ^{14}C-HD in ethanol). Calculated vs observed venous flux; cryostat depth of penetration; and VR fraction of initial value.

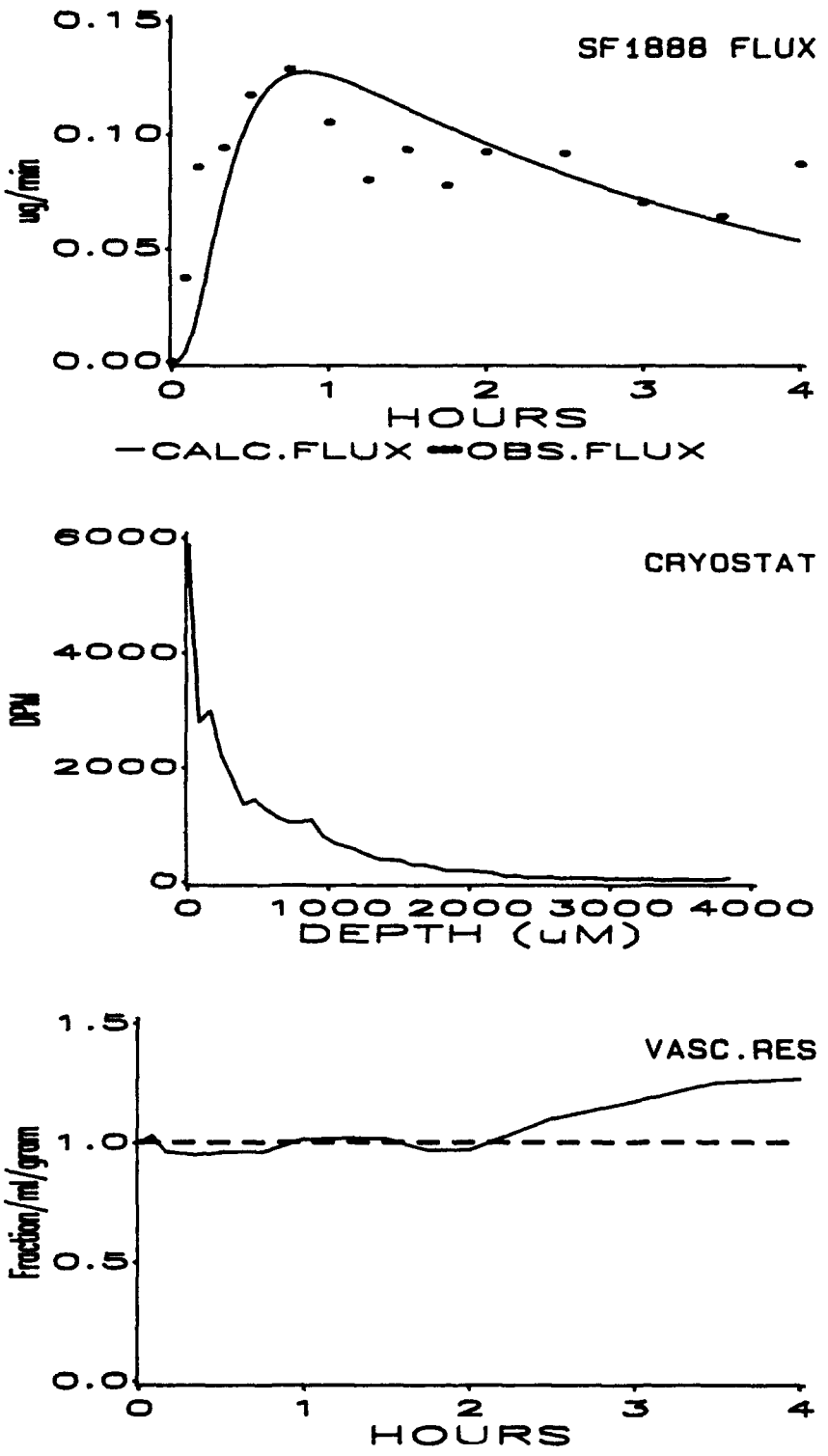

Figure 38: IPPSF 1888: (Dose = 3000 μg ^{14}C-HD in ethanol). Calculated vs observed venous flux; cryostat depth of penetration; and VR fraction of initial value.

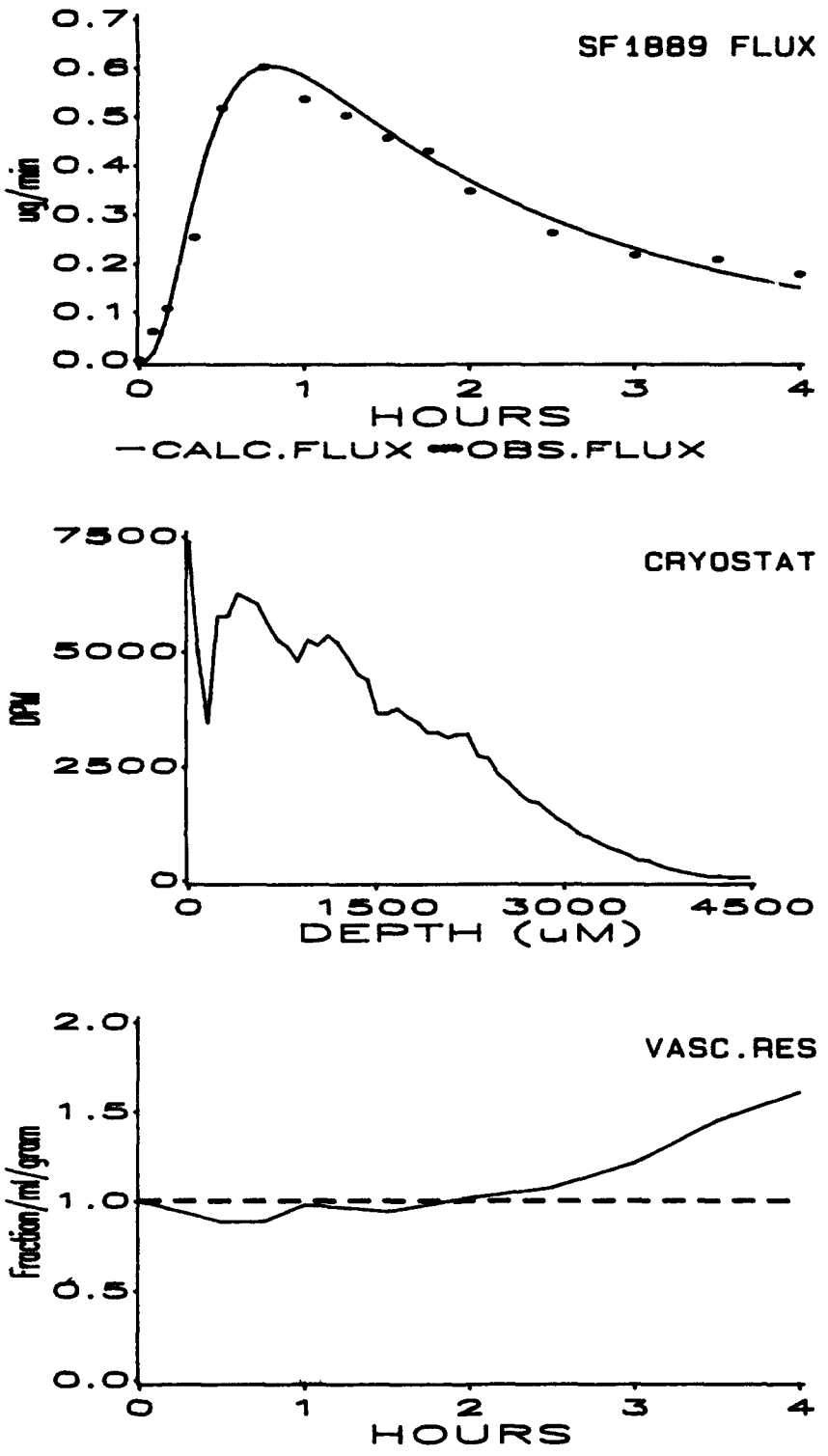

Figure 39: IPPSF 1889: (Dose = 3000 μg ^{14}C-HD in ethanol). Calculated vs observed venous flux; cryostat depth of penetration; and VR fraction of initial value.

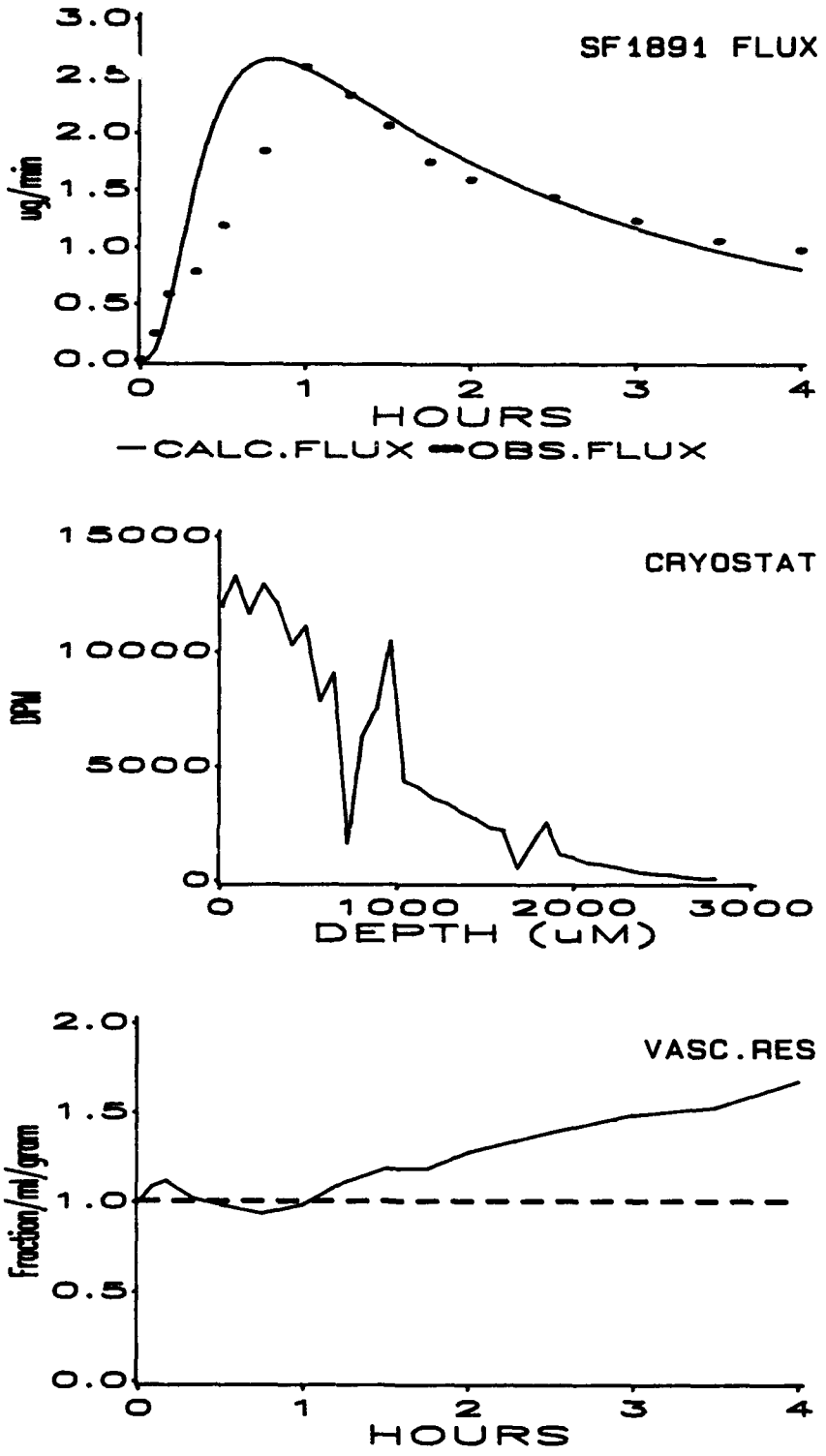

Figure 40: IPPSF 1891: (Dose = 3000 μg ^{14}C-HD in ethanol). Calculated vs observed venous flux; cryostat depth of penetration; and VR fraction of initial value.

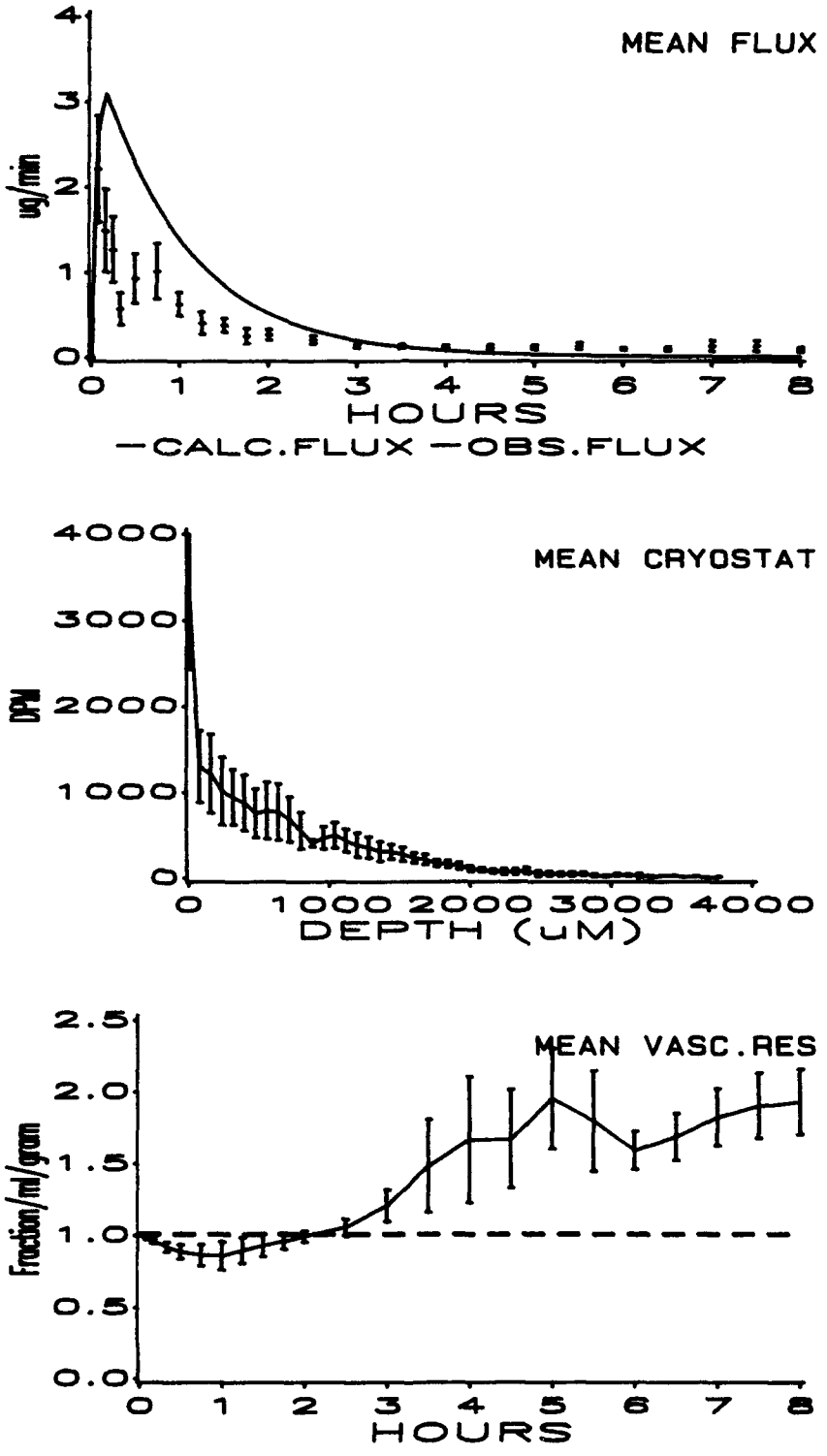

Figure 41: Mean of 8-hour IPPSFs: (Dose = 3000 μg ^{14}C-HD in ethanol). Calculated vs observed venous flux; cryostat depth of penetration; and VR fraction of initial value.

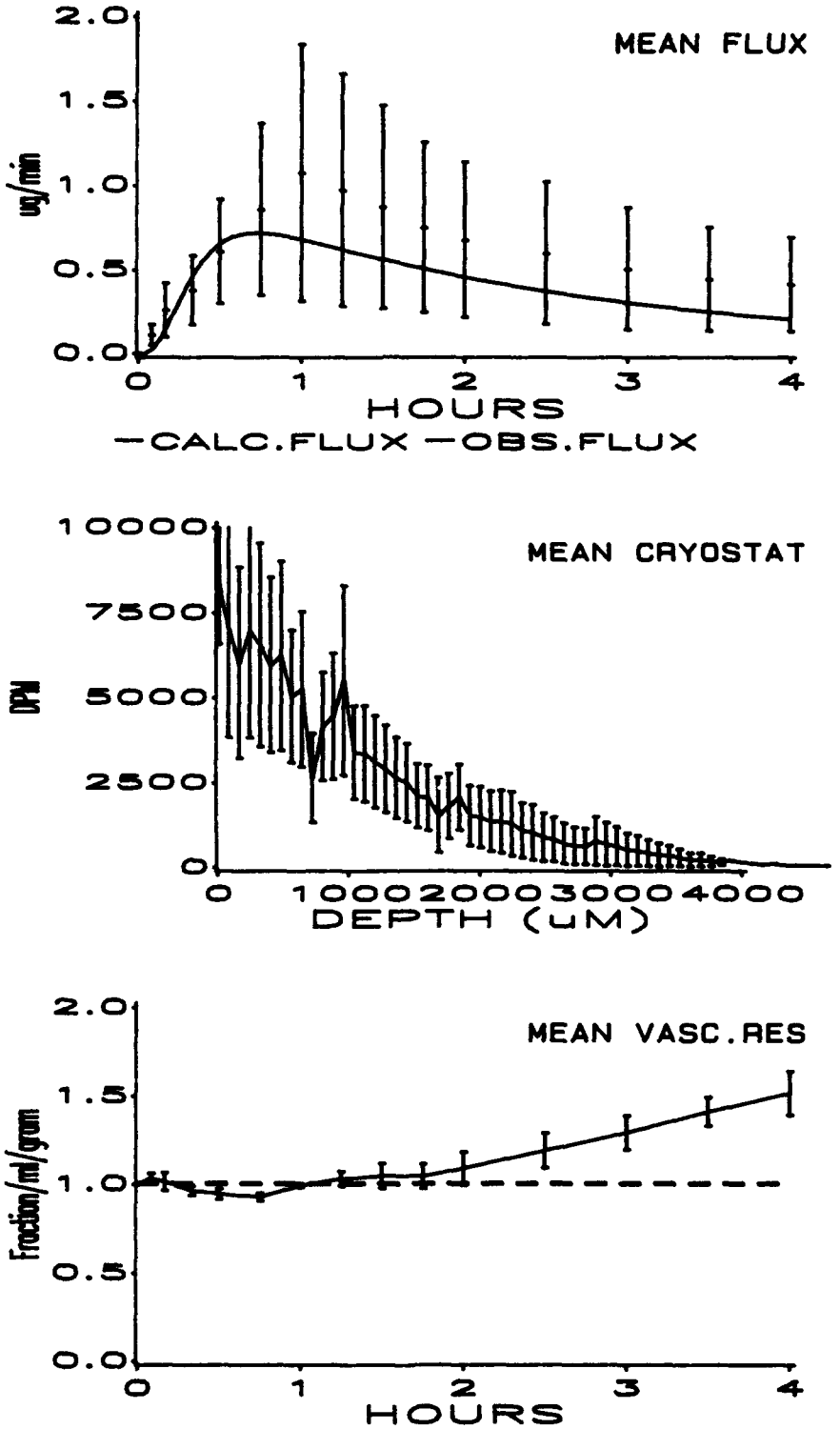

Figure 42: Mean of 4-hour IPPSFs: (Dose = 3000 μg ^{14}C-HD in ethanol). Calculated vs observed venous flux; cryostat depth of penetration; and VR fraction of initial value.

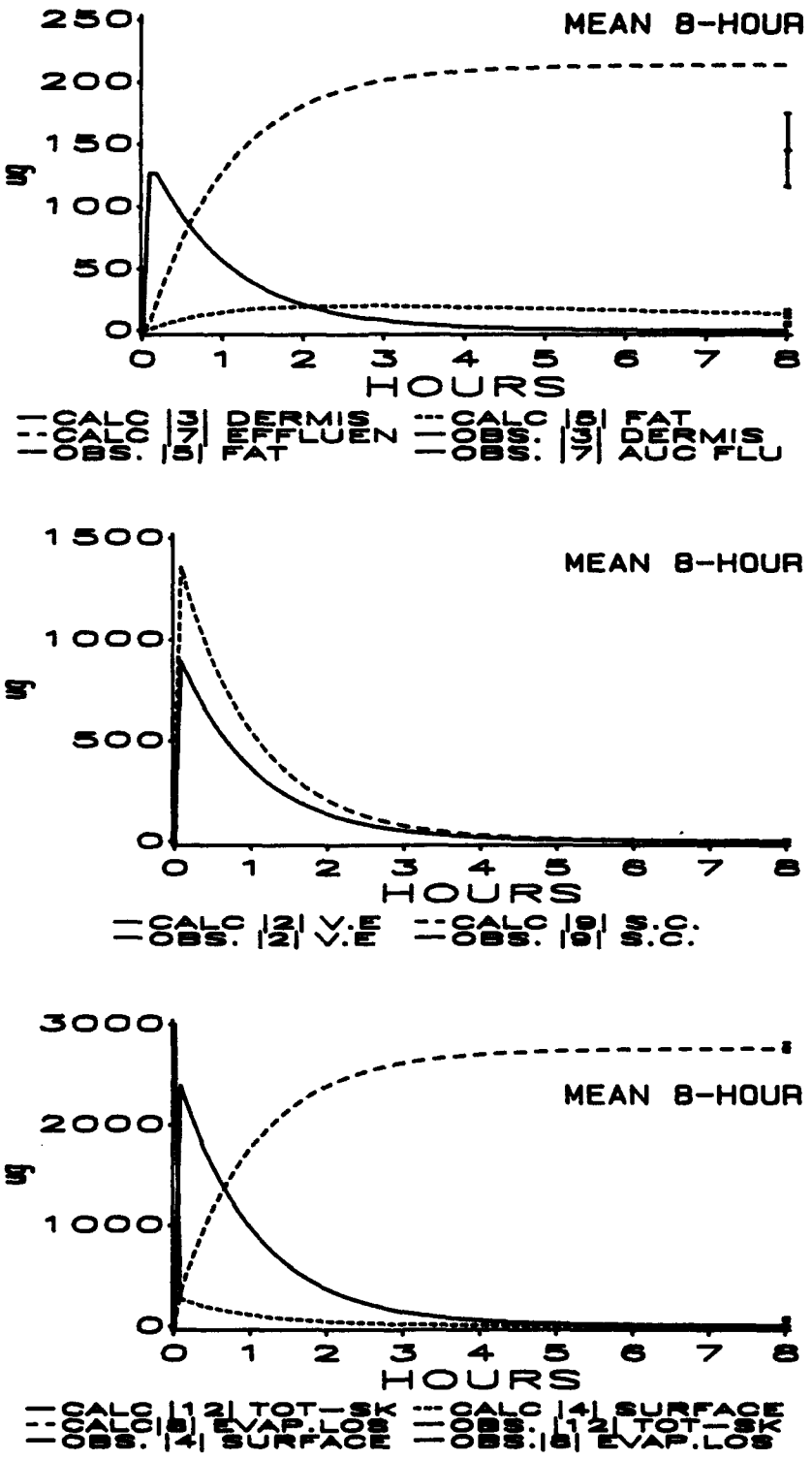

Figure 43: Mean of 8-hour IPPSFs: (Dose = 3000 µg ^{14}C-HD in ethanol). Calculated vs observed compartmental analysis: dermis, fat, and effluent; viable epidermis and stratum corneum; total skin, surface, and evaporative loss.

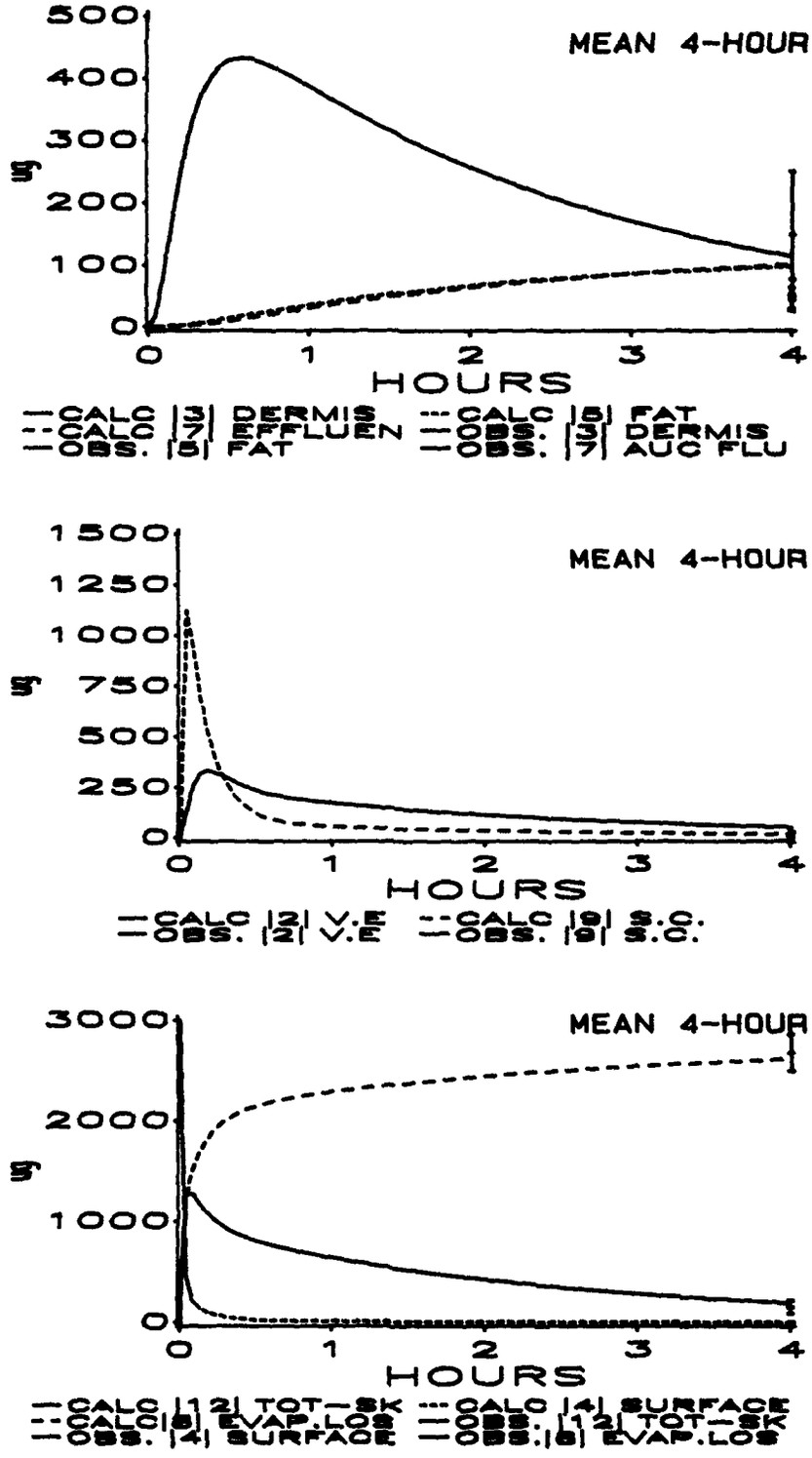

Figure 44: Mean of 4-hour IPPSFs: (Dose = 3000 μg ^{14}C-HD in ethanol). Calculated vs observed compartmental analysis: dermis, fat, and effluent; viable epidermis and stratum corneum; total skin, surface, and evaporative loss.

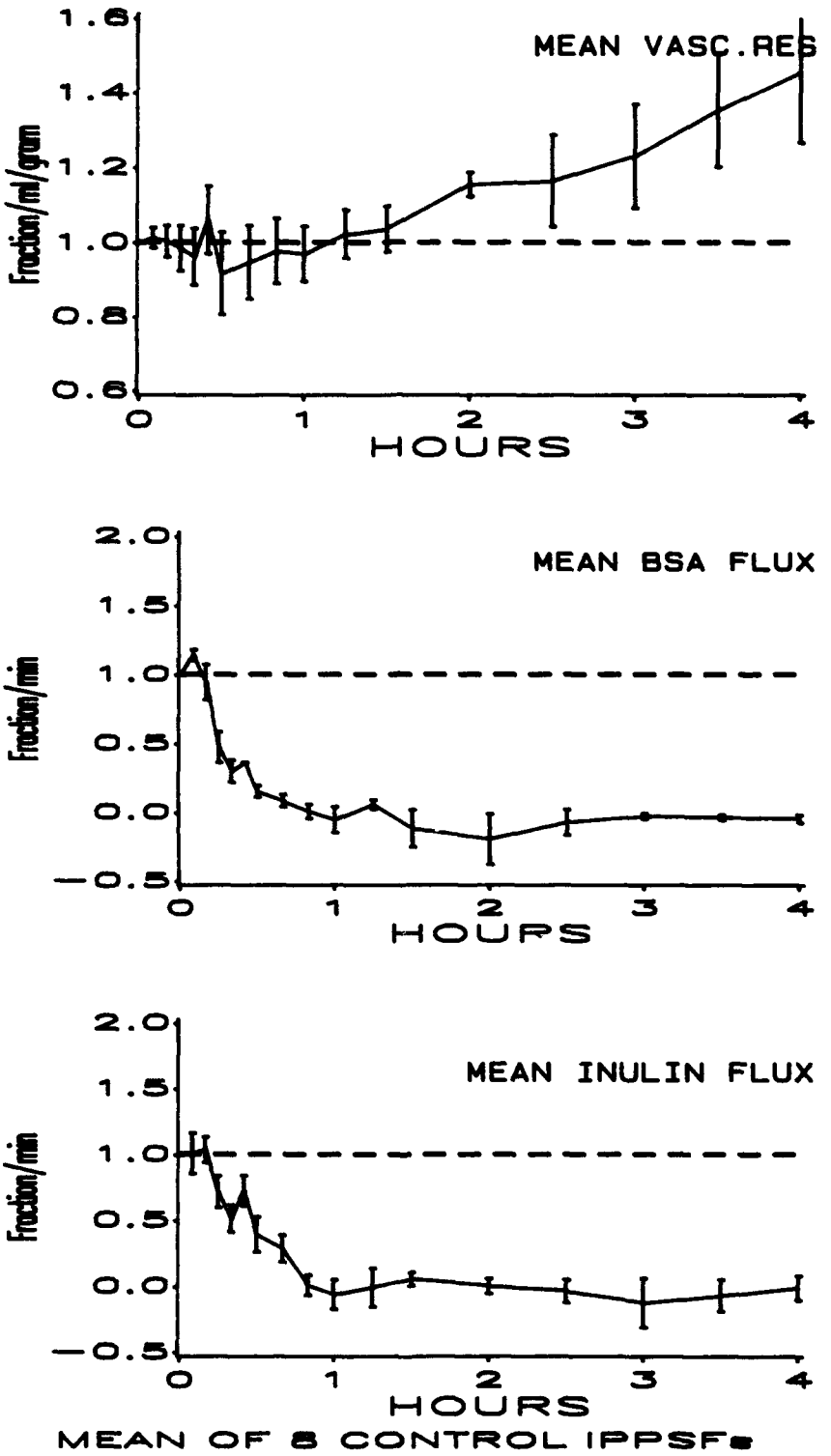

Figure 45: Mean of 5 control IPPSFs: (No Topical Dose). Mean VR; mean BSA differential flux; mean inulin differential flux.

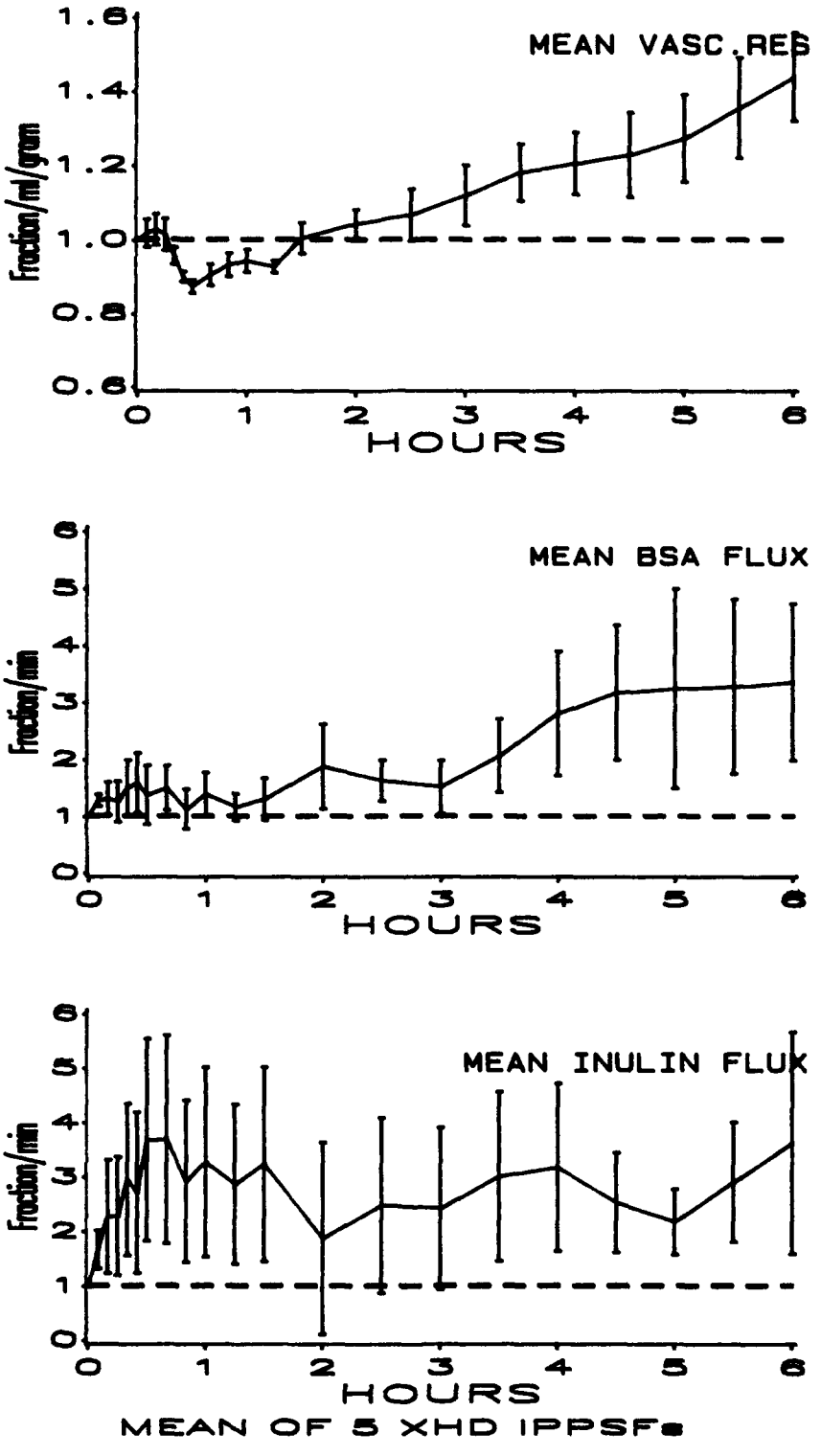

Figure 46: Mean of 5 HD IPPSFs: (Topical Dose = 1500 μg HD in ethanol). Mean VR; mean BSA differential flux; mean inulin differential flux.